EXPERIMENTAL AND NUMERICAL ADVANCES IN SCIENCE, ENGINEERING AND TECHNOLOGY

EDITED BY
Dr. RAMAZAN ŞENER

AUTHORS
ASSIST. PROF. DR. EVRIM ERSIN KANGAL
ASSIST. PROF. DR. CÜNEYT YÜCELBAŞ
ASSIST. PROF. DR. ŞULE YÜCELBAŞ
ASSIST. PROF. DR. BETÜL UZBAŞ
ASSIST. PROF. DR. HÜSEYIN GÜRBÜZ
ASSIST. PROF. DR. ÖZGE AKÇAY
ASSIST. PROF. DR. MUHAMMED ERNUR AKINER
RES. ASSIST. DR. YASEMIN AYAZ ATALAN
LECT. DR. JALE BEKTAŞ
DR. ERDAL ÇILĞIN
LECT. YASIN BEKTAŞ
GIZEMNUR EROL

İKSAD
Publishing House

EXPERIMENTAL AND NUMERICAL ADVANCES IN SCIENCE, ENGINEERING AND TECHNOLOGY

EDITED BY

Dr. RAMAZAN ŞENER

AUTHORS

ASSIST. PROF. DR. EVRIM ERSIN KANGAL
ASSIST. PROF. DR. CÜNEYT YÜCELBAŞ
ASSIST. PROF. DR. ŞULE YÜCELBAŞ
ASSIST. PROF. DR. BETÜL UZBAŞ
ASSIST. PROF. DR. HÜSEYIN GÜRBÜZ
ASSIST. PROF. DR. ÖZGE AKÇAY
ASSIST. PROF. DR. MUHAMMED ERNUR AKINER
RES. ASSIST. DR. YASEMIN AYAZ ATALAN
LECT. DR. JALE BEKTAŞ
DR. ERDAL ÇILĞIN
LECT. YASIN BEKTAŞ
GIZEMNUR EROL

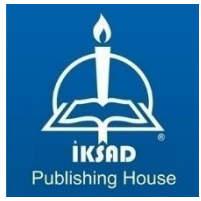

(The Licence Number of Publicator: 2014/31220)
TURKEY TR: +90 342 606 06 75
USA: +1 631 685 0 853
E mail: iksadyayinevi@gmail.com
www.iksadyayinevi.com

ISBN: 978-625-7636-73-5
Cover Design: İbrahim KAYA
May / 2021
Ankara / Turkey
Size = 16x24 cm

CONTENTS

PREFACE

Dr. Ramazan ŞENER ……..……..……1

CHAPTER 1

THE COMPARISON OF ENERGY RESOURCES IN THE CONTEXT OF GLOBAL ENERGY SUPPLY SECURITY

Res. Assist. Dr. Yasemin AYAZ ATALAN ……..3

CHAPTER 2

COMPARATIVE STUDY OF STOCHASTIC OPTIMIZATION TECHNIQUES FOR X-RAY BASED PNEUMONIA IMAGE CLASSIFICATION USING RESNET50

Lect. Dr. Jale BEKTAŞ

Lect. Yasin BEKTAŞ

Assist. Prof. Dr. Evrim Ersin KANGAL……25

CHAPTER 3

INVESTIGATION OF THE EFFECTS OF PCA, PLS, AND LDA METHODS ON COVID-19 DIAGNOSIS USING ADABOOST-RF CLASSIFIER

Assist. Prof. Dr. Cüneyt YÜCELBAŞ

Assist. Prof. Dr. Şule YÜCELBAŞ

Gizemnur EROL

Assist. Prof. Dr. Betül UZBAŞ ……45

CHAPTER 4

THE INVESTIGATION OF THE IMPACT OF USING PURE VEGETABLE OIL IN DIESEL ENGINES ON ENGINE

Dr. Erdal ÇILĞIN ……..…..63

CHAPTER 5

THE COMBINED EFFECTS OF HYDROGEN POST INJECTIONS AND FUMIGATION OF ETHANOL ON EMISSION AND PERFORMANCE IN A DIESEL ENGINE

Assist. Prof. Dr. Hüseyin GÜRBÜZ.……..…….....…87

CHAPTER 6

THE INVERSE PROBLEM OF STURM-LIOUVILLE OPERATOR WITH DISCONTINUITY CONDITIONS

Assist. Prof. Dr. Özge AKÇAY……..…..115

CHAPTER 7
A MODERN APPROACH TO THE LOADING CONFIGURATION OF PATTERNS IN FRAMES

Assist. Prof. Dr. Muhammed Ernur AKINER……139

PREFACE

This book presents the recent trends in science and engineering. The matters discussed and presented in the chapters of this book cover a wide spectrum of topics and research methods in the field of engineering. The book contains seven chapters: global energy supply security, stochastic optimization techniques, Adaboost-RF classifier for disease diagnosis, vegetable oil usage in the internal combustion engines, hydrogen post-injection in the diesel engine, the inverse problem of Sturm-Liouville operator, and the loading configuration of patterns in frames.

This book provides academics, students, and researchers with the knowledge and theoretical tools necessary to address related questions in science and engineering. I believe that this book, which consists of different fields, will be a resource for academics and researchers.

Dr. Ramazan ŞENER [1]

May 2021

[1] Automotive Engineering Department, Batman University, 72100, Batman, Turkey.
E-mail: ramazan.sener@batman.edu.tr ORCID ID: 0000-0001-6108-8673

CHAPTER 1

THE COMPARISON OF ENERGY RESOURCES IN THE CONTEXT OF GLOBAL ENERGY SUPPLY SECURITY

Res. Assist. Dr. Yasemin AYAZ ATALAN [1]

[1]Yozgat Bozok University, Faculty of Engineering and Architecture, Department of Industrial Engineering, Yozgat, Turkey.
E-mail: yasemin.ayaz@bozok.edu.tr ORCID ID: 0000-0001-7767-0342

INTRODUCTION

Energy is a crucial component in terms of carrying out daily human activities, whether in a developed or a developing country (Suganthi & Samuel, 2012). The energy requirement keeps rising with the escalation of welfare and life conditions throughout the world. The energy utilization rate and energy access are not exactly uniform everywhere (BP, 2020). Indeed, billions of people are not able to access enough amount of energy currently that is an indication of poorness (Kaygusuz, 2007).

The whole world has witnessed to the dramatic increase in global energy needs for some time now (BP, 2020). The increase in total energy consumption is roughly estimated to be 50% between 2018 and 2050 by the U.S. Energy Information Administration (EIA) as stated in the International Energy Outlook 2019 (IEO2019). The main portion of this escalation is originated from non-OECD (the Organization for Economic Cooperation and Development) nations, which concentrate in economically developing places that create demand, especially in Asia (U.S. Energy Information Administration, 2019).

The industrial sector has the biggest percentage of world energy consumption for both OECD and non-OECD countries, approaching to nearly 315 quadrillion British thermal units (Btu) by 2050. Manufacturing, agriculture, construction, refining, and mining are among the activities in the industrial sector that causes more than 50% of energy use throughout the world. Transportation ranks second with respect to the global energy utilization with 40% increase between 2018 and

2050. Non-OECD countries are responsible for most of this rise, where individual trip and freight transport related energy consumption shows faster growing trend as compared to many OECD nations. IEO forecasts that the least share of global energy usage belongs to the buildings sector, consisting of both residential and commercial constructions. In general, energy requirement globally increases in all sectors as a result of industrialization, population growth and easy access to electricity (U.S. Energy Information Administration, 2019).

1. TYPES OF ENERGY

Different forms of energy are employed all over the world as an essential constituent with the purpose of carrying out daily activities of people. Energy is divided into 3 groups in general, namely fossil fuels, nuclear energy and renewables.

Fossil fuels which include coal, oil and gas are the most dominant suppliers in the global energy mix (Johansson, 2013). EIA estimates that fossil fuels fulfill 77% of total energy use by 2040 in IEO2017 (EIA, 2017). However, there is a remarkable concern about fossil fuels over the environmental, health, economic, and energy security impacts as worldwide (Expert Group on Renewable Energy, 2005). Firstly, these sources are unsustainable and cannot replenish themselves, thus they are ultimately expose to exhaustion. Secondly, during the combustion of fossil fuels, carbon dioxide and other greenhouse gases are released into the atmosphere which in turn causes global warming. This escalation in Earth's temperature not only threats all living creatures, but also causes the glaciers to melt and so sea levels

to rise, which results in floods and negatively impact agriculture. Last but not least, fossil fuel utilization induces air pollution, acid precipitation, ozone depletion, forest destruction, and radioactive emissions that damage our environment (Shahzad, 2015). Figure 1 illustrates the global CO_2 concentrations by different fuel types, annually. It is clear from the figure that the majority of the total CO_2 emissions per year is originated from fossil fuels, endangering the environment excessively as explained above (Ritchie & Roser, 2020). In detail, coal, oil and natural gas is responsible for the 45%, 35% and 20% of the total greenhouse gas emissions throughout the world, respectively (Covert, Greenstone, & Knittel, 2016).

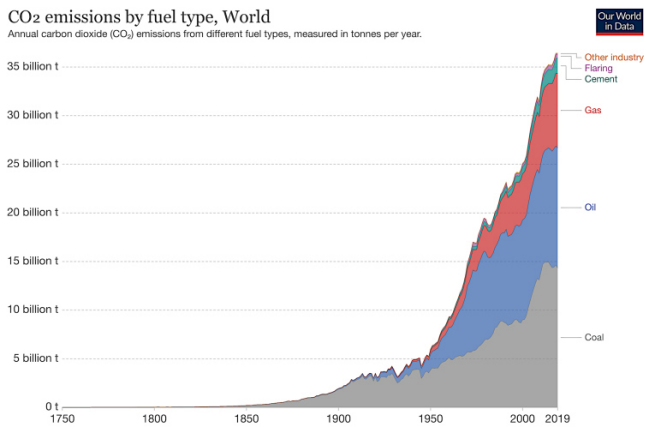

Figure 1. Global CO_2 concentrations by fuel type (Ritchie & Roser, 2020)

Nuclear energy was introduced in the early 50s, with the beginning of first nuclear reactor to operate in Idaho, United States. In the next decades, the commercial usage of nuclear power was put into practice by the U.S., UK, Russia, France, Germany and 20 other nations. Nuclear

energy was thought to reduce the momentum of global warming significantly by virtue of hindering more than 60 billion tons of CO_2 emission since 1970. The recent prediction of Nuclear Energy Agency (NEA) shows that around 1.2-2.4 Gt CO_2 emissions are suppressed from being released into the atmosphere on a yearly basis (Prăvălie & Bandoc, 2018). Recently, only 14% of electrical energy is supplied by nuclear power throughout the world (Dittmar, 2012).

On the other hand, nuclear energy technology faces some problems needed to be answered. The planning of nuclear power plants requires some safety protection issues, so that both capital costs and electricity costs increase. Radioactive gas formation during the operation period of the power plant is another worrying case about this type of energy, because of the health risk of its potential release into the atmosphere. The possibility that the expansion of the nuclear power industry will lead to the transformation of the material into nuclear weapons also retains a serious threat (Asif & Muneer, 2007). Although it is considered as an option with regard to overcome the escalating energy demand, it itself needs another feedstock to produce energy that is Uranium. It is also challenging that not only the enriched Uranium but also the nuclear waste is radioactive and hazardous (Petrescu et al., 2016). Additionally, nuclear power plants have to run at full capacity, meaning that they cannot operate on request. Moreover, they necessitate to be built close to a massive body of coolant water which can contaminate local water sources and poses hazard for aquatic life (Dittmar, 2012).

Renewable energy, classified as wind, solar, biomass, hydropower, geothermal and tidal energy, is defined as the energy that can be replenished at the same rate as it used, thus never depleted. The sustainability and cleanness of renewable energy resources help to reduce greenhouse gas emissions and so lessen the severe effects of global warming (Figure 2).

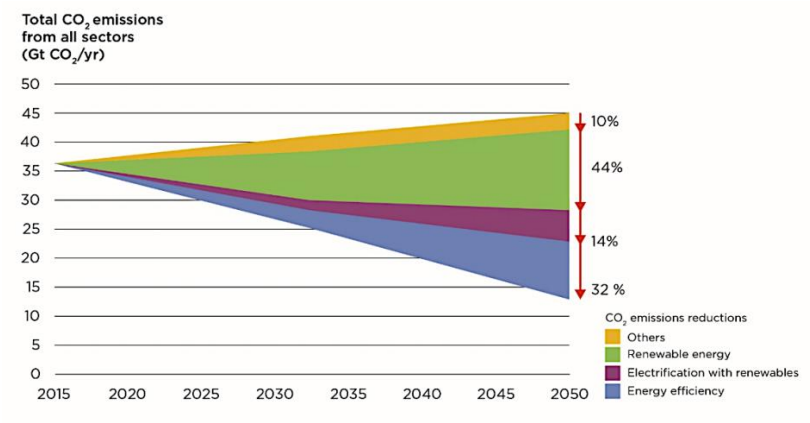

Figure 2. Primary CO_2 emission reduction potential by technology, 2015-2050 (IRENA, 2017)

The cost of energy from renewables becomes cheaper along with the improvements in technology, in contrast to unrenewables, the cost of which gets higher as these sources are exhausted and requirement of energy ascends.

Renewable energy is a relatively recent branch of industry in some regions of the world. Therefore, it can offer new job opportunities and make contribution to the economies, especially in developing countries (Shahzad, 2015). In addition, the most crucial point about re-

newable energy resources is its potential to meet more than 3000 times the present need of energy as worldwide (Ellabban, Abu-Rub, & Blaabjerg, 2014). Renewable sources of energy are the fastest growing types between 2018 and 2050, in comparison to other resources including natural gas, nuclear, petroleum, etc. (U.S. Energy Information Administration, 2019). 15 % of global energy need was met by renewable energy supply that is forecasted to increase to 28 % in 2050 (Inzlicht, Schmeichel, & Macrae, 2014)

2. ENERGY SUPPLY SECURITY

Energy, which is the most important input parameter of almost every phase of life, also indicates the level of economic development. Supply security, which refers to the availability and sustainability of energy, is a phenomenon that fundamentally affects the economic growth and development of countries and even their national security (Erdal & Karakaya, 2012).

The definition of energy security has been expanded over time and started to be used synonymously with energy supply security in the literature (Erdal & Karakaya, 2012). Energy security concept dates back to 200,000 years ago, when the Lower Paleolithic Period ended. In the past, the regions that is close to sufficient sources of combustible material (i.e., wood), not expose to extreme safety risks or do not need work more than the cost of fire itself, was believed to have high energy security. With the historical developments, this technical word lately expresses the energy to be adequately available to satisfy enough amount, affordable for both the investors and the consumers in

terms of solvency, accessible and sustainable to guarantee fuel source procurement without interference (Valentine, 2011). Energy and security have fundamentally two different aspects, where energy system is subjected to security risk or it causes risk. Figure 3 shows the analytical structure used to study the relationships between energy and security (Johansson, 2013).

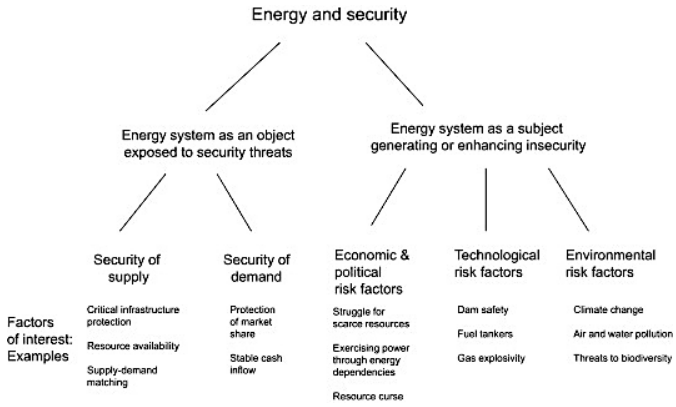

Figure 3. The analytical structure of the relationships between energy and security (Johansson, 2013)

Energy security is a significant subject attracting attention from different individuals, groups, parties, energy consumer enterprises, governments, and the society who needs energy to sustain life standards with high quality without any interruption (Ang, Choong, & Ng, 2015). The global fluctuations in energy market, the increasing competitiveness of energy suppliers, and the desire to make progress in economy while declining the poverty rate are the reasons behind this inclination of several authorities for energy security, explained as the

conception in which dependable energy is provided to customers in a cost effective way (Hughes, 2009).

There is a common misapprehension about security and independency of energy for being incorrectly employed in place of each other in some nationalities, as in the example of the United States. Likewise, evaluating energy security based on export results in ignoring the emphasis of local supply of sources and substructure (Hughes, 2009).

The risk of supply security arises from the inability to reach the existing resource rather than the possibility of running out of the potential energy source. In energy supply security, the most important concern is fossil fuels due to the uneven distribution of energy resources around the world (Erdal & Karakaya, 2012).

The energy supply security is a comprehensive term that comprises of four dimensions (symbolized as four As), namely availability, accessibility, affordability and acceptability (Figure 4) (Couder, 2015).

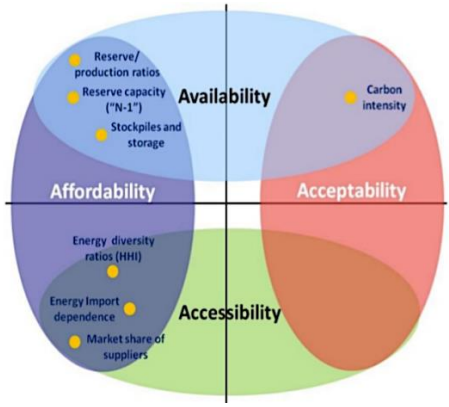

Figure 4. Four As framework of energy security (Couder, 2015)

2.1. Availability

The most important part of energy security is the existence and availability of energy source. In some sources, availability of energy is defined as the physically presence of it, especially for fossil fuels such as oil, natural gas and coal, which will be depleted in the future. It is also characterized by the ability of consumers to reach energy services they need. Therefore, availability, requires a market system in which parties who buy and sell energy goods and services agree on, regardless of the commercial, economic, political, strategic reasons (Erdal & Karakaya, 2012).

Assortment of different energy sources is an identifier of availability, by which interruptions of imported energy can be prevented or minimized. Geopolitical position is also crucial for energy availability because of the fact that wars, volatile forms of governments, and/or local events may interfere the flow of energy (Ang et al., 2015).

The International Energy Agency assumes that the exhaustion of non-renewable energy sources will bring with harsh consequences, which is caused by the imbalance among limited energy supply, escalated population and industrialization. It is a worrying fact that the predicted time of limited conventional energy sources to exist is between 30 and 150 years. Moreover, approximately 40 - 60% decrease of gas and oil generation is forecasted by 2030 (Kahia, Ben Aïssa, & Charfeddine, 2016). In opposition to finite fossil fuel stocks, renewable energy resources have the ability to provide energy for a long period depending on maintaining of sustainability when used (Johansson, 2013).

The pro-nuclear Federation of Japanese Electric Power Firms and the World Nuclear Association agree on that the remaining deposits of the world in terms of commercial uranium have a lifespan of 80-85 years. Even though there are some doubts about the availability of uranium in mid and long term, this stock is more attractive as compared to fossil fuels as it is mostly concentrated in steady countries. Indeed, Australia possess 31% of uranium reserves of the planet, while the shares of Canada and the U.S. are 9% and 5%, respectively. In short, nuclear energy might be considered as an available source for the fossil fuel dependent countries in the short term, but insufficiency of supply prevents achieving energy security in the mid to long term. Renewable energy is a more favorable source than nuclear power with regard to energy security (Valentine, 2011).

2.2. Accessibility

The accessibility of energy both refers to the distance between the production and consumption of energy from the reserve or available source and uninterrupted supply of energy. The disruption of energy, required for the daily routine of life, is an undesirable situation that prevents the production of all kinds of goods and services. In this context, it is of vital importance to take the following measures in order not to be exposed to energy cuts and to increase the security of supply Erdal & Karakaya, 2012);

- Diversification of supply sources,
- Differentiation of the generation, transmission and distribution network of supply,

- Increasing the capacity of the supply network with its pipeline and distribution infrastructure,
- Reducing the energy demand that will bring additional burden to the energy infrastructure,
- Energy storage for use in emergency power outages,
- Repair / improvement of damaged energy networks or infrastructures,
- Establishing supply and demand balance with instant information sharing in the energy market.

2.3. Affordability

The rough expression of affordability is the cost effectiveness of a product or service of interest. As a more specific statement, energy affordability refers to the quality of the energy source being financially manageable for which a fair price related to income level should be suggested in order to handle poorness. In addition, the cost of energy ought to be invariable and publicly available to help make accurate predictions on future developments in terms of resource sustainability aspect (Hafezi & Alipour, 2020).

Energy security, represents the reliable and sufficient supply of energy, fully meeting the needs of the global economy, with reasonable prices for consumer countries. Reasonable price is perceived differently in terms of those who consume and produce energy. Since the price, which is determined by the market on the basis of the supply and demand balance, is generally based on cost, it may change direction towards both ends (in favor of the seller or buyer). Compared to the

supply side of energy security and, more importantly, to the domestic supply of consumer countries, a massive power outage is as dangerous as the oil crisis, which causes a long-term security problem. Fluctuations in energy prices due to crises and speculative reasons may trigger countries to suffer economic losses, social damages, and even political instability Erdal & Karakaya, 2012).

The vital magnitude of energy costs in the energy security equation is highlighted in many researches. That US dollar is used to commercially buy and sell crude oil controls the price of energy imported internationally, for which the value of different currencies is crucial. Fossil fuel cost is unsteady leading to challenges with respect to energy supply security, which in turn complicates policy makers to achieve the national targets, such as capacity increasing, in the short-, mid-, and long term (Ang et al., 2015). It is noteworthy whether the impact of these global fluctuations in the costs of fossil fuels will be reflected on exporting countries that drastically influence on regional economies (Johansson, 2013)

In opposition to fossil fuels, the capital cost is the primary component of production price by renewable energy, namely wind power, solar energy, etc., that follows a notably declining trend with technological improvements. However, after the power plants are installed once, the energy generation prices become low and steady (Valentine, 2011).

For the case of nuclear power, the installation costs are very high and also operational costs are subject to the uranium reserves which are needed as a feedstock in nuclear energy technology (Johansson,

2013). The requirement of considering various security measures for the design of nuclear power plants leads to escalation in initial cost. Generating electricity from wind or gas costs half as much as that is derived from nuclear energy (Atalan, Tayanç, Erkan, & Atalan, 2020).

2.4. Acceptability (Sustainability)

The concept of energy security did not include environmental concerns until recently. The preference and acceptance of the energy source by the society indicates the sustainability of the resource (Erdal & Karakaya, 2012).

Actually, the relation of sustainability and environmental concerns to energy is undeniable, since global warming and air pollution are the two examples of consequence arising from emissions of carbon and other greenhouse gases. The significancy level of sustainability and the environment within the framework of energy security is also underlined by The European Commission (Ang et al., 2015).

Continuity in energy supply and environmental awareness in energy consumption is very important in terms of long term sustainability (Erdal & Karakaya, 2012). The reduction of unfavorable losses related to the society, environment, economics, technology and even politics describes sustainability. Currently, it is connected to energy that interactively defines the decline the effect of energy on environmental degradation. Energy security is now focused on several aspects, such as human rights, environment, affordability, accessibility, etc., rather than checking a single dimension of energy supply (Hafezi & Alipour, 2020).

Despite the fact that fossil fuels supply majority of the energy demand worldwide, they are finite sources of energy that cannot be reproduced again. In addition, they are hazardous for both human health and the environment because of the emissions of carbon dioxide and other greenhouse gases released after the combustion of these conventional resources. Therefore, the limited and harmful nature of fossil fuels make them unsustainable (Covert et al., 2016).

Renewable energy offers a sustainable option to meet the increasing energy need for the future in a cost-effective way. It is an eco-friendly and finite energy that help mitigate environmental degradation and so remove the pollutants endangering the health of society (Bilgen, 2014; Qazi et al., 2019).

Depending on the way of perception for sustainability term, different governments have dissimilar opinions whether the nuclear energy is sustainable or not. For instance, in South Korea nuclear power is believed to be a sustainable source, while in Denmark and Austria the opposite is accepted

(Gralla et al., 2016). Due to the supply of accessible and affordable energy cost efficiently, nuclear energy is thought to be sustainable in some communities. However, the radioactivity of both the fuel and nuclear waste with the safety risks in short and long term make this source perceived as unsustainable (Kermisch & Taebi, 2017).

CONCLUSION

Energy with the types and importance in terms of increasing demand, environmental concerns and public health is comperatively discussed in this book section. Energy security concept is described with regard to different types of energy.

Energy is the main input of the production of goods and services in economic terms. With regard to security, it is an indispensable resource that raises the standard of living that will paralyze development and welfare if interrupted. Moreover, it carries environmental risks that may endanger the lives of future generations as a result of its excessive use in fossil fuels.

Energy resources are not distributed homogenously worldwide. In some parts of the world, the possession and domination of energy resources is an indicator of wealth, causing dependency from the standpoint of exporters, while large numbers of people are trying to sustain their lives with a lack of energy in some other regions that demonstrate poverty.

Energy security is the uninterrupted reliable supply of energy in a cost efficient and sustainable way. Availability, accessibility, affordability and acceptability (or sustainability) constitutes the basic dimensions of energy supply security. The measures to be taken to increase the security of supply in energy; diversification of energy sources and suppliers, utilization of local resources, full liberalization of the domestic market, increasing cross-border investments, improving energy resource storage capacity, saving in energy consumption and increasing

energy efficiency. Renewable energy resources are considered as the best option with respect to potential to satisfy escalating energy requirement, health of society and the environment, cost, job opportunities, sustainability and energy security, etc. Governments and authorities should promote energy production by renewables in order to help minimize the dependency on foreign fossil fuel sources and so strengthen their economies besides dealing with the other environmental issues.

REFERENCES

Ang, B. W., Choong, W. L., & Ng, T. S. (2015). Energy security: Definitions, dimensions and indexes. *Renewable and Sustainable Energy Reviews*, *42*, 1077–1093. https://doi.org/10.1016/j.rser.2014.10.064

Asif, M., & Muneer, T. (2007). Energy supply, its demand and security issues for developed and emerging economies. *Renewable and Sustainable Energy Reviews*, *11*(7), 1388–1413. https://doi.org/10.1016/j.rser.2005.12.004

Atalan, Y. A., Tayanç, M., Erkan, K., & Atalan, A. (2020). Development of nonlinear optimization models for wind power plants using box-Behnken design of experiment: A case study for Turkey. *Sustainability (Switzerland)*. https://doi.org/10.3390/su12156017

Bilgen, S. (2014). Structure and environmental impact of global energy consumption. *Renewable and Sustainable Energy Reviews*, *38*, 890–902. https://doi.org/10.1016/j.rser.2014.07.004

BP. (2020). *Energy Outlook 2020 edition*. Retrieved from https://www.bp.com/content/dam/bp/business-sites/en/global/corporate/pdfs/energy-economics/energy-outlook/bp-energy-outlook-2020.pdf

Couder, J. (2015). *Literature Review on Energy Efficiency and Energy Security, including Power Reliability and Avoided Capacity Costs*. Retrieved from https://combi-project.eu/wp-content/uploads/2015/09/D7.1.pdf

Covert, T., Greenstone, M., & Knittel, C. R. (2016). Will We Ever Stop Using Fossil Fuels? *Journal of Economic Perspectives*, *30*(1), 117–138. https://doi.org/10.1257/jep.30.1.117

Dittmar, M. (2012). Nuclear energy: Status and future limitations. *Energy*, *37*(1), 35–40. https://doi.org/10.1016/j.energy.2011.05.040

EIA. (2017). International Energy Outlook 2017 Overview. U.S. Energy Information Administration, IEO2017(2017), 143. https://doi.org/www.eia.gov/forecasts/ieo/pdf/0484(2016).pdf

Ellabban, O., Abu-Rub, H., & Blaabjerg, F. (2014). Renewable energy resources: Current status, future prospects and their enabling technology. Renewable and Sustainable Energy Reviews, 39, 748–764. https://doi.org/10.1016/j.rser.2014.07.113

Erdal, L., & Karakaya, E. (2012). ENERJİ ARZ GÜVENLİĞİNİ ETKİLEYEN EKONOMİK, SİYASÎ VE COĞRAFÎ FAKTÖRLER. *Uludağ Journal of Economy and Society*, *31*(1), 107–136. Retrieved from http://193.140.245.211/bitstream/11452/18567/1/31_1_5.pdf

Expert Group on Renewable Energy. (2005). RENEWABLES 2005 BACKGROUND REPORT. *Increasing Global Renewable Energy Market Share Recent Trends and Perspectiives*, 86.

Gralla, F., John, B., Abson, D. J., Møller, A. P., Bickel, M., Lang, D. J., & von Wehrden, H. (2016). The role of sustainability in nuclear energy plans—What do national energy strategies tell us? *Energy Research & Social Science*, *22*, 94–106. https://doi.org/10.1016/j.erss.2016.09.003

Hafezi, R., & Alipour, M. (2020). *Energy Security and Sustainable Development*. https://doi.org/10.1007/978-3-319-71057-0_103-1

Hughes, L. (2009). The four 'R's of energy security. *Energy Policy*, *37*(6), 2459–2461. https://doi.org/10.1016/j.enpol.2009.02.038

Inzlicht, M., Schmeichel, B. J., & Macrae, C. N. (2014). Why self-control seems (but may not be) limited. *Trends in Cognitive Sciences*, *18*(3), 127–133. https://doi.org/10.1016/j.tics.2013.12.009

IRENA. (2017). *Perspectives for the Energy Transition- Investment Needs for a Low-Carbon Energy System*.

Johansson, B. (2013). Security aspects of future renewable energy systems–A short overview. *Energy*, *61*, 598–605. https://doi.org/10.1016/j.energy.2013.09.023

Kahia, M., Ben Aïssa, M. S., & Charfeddine, L. (2016). Impact of renewable and non-renewable energy consumption on economic growth: New evidence from the MENA Net Oil Exporting Countries (NOECs). *Energy*, *116*, 102–

115. https://doi.org/10.1016/j.energy.2016.07.126

Kaygusuz, K. (2007). Energy for Sustainable Development: Key Issues and Challenges. *Energy Sources, Part B: Economics, Planning, and Policy*, *2*(1), 73–83. https://doi.org/10.1080/15567240500402560

Kermisch, C., & Taebi, B. (2017). Sustainability, Ethics and Nuclear Energy: Escaping the Dichotomy. *Sustainability*, *9*(3), 446. https://doi.org/10.3390/su9030446

Petrescu, F. I. T., Apicella, A., Petrescu, R. V. V., Kozaitis, S. P., Bucinell, R. B., Aversa, R., & Abu-Lebdeh, T. M. (2016). Environmental Protection through Nuclear Energy. *American Journal of Applied Sciences*, *13*(9), 941–946. https://doi.org/10.3844/ajassp.2016.941.946

Prăvălie, R., & Bandoc, G. (2018). Nuclear energy: Between global electricity demand, worldwide decarbonisation imperativeness, and planetary environmental implications. *Journal of Environmental Management*, *209*, 81–92. https://doi.org/10.1016/j.jenvman.2017.12.043

Qazi, A., Hussain, F., Rahim, N. A., Hardaker, G., Alghazzawi, D., Shaban, K., & Haruna, K. (2019). Towards Sustainable Energy: A Systematic Review of Renewable Energy Sources, Technologies, and Public Opinions. *IEEE Access*, *7*, 63837–63851. https://doi.org/10.1109/ACCESS.2019.2906402

Ritchie, H., & Roser, M. (2020). CO2 emissions by fuel. Retrieved April 29, 2021, from https://ourworldindata.org/emissions-by-fuel

Shahzad, U. (2015). The Need for Renewable Energy Sources. *International Journal of Information Technology and Electrical Engineering*.

Suganthi, L., & Samuel, A. A. (2012). Energy models for demand forecasting—A review. *Renewable and Sustainable Energy Reviews*, *16*(2), 1223–1240. https://doi.org/10.1016/j.rser.2011.08.014

U.S. Energy Information Administration. (2019). *International Energy Outlook 2019 with projections to 2050*. Retrieved from https://www.eia.gov/outlooks/ieo/pdf/ieo2019.pdf

Valentine, S. V. (2011). Emerging symbiosis: Renewable energy and energy security. *Renewable and Sustainable Energy Reviews*, *15*(9), 4572–4578.

https://doi.org/10.1016/j.rser.2011.07.095

CHAPTER 2

COMPARATIVE STUDY OF STOCHASTIC OPTIMIZATION TECHNIQUES FOR X-RAY BASED PNEUMONIA IMAGE CLASSIFICATION USING RESNET50

Lect.Dr. Jale BEKTAŞ [1]

Lect. Yasin BEKTAŞ [2]

Assist. Prof. Dr. Evrim Ersin KANGAL [3]

[1] Mersin University, Erdemli School of Applied Technology and Management, Department of Computer Technology and Information Systems, Mersin, Turkey.
E-mail: jale@mersin.edu.tr ORCID ID: 0000-0002-8793-1486

[2] Mersin University, Vocational School of Erdemli, Department of Computer Technologies, Mersin, Turkey.
E-mail: yasinbektas@mersin.edu.tr ORCID ID: 0000-0002-2761-5780

[3]Mersin University, Erdemli School of Applied Technology and Management, Department of Computer Technology and Information Systems, Mersin, Turkey.
E-mail: evrim.kangal@mersin.edu.tr ORCID ID: 0000-0001-5906-3143

INTRODUCTION

In the United States alone, more than 1 million people are diagnosed with pneumonia every year, and 50,000 of the cases die (Centers for Disease Control and Prevention, 2021). The most common method for diagnosing pneumonia is chest X-Ray (World Health Organization, 2001). However, detecting pneumonia on chest X-rays is also a tedious and challenging process for specialist radiologists.

A number of artificial intelligence (AI) systems based on machine learning (Maruyama et al., 2018) and deep learning (DL) (Gupta et al. 2021) have been proposed by researchers, as this paves the way for faster interpretation of radiographic images by experts in disease diagnoses. Experts in determining the disease infected with pneumonia with these methods are mainly focused on CT imaging and have very supportive results at the decision stage (Zhao et al., 2018). One of the most critical challenges to this success is the optimization problem in DL. Finding optimal weight values to minimize error in the calculation process of the loss function is a situation that directly affects the ability to learn. The choice of stochastic optimization techniques plays an important role and also is needed expertise for choosing in this process (Li et al., 2021).

Feature selection is a keystone (Urbanowicz et al., 2018) in many radiographic image classification problems (Nayak et al., 2021). Instead of all complex relationships to diagnose an image, only those who best identify that image are efficient and effective in classification. More features don't always mean better classification performance. Therefo-

re, choosing the most compact subset by reducing the dimensionality of the property space requires good editing and flow in the model. In this way, an increase in classification performance is inevitable and the cost of calculation is reduced.

In previous studies (Tuncer et al., 2020), Residual Exemplar Local Binary Pattern (ResExLBP) method which uses iterative ReliefF (IRF) based feature selection is suggested. After feature selection phase, five classifiers which are Decision tree (DT), linear discriminant (LD), support vector machine (SVM), k nearest neighborhood (kNN), and subspace discriminant (SD) were utilized to classify COVID-19 chest X-ray images. This method achieved 99.69% accuracy with SVM. The deep LSTM model (Demir, 2021), which is learning from scratch an application of the Sobel gradient and marker-controlled preprocessing schemes to raw images is suggested. These preprocess operations are applied to increase the performance of the model to detect COVID-19, pneumonia and normal (healthy) chest X-ray images. In (Stephen et al., 2019) a method of X ray image classification based on pneumonia is presented based on Convolutional Neural Networks (CNN-Conv). During implementation, the CNN architecture achieved with the Acc of 0.94%. In (Jaiswal et al., 2019), a deep R-CNN method of segmenting with different threshold values using global and local features for pixel-wise operations were developed. In addition to this, autonomous hyper-parameters determining have been a challenging subject for researchers. Therefore, different state-of-art architectures are experimented in a novel study which generates SGD methods with genetic algorithms (Ma et al., 2020). Moreover, to the contantry

of SGD, the Adam method achieves a more satisfactory result by using memory effectivelywhen classifying chest X-Rays (Montalbo, 2021). This has shown us the importance of experimenting with SGD derivatives.

In this work, Resnet-50 Network, whose success on medical images is indisputable in the classification process, was used. The effect of stochastic optimization techniques such as Stochastic Gradient Descent, Adadelta, RMSProp and Adam on Resnet-50 was experimented using Chest X-Ray image data. In the next step, the effect of ReliefF, which is a feature selection method, on existing analyses and selected hyperparameters, is also discussed.

1. MATERIAL AND METHODS

In the process of classifying images, there are many hyper parameters that affect the performance of DL use. The main ones are feature selection and optimization parameters (Koutsoukas et al., 2017). Ignoring the use of feature selection in the training process can lead to a permanent deterioration in generalization performance. This disruption triggers the need to research different techniques to train models. In addition, larger training sets increase training time. Another problem in learning is the process of achieving optimal weight values during the training process. Finding weight values that minimize cost is a situation that directly affects the ability to learn, and the choice of stochastic optimization techniques plays an important role in this process. Incorrect algorithm selection can lead to a lack of generalization ability, and the inability to reasonably obtain these values using a de-

terministic optimization technique also leads to serious costs for learning times (Xu et al., 2019).

1.1. Image Dataset

Chest X-Ray image data consists of a total of 5856 images with 2 categories of 1583 normal and 4273 infected is available on kaggle website. Class activation mapping which utilizes gradient weighting (Grad-CAM) (Selvaraju et al., 2017) is used to determine and extract region of Interest (ROI) areas for images when dividing CXRs into normal and infected classes. Grad-CAM creates heat maps that are indicated by colored pixels and show high-level regions. Beyond visual explanation, Grad-CAM can be used as an approach to visualizing classification predictions. Figure 1 and Figure 2 shows the visualization of the heat map of the ROI for two different classes using Grad-CAM, respectively.

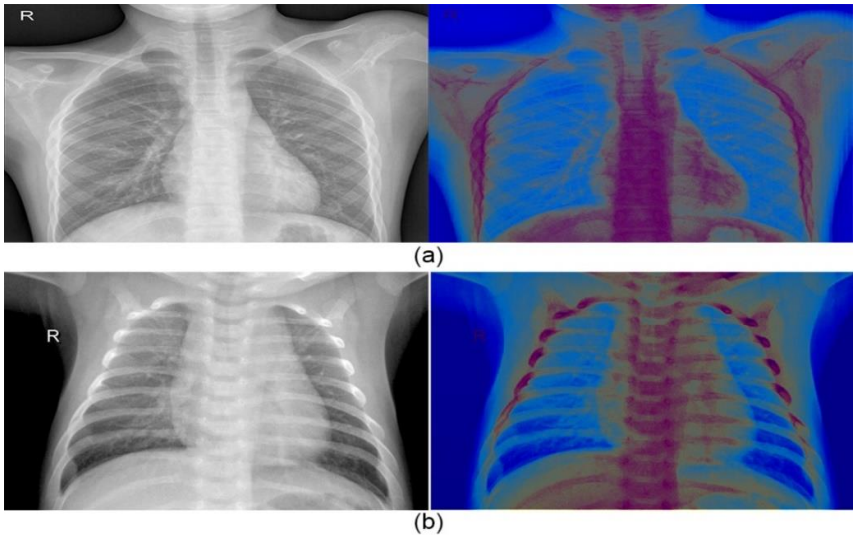

Figure 1. Two non-infected samples from image dataset (a)Sample#1, (b)Sample #2. Left: original gray scale image Right: Grad-CAM visualization.

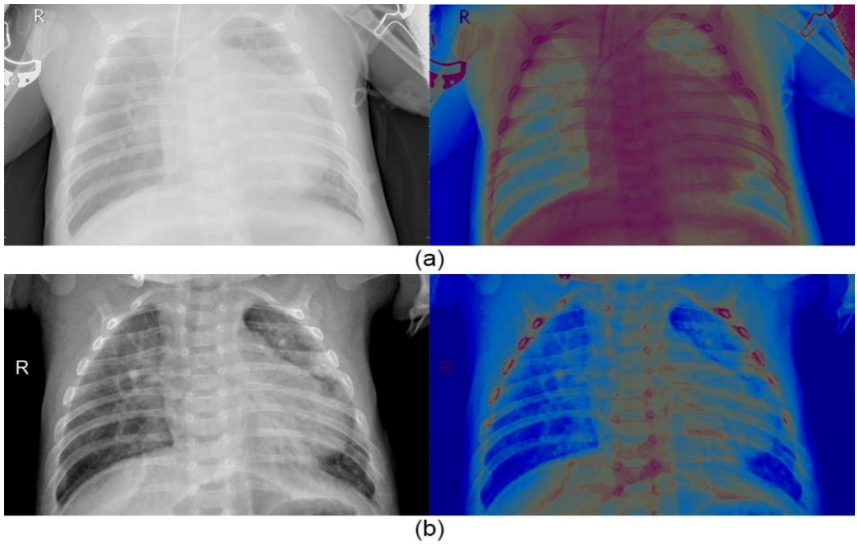

Figure 2. Two pneumonia samples from image dataset (a)Sample#1, (b)Sample #2. Left: original gray scale image Right: Grad-CAM visualization.

1.2. Background on Very Deep Resnets

In studies, it has been proven that the depth level of the network used in DL is one of the key factors of model expression (Rajpal et al., 2021). Image classification one of the popular state-of-the-art designs, the Resnet-50, was utilized in architectural design. Resnet-50 has minimal risk of data loss from the first layers and in layer additions. In the ResNet architecture, the path from input to output is mapped by a nonlinear *H(x)* function and represented by another nonlinear function defined as $F_i(x) = H_i(x) - x$ for the Residual block. In addition, by making a shortcut link from input to output, the input value *x* is added arithmetic to the function *F(x)*. Then the function $F_i(x) = F_i(x) + x$ is passed together in Relu. In this method, the input layer is added to the end of the second layer and the values in the past layers are more

strongly transferred to the next layers.

Convolutional (conv), Rectified Linear Unit (ReLU) and batch normalization (Batch Norm) layers are the basis structs of a residual block.

1.3. Proposed ResNet Classification Architecture

The Resnet-50 model was utilized only by revising in accordance with the output layer classification sample without changing the layer architecture. When calling the Resnet-50 network, the pooling parameter is given as avg. Whilst the training process, weight values were not updated, pretrained tuning weight values were used. Input shape is set to 128 x 128. Proposed Resnet-50 classification architecture is given in Figure 3.

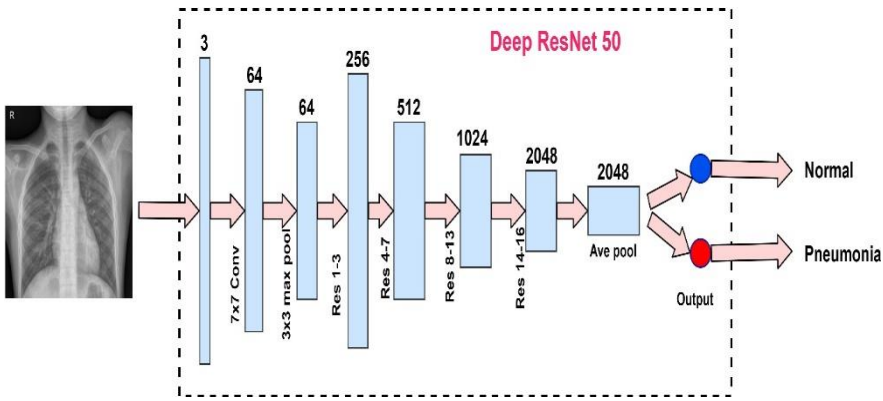

Figure 3. Resnet-50 classification architecrure which is applied to Chest X-Ray images.

1.3.1. Training Process of Classification

Whilst the train process, the image augmentation technique was used. Batch size value selected as 8 and the training process with 100

epochs was operated. SGD, AdaDelta, RMSProp and Adam functions were used as optimization functions in the training process. The learning rate is 0.01 for all optimization techniques and the momentum is given as 0.9. Momentum is the parameter that accelerates the optimization techniques in the relevant direction and reduces the oscillations. One of the main momentum-based techniques, Nesterov's accelerated gradient, was used. Decay value is optimized as 0.0005.

1.4. Optimization Algorithms

1.4.1. Stochastic gradient descent (SGD) algorithm

Gradient descent (GD) is a widely used optimization algorithm that converges the model to obtain appropriate parameters in the shortest possible time (Ketkar, 2017). GD can help CNN based models represent the most appropriate weight values in each training iteration. However, the performance of GD appears to be declining in validation and testing processes due to the excessive risk of being stuck in local solutions. Therefore, SGD is widely recommended to solve this issue. During training, GD scans all data in each iteration, while SGD translates only part of it, which means that it chooses only one stochastic training sample instead of all. While stepping each iteration in training, samples are selected randomly. Weight updates as follows:

$$w_{i+1} = w_i - \eta \frac{\partial L}{w_i} \quad (1)$$

Where w denotes weight parameter, η is learning rate, L represents the loss function.

1.4.2. RMSProp Algorithm

The RMSProp (Hinton et al., 2012) algorithm has been developed against the problem of early and memorized termination of the training process. It is improved by combining both the superiority of momentum and the application effectiveness of Adagrad in Eq.2

$$\rho \leftarrow \rho.r + (1-\rho).g^2 \quad (2)$$

Cumulative squared gradient is calculated according to the above formula. The parameter ρ is used to check the effect of past gradients and is usually set to 0.9. It provides a balance between the historical effects of gradients and their second degree momentums. r is the gradient cumulative variable.

$$\Delta w \leftarrow -\eta.g/\left(\delta + \sqrt{r}\right) \quad (3)$$

The sum of squared gradients become larger when the number of iterations increases. Therefore, to update the parameters δ is used to guarantee the nonzero denominator.

1.4.3. Adaptive Momentum (Adam) Algorithm

Adaptive Momentum (Adam) optimization algorithm is an extension to SGD and as determinedas RMSprop and SGD with momentum entegration (Kingma and Ba, 2014). The learning rate is optimized with Square gradients (RMSProp) and takes advantage of momentum using the moving means of the gradient (SGD). Adam uses exponentially moving means computed on the gradient and predicts the mo-

ments.

$$m_t = \beta_1 m_{t-1} + (1 - \beta_1) g_t \quad (4)$$

$$v_t = \beta_1 v_{t-1} + (1 - \beta_2) g_t^2 \quad (5)$$

where *m* and *v* are moving averages, g is gradient on current mini-batch, and β_1 and β_2 values are new hyperparameters of the algorithm. Given the values between 0.9 and 0.999 respectively would result in the network performing better.

1.4.4. Adaptive Delta (AdaDelta) Algorithm

AdaDelta (Zeiler, 2012) is an extension of Adagrad, which attempts to uniformly reduce the gradient descent rate. In the AdaDelta stochastic optimization technique, not all past square gradients are addressed, but instead past gradients are bounded by *w* as a fixed dimension. The sum of gradients is recursively defined as a skewed mean of all of the past square gradients.

$$E[g^2]_t = \gamma E[g^2]_{t-1} + (1 - \gamma) g_t^2 \quad (6)$$

The moving average $E[g^2]_t$ in the time step. As a fraction γ similar to the term Momentum and depends only on the previous average and current gradients. Given the value approximately 0.9 to γ would result in the network performing better.

1.5. Feature Selection with ReliefF

In Relief feature selection (Zhou, 2015; Jia et al., 2013) the concept of Margin is used to evaluate the classification capacity of feature size.

The Margin maintains the classification for the same samples within the area at the maximum distance between the classification regions. In addition, ReliefF is often preferred as a pre-model schema for the selection of features that will best identify the data.

$$w_i = w_i - \frac{\sum_{k=1}^{K} D_H(k)}{n.k} + \sum_{c=1}^{C-1} p_c \cdot \frac{\sum_{k=1}^{K} D_M(k)}{n.k} \quad (7)$$

where $D_H(k)$ is the sum of distance between the selected instance and its k_{th} nearest neighbor in H or M, p_c is the prior probability of class c. Following pseudo-code of the ReliefF algorithm is designed according to Eq.7 presented in the reliefF procedure.

Procedure: Pseudo-code of ReliefF (ReliefF(D))

Input: Feature data matrix*: D,* repeat times*: n,* the number of the neighbors*: k*

Output: *Vector w for the feature attributes ranking*

00:Begin

01:for i=1 to n do

02: S_i instance is selected randomly

03: *K* nearest hits *H* and the nearest misses *M* are found

04: *for j=1 to all features do*

05: W_i estimations are updated

06: *End*

07:End

08:End

---

2. EXPERIMENTAL RESULTS

The evaluation metrics which were used for the analysis of the experimens are accuracy (Acc), Loss, and Auc. The mathematical equations fort the Acc is given in Eq.8.

$$Acc = \frac{TP+TN}{TP+FP+FN+TN} \quad (8)$$

Chest X-Ray image data was used which is a total of 5856 images with 2 categories of 1583 normal and 4273 infected. 70% -30% of the images were divided for training and validation, respectively. Comprehensive experiments were performed on Chest X-Ray dataset to compare our Resnet-50 classification network with ReliefF-Resnet50 ensemble. Hardware used in the process from effective attributes selected by the ReliefF feature selection preliminary scheme to the operating stage in the classification architecture was Intel(R) Core(TM) i7-4700HQ 2.40GHz processor, NVIDIA GeForce GTX 765M GPU card, and 16GB RAM. Chest images were loaded as W x H x 3 size and resized as for the W x H grayscale conversion to 500 X 500 size. In the experiment on the dataset a 250000 dimension feature space were obtained. Then, each feature component in the feature space was considered as a single feature.

Table 1 shows average performance comparisons of Resnet-50 and reliefF-ResNet50. It can be seen that the adadelta optimization technique shows the best performance among others in the chest X-ray dataset, as well as the effectiveness of the selected parameters. When the feature selection was combined with Resnet-50, the classification

network achieved the highest performance measurements with 0.99% Acc, 0.997 Auc. The AdaDelta optimization technique has shown the best output when using both the Resnet-50 and the ReliefF-Resnet50 method.

Table 1. The comparison of classification performances between Resnet-50 and ReliefF-Resnet50 according to stochastic optimization techniques.

	Resnet-50			ReliefF-Resnet50		
	Loss	Acc	Auc	Loss	Acc	Auc
SGD	0.548	0.904	0.957	***0.001***	***0.980***	0.996
Adam	0.994	0.756	0.815	0.087	0.897	0.945
RmsProp	0.421	0.845	0.905	0.393	0.891	0.930
AdaDelta	***0.076***	***0.929***	***0.976***	0.005	***0.988***	***0.997***

The classification architecture was performed with SGD, AdaDelta, RMSProp, and Adamstochastic optimization techniques and results were obtained by using Resnet-50 and ReliefF-Resnet50 ensemble, respectively. Classification performances with optimization techniques were shown in Figure 4, Figure 5 respectively.

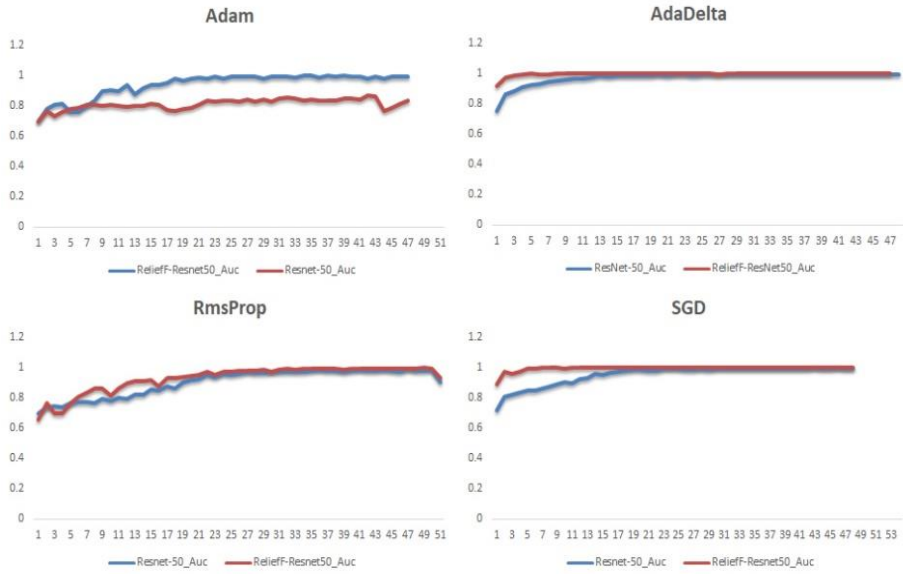

Figure 4. Auc progress for different stochastic optimization techniques.

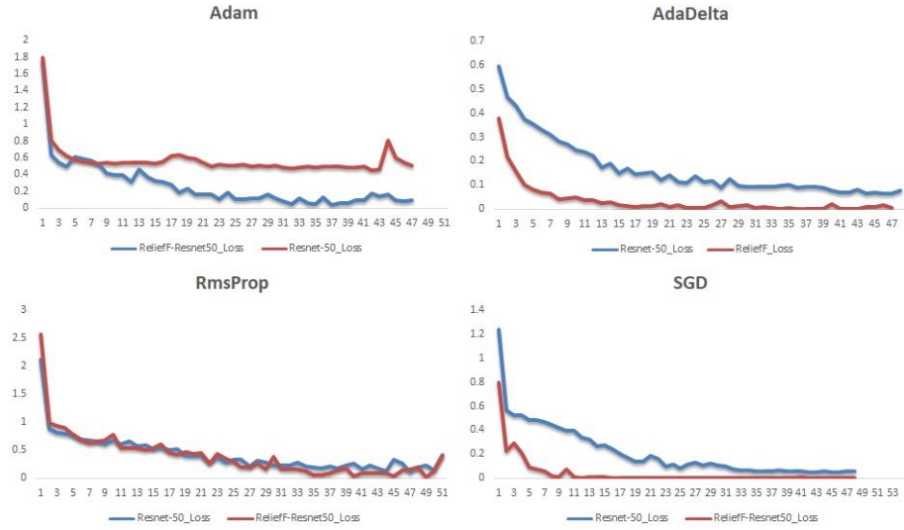

Figure 5. Loss progress for different stochastic optimization techniques.

When the differences in Acc performance between Resnet50 and ReliefF-Resnet50 were examined, the difference was 0.076 for SGD, 0.141 for Adam, 0.046 for RmsProp, and 0.059 for Adadelta. The use of ReliefF has resulted in improvement for all optimization techniques. These results further proves that although the proposed Resnet-50 model is effective, its effectiveness increases even more when used with feature selection.

CONCLUSIONS

Due to the advantages of DL, such as low risk of any data loss in layer additions, weight sharing, and reduced down-sampling size, it has been widely used in research projects. In contrast, the optimization problem is one of the most critical challenges in DL, such as Resnet-50. Finding optimal weight values that will minimize loss function calculation is a challenge to select optimal stochastic optimization techniques. Incorrect selection of the algorithm can lead to being stuck at the local minimum and lack the ability to generalize. On the other hand, a feature selection method may be needed for issues such as identifying sensitive features in medical images and reducing feature dimension. Therefore in this work, we integrated the ReliefF algorithm scheme into the classifier to reduce feature sizes for feature selection of chest x-Ray images, which improved classification performance and speed. In addition to the studies in the literature using the stochastic optimization techniques, we tested which technique best suited to the scheme we proposed using Adam, RmsProp, AdaDelta and SGD methods. Experiments using the ReliefF-Resnet50 also show

that ReliefF feature selection method can effectively improve classification accuracy and ease of integration in classification for X-Ray images. However, it has been revealed that the AdaDelta method is the best optimization technique for chest X-Ray images. However, SGD had the best improvement with the ReliefF-Resnet50 ensemble.

Acknowledgements

This work was supported by Scientific Research Projects Coordination Unit of Mersin University with the project number of 2020-1- AP2-4093.

REFERENCES

Centers for Disease Control and Prevention, (2021). Pneumonia an infection of the Lungs. CDCP. [Online] Available: https://www.cdc.gov/fungal/diseases /pneumocystis-pneumonia/ (January 19, 2021).

Demir, F. (2021). DeepCoroNet: A deep LSTM approach for automated detection of COVID-19 cases from chest X-ray images. Applied Soft Computing, 103, 107160.

Gupta, A., Gupta, S., & Katarya, R. (2021). InstaCovNet-19: A deep learning classification model for the detection of COVID-19 patients using Chest X-ray. Applied Soft Computing, 99, 106859.

Hinton, G., Srivastava, N., & Swersky, K. (2012). Neural networks for machine learning lecture 6a overview of mini-batch gradient descent. Cited on, 14(8).

Jaiswal, A. K., Tiwari, P., Kumar, S., Gupta, D., Khanna, A., & Rodrigues, J. J. (2019). Identifying pneumonia in chest X-rays: A deep learning approach. Measurement, 145, 511-518.

Jia, J., Yang, N., Zhang, C., Yue, A., Yang, J., & Zhu, D. (2013). Object-oriented feature selection of high spatial resolution images using an improved Relief algorithm. Mathematical and Computer Modelling, 58(3-4), 619-626.

Ketkar, N. (2017). Stochastic gradient descent. In Deep learning with Python (pp. 113-132). Apress, Berkeley, CA.

Kingma, D. P., & Ba, J. (2014). Adam: A method for stochastic optimization. arXiv preprint arXiv:1412.6980.

Koutsoukas, A., Monaghan, K. J., Li, X., & Huan, J. (2017). Deep-learning: investigating deep neural networks hyper-parameters and comparison of performance to shallow methods for modeling bioactivity data. Journal of cheminformatics, 9(1), 1-13.

Li, Z., Yang, W., Peng, S., & Liu, F. (2020). A survey of convolutional neural networks: analysis, applications, and prospects. arXiv preprint arXiv:2004.02806.

Ma, B., Li, X., Xia, Y., & Zhang, Y. (2020). Autonomous deep learning: A genetic DCNN designer for image classification. Neurocomputing, 379, 152-161.

Maruyama, T., Hayashi, N., Sato, Y., Hyuga, S., Wakayama, Y., Watanabe, H., ... & Ogura, T. (2018). Comparison of medical image classification accuracy among three machine learning methods. Journal of X-ray Science and Technology, 26(6), 885-893.

Montalbo, F. J. P. (2021). Diagnosing Covid-19 chest x-rays with a lightweight truncated DenseNet with partial layer freezing and feature fusion. Biomedical Signal Processing and Control, 102583.

Nayak, S. R., Nayak, D. R., Sinha, U., Arora, V., & Pachori, R. B. (2021). Application of deep learning techniques for detection of COVID-19 cases using chest X-ray images: A comprehensive study. Biomedical Signal Processing and Control, 64, 102365.

Rajpal, S., Lakhyani, N., Singh, A. K., Kohli, R., & Kumar, N. (2021). Using handpicked features in conjunction with ResNet-50 for improved detection of COVID-19 from chest X-ray images. Chaos, Solitons & Fractals, 145, 110749.

Selvaraju, R. R., Cogswell, M., Das, A., Vedantam, R., Parikh, D., & Batra, D. (2017). Grad-cam: Visual explanations from deep networks via gradient-based localization. In Proceedings of the IEEE international conference on computer vision (pp. 618-626).

Stephen, O., Sain, M., Maduh, U. J., & Jeong, D. U. (2019). An efficient deep learning approach to pneumonia classification in healthcare. Journal of healthcare engineering, 2019.

Tuncer, T., Dogan, S., & Ozyurt, F. (2020). An automated Residual Exemplar Local Binary Pattern and iterative ReliefF based COVID-19 detection method using chest X-ray image. Chemometrics and Intelligent Laboratory Systems, 203, 104054.

Urbanowicz, R. J., Meeker, M., La Cava, W., Olson, R. S., & Moore, J. H. (2018). Relief-based feature selection: Introduction and review. Journal of biomedical informatics, 85, 189-203.

World Health Organization, (2001), Standardization of interpretation of chest radiographs for the diagnosis of pneumonia in children. [Online] Available: https://apps.who.int/iris/handle/10665/66956 (December 17, 2020)

Xu, Q., Zhang, M., Gu, Z., & Pan, G. (2019). Overfitting remedy by sparsifying regularization on fully-connected layers of CNNs. Neurocomputing, 328, 69-74.

Zeiler, M. D. (2012). Adadelta: an adaptive learning rate method. arXiv preprint arXiv:1212.5701.

Zhao, X., Liu, L., Qi, S., Teng, Y., Li, J., & Qian, W. (2018). Agile convolutional neural network for pulmonary nodule classification using CT images. International journal of computer assisted radiology and surgery, 13(4), 585-595.

Zhou, X. (2015). Feature selection for image classification based on a new ranking criterion. Journal of Computer and Communications, 3, 74.

CHAPTER 3

INVESTIGATION OF THE EFFECTS OF PCA, PLS, AND LDA METHODS ON COVID-19 DIAGNOSIS USING ADABOOST-RF CLASSIFIER

Assist. Prof. Dr. Cüneyt YÜCELBAŞ [1]

Assist. Prof. Dr. Şule YÜCELBAŞ [2]

Gizemnur EROL[3]

Assist. Prof. Dr. Betül UZBAŞ [4]

[1] Hakkari University, Electrical and Electronics Engineering Department, Hakkari, Turkey. E-mail: cuneytyucelbas@hakkari.edu.tr ORCID ID: 0000-0002-4005-6557
[2] Hakkari University, Electrical and Electronics Engineering Department, Hakkari, Turkey. E-mail: suleyucelbas@hakkari.edu.tr ORCID ID: 0000-0002-6758-8502
[3] Konya Technical University, Computer Engineering Department, Konya, Turkey. E-mail: gizemnurerol0@gmail.com ORCID ID: 0000-0001-9347-9775
[4] Konya Technical University, Computer Engineering Department, Konya, Turkey. E-mail: buzbas@ktun.edu.tr ORCID ID: 0000-0002-0255-5988

INTRODUCTION

Coronavirus is a type of virus, was first seen in Wuhan, China, in early December 2019. This virus is an infectious virus that causes respiratory infection and can be passed from person to person. The World Health Organization (WHO) uses the term COVID-19 to describe the disease caused by the Coronavirus. This organization declared the COVID-19 disease as a pandemic on March 11, 2020. The clearest symptoms of COVID-19 are fever, cough, shortness of breath, and breathing difficulties. In more severe cases, an infection can cause pneumonia, acute respiratory failure, kidney failure, and even death (Lalmuanawma, Hussain, & Chhakchhuak, 2020; Mahase, 2020). Experts use many sources to detect COVID-19 in patients. The first of these are the symptoms of this disease in people. The second is the Polymerase Chain Reaction (PCR) antigen test, which is performed by taking a swab sample from the nose and throat. If the PCR test of the person applying to the hospital is positive, it means that the virus is active in that person. Third, antibody-antigen testing is utilized. In order to perform this test, blood samples are taken from people. As a last method, the diagnosis of COVID-19 can also be made by lung tomography. All these diagnostic resources guide the initiation of the treatment protocol by the experts (Guo et al., 2020; Li et al., 2020; Zou et al., 2020). In addition, due to the fact that the disease has become pandemic, there has been a shortage of personnel per person in many hospitals and health units. As a result of this situation, the importance of artificial intelligence (AI) algorithms that can act as experts with various inputs and teachings has increased.

COVID-19 disease can also be diagnosed by AI-trained systems, thanks to both blood samples and tomography outputs. These systems can support experts in the decision phase of the diagnosis of COVID-19, as in other diseases. In addition to this situation, the same systems allow patients to make pre-screening with their existing biochemistry tests (Ai et al., 2020; Naudé, 2020; Shiraishi, Li, Appelbaum, & Doi, 2011).

In order to overcome the COVID-19 pandemic with the least damage and in a controlled manner, it has been observed that machine learning algorithms are actively used in a wide range in this process. In the first stage, AI-based systems were used to quickly and automatically determine the body temperature of people in the entrance and exit areas of crowded places such as airports, train stations, shopping malls (Chun, 2020). Another purpose of using these systems in the process was to detect and control the social distance between people as a result of the processing of images taken from cameras (Rivas, 2020). Since the beginning of the COVID-19 pandemic in the literature, many studies have been conducted for the purposes of diagnosis, treatment, monitoring, prediction, and prevention of its spread(Hu, Ge, Jin, & Xiong, 2020; Jin et al., 2020; Lalmuanawma et al., 2020; Naudé, 2020; Salman, Abu-Naser, Alajrami, Abu-Nasser, & Alashqar, 2020; Vaishya, Javaid, Khan, & Haleem, 2020).In the study conducted by Naudé, the contribution of AI systems to the COVID-19 pandemic was investigated (Naudé, 2020). In the study, it was emphasized that the contribution of these systems is generally in areas such as early warning, diagnosis, monitoring, data editing, and treatment (Naudé,

2020).In another study(Jin et al., 2020), researchers have tried to detect COVID-19 through chest computer tomography (chest CT) images using an AI system. In (Lalmuanawma et al., 2020; Vaishya et al., 2020), similar to other studies, the AI applications during the pandemic process were investigated. In these studies (Lalmuanawma et al., 2020; Vaishya et al., 2020), the importance of real-time AI systems in preventing the spread of the disease has been emphasized. In another study in this area, researchers have tried to predict through AI when the COVID-19 disease in China could end (Hu et al., 2020).In (Salman et al., 2020), a deep learning model was used to diagnose the disease using X-ray images. There are also studies in which size reduction methods are applied after extracting the necessary features from X-ray images of COVID-19 patients (Ahishali et al., 2020; Albadr et al., 2020; Doanvo et al., 2020; Khuzani, Heidari, & Shariati, 2020; Rasheed, Hameed, Djeddi, Jamil, & Al-Turjman, 2021; Sharma & Dyreson, 2020; Sonbhadra, Agarwal, & Nagabhushan, 2020; Wan, Wang, Peter, Xu, & Zhang, 2016; Yamac et al., 2020). It has been observed that principal component analysis (PCA) is preferred as a dimension reduction method in almost all of these studies (Ahishali et al., 2020; Albadr et al., 2020; Doanvo et al., 2020; Khuzani et al., 2020; Rasheed et al., 2021; Sonbhadra et al., 2020; Wan et al., 2016; Yamac et al., 2020). When the diagnostic studies in the literature were examined, it was seen that the common purpose of most of them was to detect the disease in the shortest time with the highest accuracy.

In this study, the effects of PCA, Linear Discriminant Analysis (LDA), and Partial Least Squares (PLS) dimension reduction methods in the diagnosis of COVID-19 using blood values of individuals were analyzed. For this purpose, 13-parameter blood analysis results obtained from 279 people, 177 of whom were positive for PCR test and 102 of whom were negative, were used as data (Brinati et al., 2020). Since there are deficiencies in the data, this problem was solved by using the K-Nearest Neighbor (KNN) algorithm and the raw data set was obtained. Then, each dimension reduction method mentioned above was applied to this data set for dimensions between 2 and 12. Raw data sets and data matrices created using PCA, LDA, PLS methods were presented to Naive Bayes, SMO-SVM, J48, decision trees, and Adaboost-Random Forest (Adaboost-RF) classifiers. Since the best performance results were achieved with Adaboost-RF in all data, the study was continued with this classifier. Among the coefficients of each method, the highest classification accuracy result was reached with the data matrix reduced to 10 dimensions. In order to achieve the best average result, the Adaboost-RF classifier was applied to the data matrices and raw data set obtained by changing its '*seed*' training parameter between 1 and 25. Then, the statistical success criteria reached for each '*seed*' value were averaged. According to the results obtained; it has been proven that the PCA method performs better than both the raw data set and the others. Figure 1 shows the general flow processes for the study.

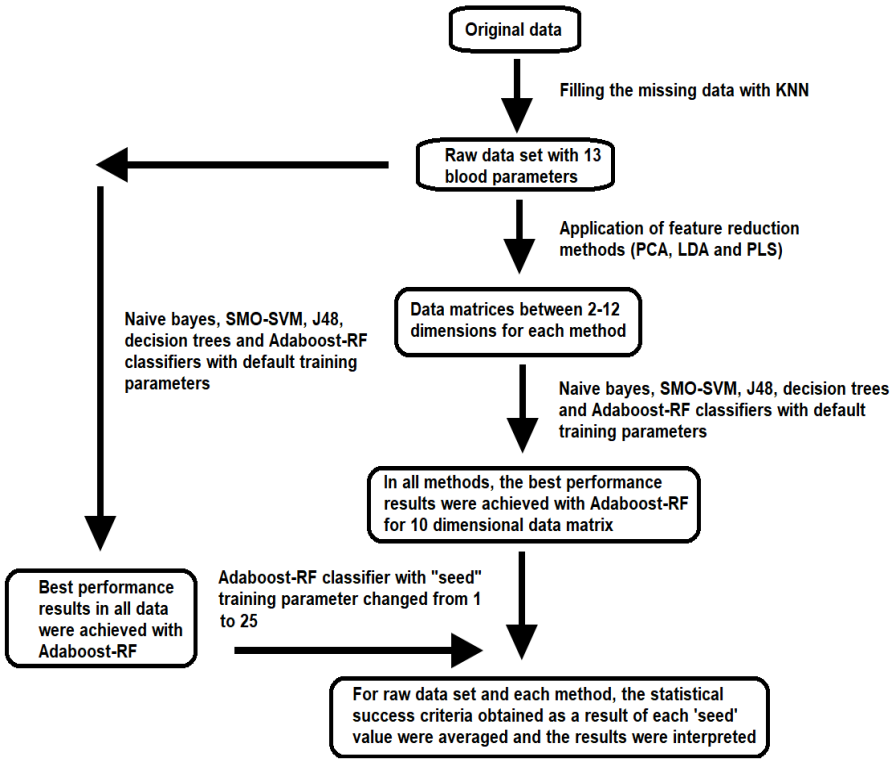

Figure 1. General flow diagram of the study.

Thanks to this study, it was aimed to reduce the existing data to less size in order to reduce the system working density. In addition, it has been tried to reach much higher success rates with reduced data than existing data. Unlike studies using the same data in the literature, gender and age factors were eliminated from the data used in the application. For this reason, only the effect of dimension reduction methods on blood parameters could be studied in detail. In addition, the effect of size reduction methods on one-dimensional data in the diagnosis of COVID-19 was also noted. The situations mentioned above reveal the importance of the study carried out.

1. MATERIALS AND METHODS

In this study, records of 279 patients (who applied to San Raffaele Hospital between February and March 2020 in Milan, Italy, and whose blood samples were taken) were used as the data set (Brinati et al., 2020). In the specified data set, there are 13 blood parameters belonging to patients with PCR test results (177 positive and 102 negative). The features and the units in the data set used for the study are shown in Table 1.

Table 1. Features and measurement units of the data set (Brinati et al., 2020)

Attribute	**Unit**
WBC	$x10^9$ cells/L
Neutrophils	$x10^9$ cells/L
Lymphocytes	$x10^9$ cells/L
Monocytes	$x10^9$ cells/L
Eosinophils	$x10^9$ cells/L
Basophils	$x10^9$ cells/L
Platelets	$x10^9$ cells/L
CRP	mg/L
AST	U/L
ALT	U/L
ALP	U/L
GGT	U/L
LDH	U/L

Since there are missing data in the data set(Brinati et al., 2020) used in the study, this problem was solved first by using the KNN method. KNN, which is a classification algorithm, is also used to complete missing parts in any data set (Cabitza et al., 2021; Jadhav, Pramod, & Ramanathan, 2019). The missing data wanted to be filled in this study were completed by taking the average of the nearest 5 neighbors that do not contain missing values.

In order to obtain data matrices with new dimensions, 3 different dimension reduction methods were applied to the completed data: PCA, classical LDA, and PLS. PCA, the first of these methods, is an effective statistical tool that aims to reduce the dimension of the data by recycling features that may affect the classification performance at a minimum or negative level. PCA aims to detect the targets at a higher success rate thanks to the transformation on data (Hotelling, 1933; Yıldız, Çamurcu, & Doğan, 2010). Classical LDA is a multivariate statistical method developed to ensure that data with a known number of features are assigned to their real classes with minimum error (Fisher, 1936). However, it is known that the LDA method cannot find effective solutions against outlier data, and new LDA methods developed against this situation have been brought to the literature (Alkan, Atakan, & Alkan, 2018). Finally, large numbers of linearly connected samples can be reduced with PLS to a smaller number of new dimensions that do not require a linear connection between them (Bulut & Alın, 2009).

All the data prepared were separated as training and testing using the 10-fold cross-validation method before being given to the classifiers. Then, Naive Bayes, SMO-SVM, J48, decision trees, and Adaboost-RF classifiers were used to classify data matrices and raw data sets. Since the best performance results were achieved with Adaboost-RF in all data, the study continued with this classifier. After changing the '*seed*' training parameter of the Adaboost-RF classifier between 1 and 25, it was tried for all data respectively. The general purpose of boosting algorithms is to combine a large number of underpowered and low-precision classifiers to obtain a single, more efficient, and sensitive classifier (Leshem & Ritov, 2007). Therefore, it is not surprising that the Adaboost-RF algorithm has better performance outputs. Finally, the classes were determined as "1" for those with COVID-19 and "0" for those that do not. Kappa coefficient, Precision, MCC, ROC area and accuracy (ACC) criteria were used for statistical performance analysis (Yücelbaş et al., 2017).

2. EXPERIMENTAL RESULTS

In this study, PCA, LDA, and PLS methods were applied to redimension blood parameters of the patients which were used for diagnosing COVID-19 and to separate with a high accuracy rate. By applying these methods to raw data, coefficients from 2 to 12 were obtained for each. These coefficients were presented one by one for each method to the Adaboost-RF classifier, which was decided as a result of various evaluations. As a result, it was seen that the highest performance outputs in all methods were achieved with 10-coefficient

data matrices. Then, it was tested for all 10-coefficient data matrices by changing '*seed*' parameter belonging to the Adaboost-RF classifier in the range of 1-25 and average results were obtained. Likewise, for the raw dataset too, classification rates were registered by changing '*seed*' value on the same range, and the mean of these rates were taken. Table 2 shows the 10-coefficient data matrices belonging to all methods and mean performance of outcomes that were obtained with raw dataset.

Table 2. The 10-coefficient data matrices belonging to the all methods and mean performance of outcomes obtained as a result of classification of the raw dataset with Adaboost-RF (TNI: total number of instances, CCI: correctly classified of instances)

Dimensionality reduction methods	**PCA**	**LDA**	**PLS**	**Raw data set**
TNI	279			
~ CCI	224	167	220	220
Kappa	0.554744	0.050796	0.524888	0.518984
Precision	0.80396	0.5638	0.78492	0.78564
MCC	0.56596	0.05508	0.53064	0.52844
ROC Area	0.8288	0.5384	0.82508	0.80708
ACC (%)	80.3824	60.0236	78.7896	78.748

When Table 2 is analyzed, approximately 224 of 279 data were accurately estimated thanks to the PCA method. As a consequence of classification with Adaboost-RF of the data matrix obtained by applying PCA, ACC rate and Kappa coefficient were obtained as 80.38% and 0.5547, respectively. When the PCA method was applied,

it was reached higher accuracy rates as against the other methods. Additionally, it was observed that statistical performance results obtained were nearly even by using the raw dataset and the data matrices obtained by applying PLS. According to Table 2, it was observed that data that were redimensioned by applying LDA method was not sufficiently successful in the field of classification as against the other data. Figure 2 shows the change in the classification accuracy rates that were separately obtained with all data for each changing '*seed'* value of Adaboost-RF classifier in the range of 1-25.

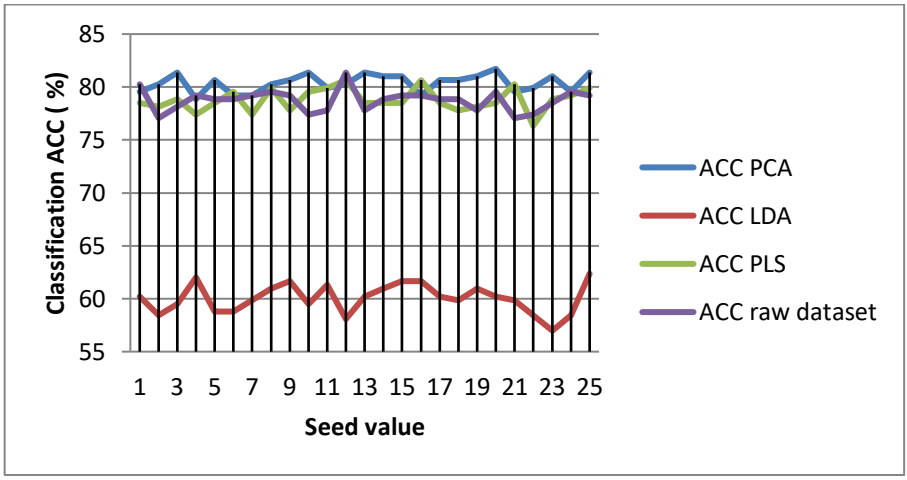

Figure 2. The change in the classification accuracy rates that were separately obtained with the all data for each '*seed*' value of Adaboost-RF classifier

When the graph in Figure 2 was analyzed, the best classification rate was obtained as 81.72% for 20 '*seed'* value in PCA method. In addition, it was seen that better performance results were achieved at 12 '*seed'* value for the raw data set and 16 for the PLS method.

DISCUSSION AND CONCLUSION

Expert systems using artificial intelligence and machine learning algorithms are actively used in many areas such as the defense industry, smart home, security systems, and health sector. In addition, these systems are generally used for diagnostic purposes in the health sector. Today, it is seen that AI systems are used in order to diagnose COVID-19 disease in a faster and more reliable way which is the first agenda item and the problem of the whole world. In this study, for the same purpose, the effect of PCA, LDA, and PLS size reduction methods on the diagnosis of COVID-19 was analyzed through the blood values of individuals (Brinati et al., 2020). Data matrices created by using PCA, LDA and PLS methods with the raw data set obtained as a result of pre-processing were presented to Naive Bayes, SMO-SVM, J48, decision trees, and Adaboost-RF classifiers. As the performance outputs of Adaboost-RF, one of these classifiers, are much better than the others, the analyzes in the study were carried out with this. According to the results obtained; it was seen that the PCA method performed more successfully than both the raw data set and the others. The average classification accuracy was obtained as 80.38% using the PCA method. PCA was followed by PLS, raw data set, and LDA with mean classification rates of 78.79%, 78.75% and 60.02%, respectively.

When the study is evaluated in general, it was seen that PCA, one of the size-reduction methods used in classifying the COVID-19 data, positively affected the system performance. The fact that the

performance outputs obtained as a result of the PCA method are better than those obtained with the raw data set shows that this method can be effective in one-dimensional data as well as image data. Using the PLS method, results were obtained close to the raw data set. It is thought that better results can be obtained if PLS can be applied to clearer data. In addition, LDA has been the most unsuccessful method in diagnosing COVID-19. This situation showed that the LDA method should be developed as the researchers recommend in the literature. As a result, it is thought that PCA and PLS methods can produce more effective results on data sets with minimal missing data and a large number of subjects. In future studies, it is estimated that COVID-19 detection will be more successful as a result of presenting the blood values and lung images of the same person to artificial intelligence systems at the same time.

REFERENCES

Ahishali, M., Degerli, A., Yamac, M., Kiranyaz, S., Chowdhury, M. E., Hameed, K., et al. (2020). Advance warning methodologies for covid-19 using chest x-ray images. *arXiv e-prints*, arXiv: 2006.05332.

Ai, T., Yang, Z., Hou, H., Zhan, C., Chen, C., Lv, W., et al. (2020). Correlation of chest CT and RT-PCR testing for coronavirus disease 2019 (COVID-19) in China: a report of 1014 cases. *Radiology, 296*(2), E32-E40.

Albadr, M. A. A., Tiun, S., Ayob, M., Al-Dhief, F. T., Omar, K., & Hamzah, F. A. (2020). Optimised genetic algorithm-extreme learning machine approach for automatic COVID-19 detection. *PloS one, 15*(12), e0242899.

Alkan, B., Atakan, C., & Alkan, N. (2018). Dayanikli lineer diskriminant analizi için yeni bir yaklaşim. *Erciyes Üniversitesi Fen Bilimleri Enstitüsü Fen Bilimleri Dergisi, 34*(2), 12-19.

Brinati, D., Campagner, A., Ferrari, D., Locatelli, M., Banfi, G., & Cabitza, F. (2020). Detection of COVID-19 infection from routine blood exams with machine learning: a feasibility study. *Journal of medical systems, 44*(8), 1-12.

Bulut, E., & Alın, A. (2009). Kısmi En Küçük Kareler Regresyon Yöntemi Algoritmalarından Nipals Ve Pls-Kernel Algoritmalarının Karşılaştırılması Ve Bir Uygulama.*Dokuz Eylül Üniversitesi İktisadi İdari Bilimler Fakültesi Dergisi, 24*(2), 127-138.

Cabitza, F., Campagner, A., Ferrari, D., Di Resta, C., Ceriotti, D., Sabetta, E., et al. (2021). Development, evaluation, and validation of machine learning models for COVID-19 detection based on routine blood tests. *Clinical Chemistry and Laboratory Medicine (CCLM), 59*(2), 421-431.

Chun, A. (2020). In a time of coronavirus, Chinas investment in AI is paying off in a big way. *South China Morning Post, 18*.

Doanvo, A., Qian, X., Ramjee, D., Piontkivska, H., Desai, A., & Majumder, M. (2020). Machine learning maps research needs in covid-19 literature. *Patterns, 1*(9), 100123.

Fisher, R. A. (1936). The use of multiple measurements in taxonomic problems. *Annals of eugenics, 7*(2), 179-188.

Guo, L., Ren, L., Yang, S., Xiao, M., Chang, D., Yang, F., et al. (2020). Profiling early humoral response to diagnose novel coronavirus disease (COVID-19). *Clinical Infectious Diseases, 71*(15), 778-785.

Hotelling, H. (1933). Analysis of a complex of statistical variables into principal components. *Journal of educational psychology, 24*(6), 417.

Hu, Z., Ge, Q., Jin, L., & Xiong, M. (2020). Artificial intelligence forecasting of covid-19 in china. *arXiv preprint arXiv:2002.07112*.

Jadhav, A., Pramod, D., & Ramanathan, K. (2019). Comparison of performance of data imputation methods for numeric dataset. *Applied Artificial Intelligence, 33*(10), 913-933.

Jin, C., Chen, W., Cao, Y., Xu, Z., Tan, Z., Zhang, X., et al. (2020). Development and evaluation of an artificial intelligence system for COVID-19 diagnosis. *Nature communications, 11*(1), 1-14.

Khuzani, A. Z., Heidari, M., & Shariati, S. A. (2020). COVID-Classifier: An automated machine learning model to assist in the diagnosis of COVID-19 infection in chest x-ray images. *medRxiv*.

Lalmuanawma, S., Hussain, J., & Chhakchhuak, L. (2020). Applications of machine learning and artificial intelligence for Covid-19 (SARS-CoV-2) pandemic: A review. *Chaos, Solitons & Fractals*, 110059.

Leshem, G., & Ritov, Y. (2007). *Traffic flow prediction using adaboost algorithm with random forests as a weak learner.* Paper presented at the Proceedings of world academy of science, engineering and technology.

Li, Z., Yi, Y., Luo, X., Xiong, N., Liu, Y., Li, S., et al. (2020). Development and clinical application of a rapid IgM-IgG combined antibody test for SARS-CoV-2 infection diagnosis. *Journal of medical virology, 92*(9), 1518-1524.

Mahase, E. (2020). Coronavirus: covid-19 has killed more people than SARS and MERS combined, despite lower case fatality rate: British Medical Journal Publishing Group.

Naudé, W. (2020). Artificial Intelligence against COVID-19: An early review. *IZA – Institute of Labor Economics*.

Rasheed, J., Hameed, A. A., Djeddi, C., Jamil, A., & Al-Turjman, F. (2021). A machine learning-based framework for diagnosis of COVID-19 from chest X-ray images. *Interdisciplinary Sciences: Computational Life Sciences*, 1-15.

Rivas, A. (2020). Drones and artificial intelligence to enforce social isolation during COVID-19 outbreak. *Medium Towards Data Sci, 26*.

Salman, F. M., Abu-Naser, S. S., Alajrami, E., Abu-Nasser, B. S., & Alashqar, B. A. (2020). Covid-19 detection using artificial intelligence.

Sharma, V., & Dyreson, C. (2020). Covid-19 detection using residual attention network an artificial intelligence approach. *arXiv preprint arXiv:2006.16106*.

Shiraishi, J., Li, Q., Appelbaum, D., & Doi, K. (2011). *Computer-aided diagnosis and artificial intelligence in clinical imaging.* Paper presented at the Seminars in nuclear medicine.

Sonbhadra, S. K., Agarwal, S., & Nagabhushan, P. (2020). Target specific mining of COVID-19 scholarly articles using one-class approach. *Chaos, Solitons & Fractals, 140*, 110155.

Vaishya, R., Javaid, M., Khan, I. H., & Haleem, A. (2020). Artificial Intelligence (AI) applications for COVID-19 pandemic. *Diabetes & Metabolic Syndrome: Clinical Research & Reviews, 14*(4), 337-339.

Wan, X., Wang, D., Peter, W. T., Xu, G., & Zhang, Q. (2016). A critical study of different dimensionality reduction methods for gear crack degradation assessment under different operating conditions. *Measurement, 78*, 138-150.

Yamac, M., Ahishali, M., Degerli, A., Kiranyaz, S., Chowdhury, M. E., & Gabbouj, M. (2020). Convolutional sparse support estimator based covid-19 recognition from x-ray images. *arXiv preprint arXiv:2005.04014*.

Yıldız, K., Çamurcu, Y., & Doğan, B. (2010). Veri madenciliğinde temel bileşenler analizi ve Negatifsiz matris çarpanlarına ayırma tekniklerinin karşılaştırmalı analizi. *Akademik Bilişim, 10*, 248.

Yücelbaş, Ş., Yücelbaş, C., Tezel, G., Özşen, S., Küççüktürk, S., & Yosunkaya, Ş. (2017). Pre-determination of OSA degree using morphological features of the ECG signal. *Expert Systems with Applications, 81*, 79-87.

Zou, L., Ruan, F., Huang, M., Liang, L., Huang, H., Hong, Z., et al. (2020). SARS-CoV-2 viral load in upper respiratory specimens of infected patients. *New England Journal of Medicine, 382*(12), 1177-1179.

CHAPTER 4

THE INVESTIGATION OF THE IMPACT OF USING PURE VEGETABLE OIL IN DIESEL ENGINES ON ENGINE EFFICIENCY AND EMISSIONS

Dr. Edal ÇILĞIN [1]

[1] Dicle University, Vocational School of Technical Sciences, Diyarbakır, Turkey. E-mail: cilgin_erdal@hotmail.com.tr ORCID ID: 0000-0003-2365-734X

INTRODUCTION

The global energy demand is rising day by day as a result of countries' socioeconomic growth, and this demand is once again dependent on energy supply (Kumar and Chauhun, 2013). Developing countries generally have to purchase crude oil to meet these increasing energy needs. Therefore, most of their economies are spent on energy purchases (Oumer et al, 2018). Furthermore, air pollution, market competition, and fuel prices, and dwindling oil reserves have prompted all countries around the world to search out alternative, reliable, and renewable fuels to replace fossil-based fuels. (Gulum and Çakmak, 2015). Renewable fuels such as alcohol, vegetable oil, and biodiesel are seen as a viable option to meet the energy demands while also reducing emissions. (Imdadul et al, 2016). The use of vegetable oils is very old. They have been used since the invention of diesel engines.

These oils obtained from plants have some advantages over petroleum-based fuels. These advantages are they are sustainable, biodegradable, low aromatic, and sulfur content. (Demirbas, 2017). Plants absorb most of the CO_2 released during combustion during their growth. Therefore, the use of vegetable oils can reduce greenhouse gas emissions from the transportation sector. (Atabani et al, 2012). However, the use of vegetable oils, whether pure or transformed into biodiesel, has started to cause some drawbacks. Producers have largely devoted their agricultural land to oilseed planting to obtain these vegetable oils obtained from oil seeds. The filling of agricultural lands with oilseed crops negatively affected food prices. This heightened the

controversy over the use of edible food for fuel production, as well as the question of food versus fuel, and drew widespread condemnation around the world. The process economy was influenced by the selection of non-edible raw materials with low production costs and high productivity in order to promote biofuel production and compete with other available resources. As a result, research focused on inactive cooking oils because they were cheaper. In addition, these oils were not only cheap but did not threaten food safety (Garcia, 2019). Besides these listed positive properties, there were some downsides of waste cooking oil.

It took a lot of effort, especially for it to be cleaned, filtered and fueled. In addition, if the oil contains high amounts of free fatty acids, this can form soap during the transesterification process, thus reducing the biodiesel yield (Garcia, 2018). All these negativities continued the search for more suitable raw materials and determined microalgae as new raw materials. Microalgae are micro-organisms that consume CO_2 emission very effectively compared to plants that are terrestrial biodiesel sources. (Oliveire et al, 2020). They are viewed as a promising raw material for use in a variety of industries, including food, feed, and biofuels. (Morais et al, 2020). Compared to traditional crops, microalgae offer numerous advantages for biofuel production (Mata et al, .2010). Ability to survive in wastewater, brine, or seawater, high growth and efficiency, high lipid or carbohydrate content. Moreover, more than 50% of the biomass of many microalgae species contains lipids (Mata, et al, 2013). Biofuels obtained from microalgae-based

oils are more advantageous than fossil fuels because they are both locally produced and energy-independent and more environmentally friendly (Mata et al, 2012). The high lipid yield of some micro algae species is the key to being attractive as a biomass raw material for producing biofuels. The rapid growth rates and high lipid content of green algae (chlorophyta) and diatoms (Bacillariophyta) made them particularly attractive raw materials for biofuel production. Microalgae, glucose, acetate etc. It grows by consuming organic carbon sources or inorganic carbon sources such as CO_2 and provides lipid accumulation. This study has the potential to respond to the increasing global energy need and to contribute to the prevention of global warming, partially by converting excess carbon dioxide in the atmosphere into an efficient product through photosynthesis. In addition, the experimental use of the oil obtained from microalgae in diesel engines, which provides the advantage of removing pollutants such as nitrogen and phosphorus in nature, which do not pose a great danger on drinking water resources such as terrestrial energy plants during production, through wastewater treatment was investigated. For this purpose, firstly pure microalgae oil was mixed with 2% and 4% diesel fuel by volume and two different fuels named as PVO-2 and PVO-4 respectively were obtained. The test fuels obtained were examined in a test engine at an engine speed of 1500 rpm and under different load conditions.

İlkılıç and Öner (2003) stated in their study that the viscosity of oils obtained from plants should be reduced in order to be used in internal combustion diesel engines.

Bao and He (2002) tested a blend of rapeseed oil and diesel fuel as fuel in 2002.They reported that there was no need for any modifications to use this mixture fuel. In their work, Bao and He said that viscosity should be reduced in the use of vegetable oil.

Aydın and Keskin (2000) used a single cylinder diesel engine to measure blends of cotton oil methyl ester and diesel in various proportions (30/70, 50/50, and 70/30). According to the researchers, cotton oil methyl ester has similar torque values to diesel fuel in the engine at high engine speeds, similar power values to diesel fuel at high and low engine speeds, and higher actual fuel consumption than diesel fuel. According to their findings, cotton oil methyl ester / diesel fuel mixtures can be easily used as a diesel fuel substitute in diesel engines, and automobiles using these mixtures as alternative fuels can pass the exhaust emission test successfully.

In their reports, Oğuz and Öğüt (2001) reported that the high viscosity problem must be solved first before vegetable oils can be considered as a diesel fuel substitute. Furthermore, using different methods on pure vegetable oils, the high viscosity problem is attempted to be solved. Dilution, microemulsion, pyrolysis, supercritical, and re-esterification (transesterification) methods are the most common.

According to Baş et al. (1993), vegetable oils can be used as a fuel in traditional diesel engines with minor fuel system modifications. However, when vegetable oils are evaluated in terms of diesel engine fuel, the most important problem is that their viscosity is high and this causes blockages in fuel systems, deterioration of the combustion quality and carbon deposits in the combustion chamber, and in case of accelerating the research to eliminate the negative features of vegetable oils, an alternative renewable to petrol is It is stated in the researches that the energy source will be gained.

The effects of using vegetable oil as an alternative fuel in a single cylinder diesel engine on engine efficiency and exhaust emissions were examined by Yücesu et al. (2001). Crude sunflower oil, crude cottonseed oil, crude soybean oil, sunflower oil methyl esters extracted from them, cottonseed oil methyl esters, soybean oil methyl esters, poppy oil, rapeseed oil, and corn oil processed with No 2-D diesel fuel were all used in his research. as a source of energy as a result of the tests, the performance values of vegetable oils are lower than diesel fuel, the smoke darkness is higher in vegetable oils, they stated that NO_X emissions were higher than No 2-D diesel fuel. On the other hand, it was stated that the engine performance values of vegetable oil methyl ester-based fuels were better than crude oils and closer to diesel fuel performance values.

In a study by Demirsoy and Kındıroğlu (1997), they used different proportions of sunflower, soybean, and cotton oils with diesel oil as fuel in a single cylinder direct injection diesel engine. They claim that

when vegetable oil blends with diesel are compared to diesel, they have about the same power values and more specific fuel consumption at high revs, and that the specific fuel consumption increases as the oil ratio in the mixture increases.

Barsic and Humke (1982) used crude soybean oil as a fuel in a naturally aspirated, 6-cylinder, direct injection diesel engine with a 50 percent mixture of No.2-D diesel fuel to assess engine efficiency and emission characteristics. They compared it with the values of. 2-D diesel fuel and found that due to the higher density and viscosity of crude soybean oil compared to diesel oil, more soybean oil was transferred at full gas compared to diesel fuel, and in turn, the engine power increased, furthermore, the CO_2, HC and particulate matter emissions were. They noted that it was higher than its fuel, and its NO_x emissions were lower.

1. MATERIALS AND METHOD

A four-cylinder four stroke water-cooled direct injection diesel engine was used in the tests. An alternator is attached to the diesel engine. The alternator output enters the electricity supply control panel. Voltage and current values are controlled on the panel and controlled by heater switches with resistors. A digital timer was used to determine the fuel consumption times in the experiments. Instead of the fuel tank of the engine, another fuel tank is placed on the scale and connected to the fuel line by means of pipes. Features of the analyzer measuring exhaust gas emissions. It is given in Table 1. After the engine reached

its operating temperature, the receivers connected to the generator were gradually brought into the circuit, and electrical energy was drawn in three different locations. Diesel Engine Technical Specifications given in Table 2.

Table 1. Technical specifications of the gas analysis device.

Parameter	Measuring Range	Precision
HC	0–20,000 ppm	1 ppm
CO_2	0–21%	0.1%
CO	0–10.5%	0.001%
O_2	0–21.7%	0.01%
NOx	0–5000 ppm	1 ppm

Table 2. Diesel engine specifications.

Engine power	18 kW@1500 rev/min
Engine cooling system	Water-cooled
Intake system	Naturally aspirated
Engine model	4DW81-23D
Diameter Stroke	85×100 mm
Number of cylinders	4
Combustion system	Direct injection
Compression ratio	17:1

2. RESULTS AND DISCUSSION

2.1. Brake Specific Fuel Consumption (BSFC)

Specific fuel consumption is the value in grams of the fuel that the engine should consume per kWh of work in stable operation. The amount of power obtained is proportional to the fuel injected by mass in the basic fuel consumption diagram (Boyalı, 2008). When Figure 1 and 2 is examined, it is seen that PVO-2 has a specific fuel consumption of 0.4914% and PVO-4 has a higher specific fuel consumption of 2.9543 g/kWh compared to ULSD fuel. As the amount of pure oil in blended fuels increases, the increase in specific fuel consumption can be attributed to the decrease in thermal value (İlkılıç et al. 2015). Another point that stands out in the specific fuel consumption curve is that the minimum fuel consumption is obtained at the loads where the maximum engine power values are produced in all experimental fuels, and the specific fuel consumption increases in smaller loads other than this load, thus in smaller power generations. While Pulkrabek states that the increase in fuel consumption at low rotational speeds is due to higher heat loss due to longer cycle times (Pulkrabek, 2003). Stone, on the other hand, stated that the loading on the engine increases the turbulence in the cylinder, so the combustion and the engine power increase, and the increasing engine power decreases the specific fuel consumption (Stone, R.1989).

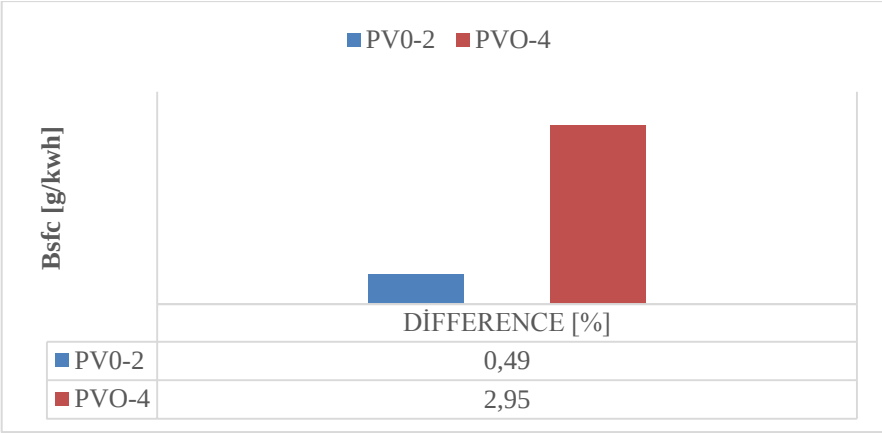

Figure 1. Specific fuel consumption differences in percentage of test fuels compared to ULSD fuel.

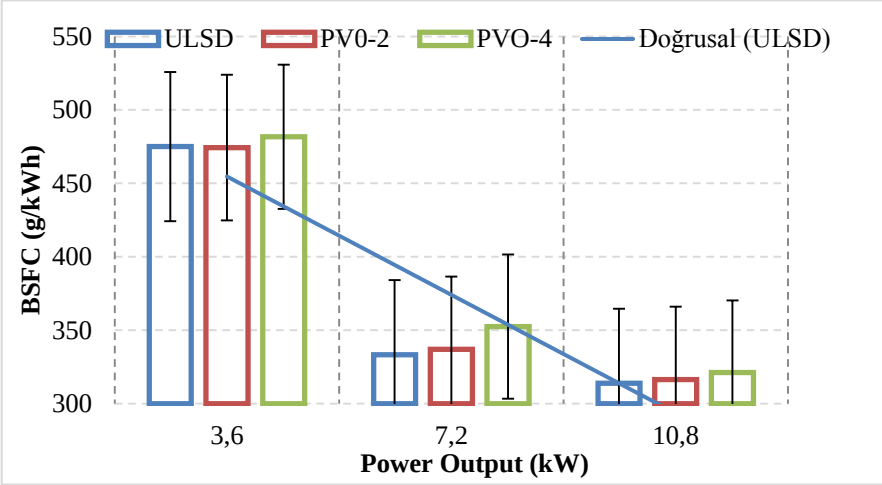

Figure 2. BSFC variation of the test fuels depending on the load.

2.2. Effective Yield (η_e)

The effective parameters of the engine, in which the mechanical resistances and the useful work used in intake and exhaust times are taken into account, are different from the indicated parameters (Keleş,

G. 2012). Mechanical losses are expressed as the loss of mechanical power per unit displacement that is expended to overcome many resistances in the motor. Effective parameters of the engine; average effective pressure, effective power, torque, mechanical efficiency, effective efficiency and specific fuel consumption. One of these effective parameters is the effective performance, which is defined as the ratio of work taken from the motor shaft to total energy given. Effective efficiency, also known as overall efficiency, is a critical feature since it is informative about the operation of the engine. When the effective efficiency change of ULSD fuel and pure oil-diesel blends was examined, the yields were obtained in Figure (3,4,) with PVO-2 to 22,185%, with PVO-4 fuel and 21,653% with ULSD fuel, with an average of 22,189%. It has been determined that the efficiency values show a decrease parallel to the pure oil ratio in mixed fuels. The probable reason was that vegetable oils had lower thermal values than diesel fuel (Scholl, K.W. 1993).

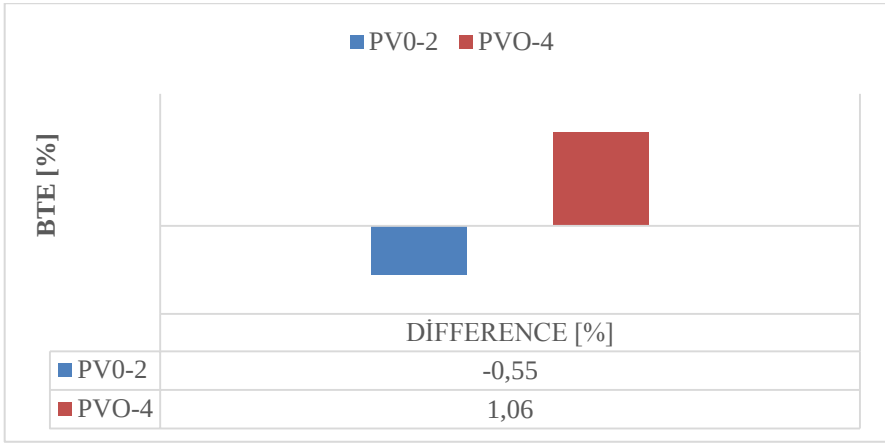

Figure 3. Percentage effective efficiency differences of test fuels compared to ULSD fuel.

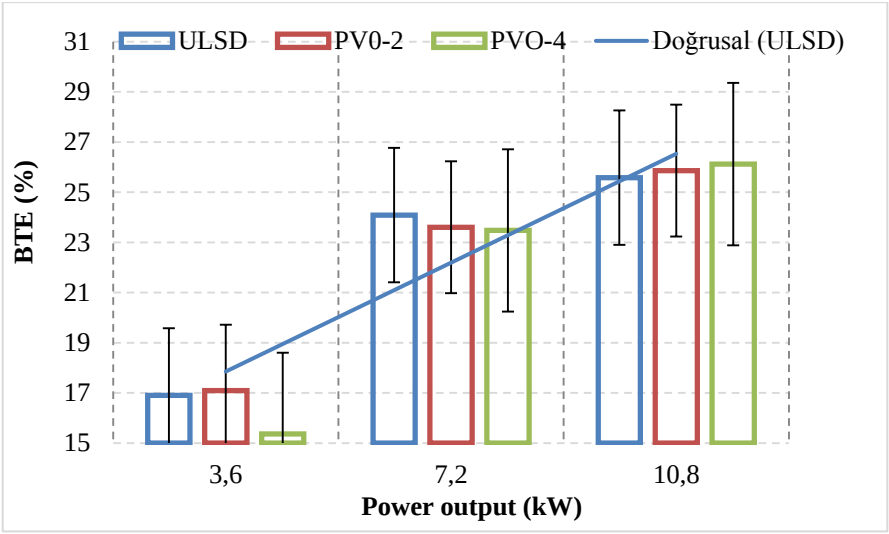

Figure 4. Efficiency changes of test fuels depending on the load.

2.3. Engine Emissions

Internal combustion engine exhaust emissions are a major source of air pollution. In reality, internal combustion gasoline and diesel engines are responsible for half of the emissions generated by the burning of fossil fuels. (Birsen, B. 2008). Carbon monoxide (CO), carbon dioxide (CO_2), hydrocarbon (HC), and nitrogen oxides (NO_x) are the most common exhaust emissions from internal combustion engines.

2.3.1. Carbon Monoxide (CO)

CO, which is formed when the carbon (C) in the fuel is not completely combusted, is a colorless, odorless and poisonous gas. CO is formed as a result of partial combustion of C-containing compounds. The

main reason for the presence of CO among exhaust emissions is due to insufficient oxygen or the inhomogeneity of some parts in the combustion chamber. Figure 5.6. As the engine load increased, the (CO) emission changed to (CO_2) emission as the cylinder temperature increased, resulting in low (CO) emissions for all test fuels. Indeed, as seen in Figure 7, 8, as the engine is loaded, the increase in CO_2 emission in all fuels can be claimed as a proof of this. When the experimental fuels were compared, an average reduction of 13.65% was observed in the CO emission values obtained by using PVO-2 and PVO-4 fuels compared to diesel fuel.

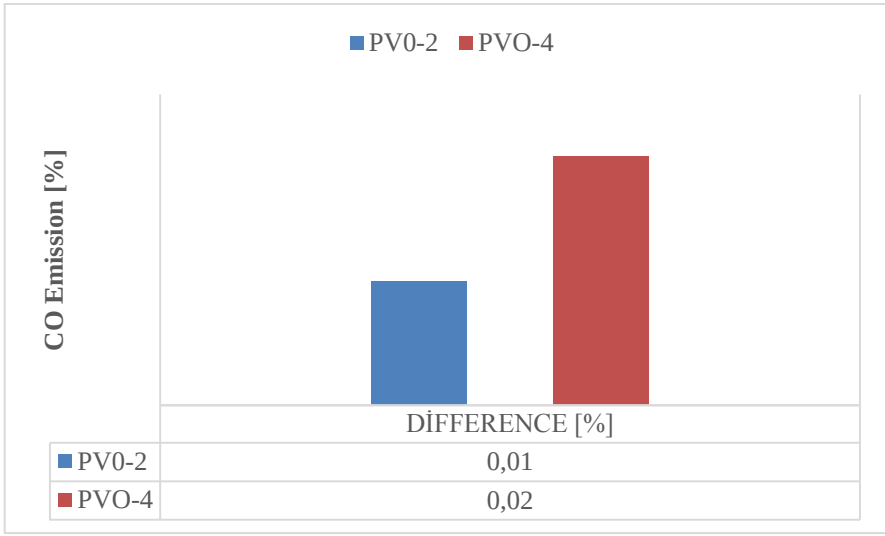

Figure 5. Percentage carbon monoxide differences of test fuels compared to ULSD fuel.

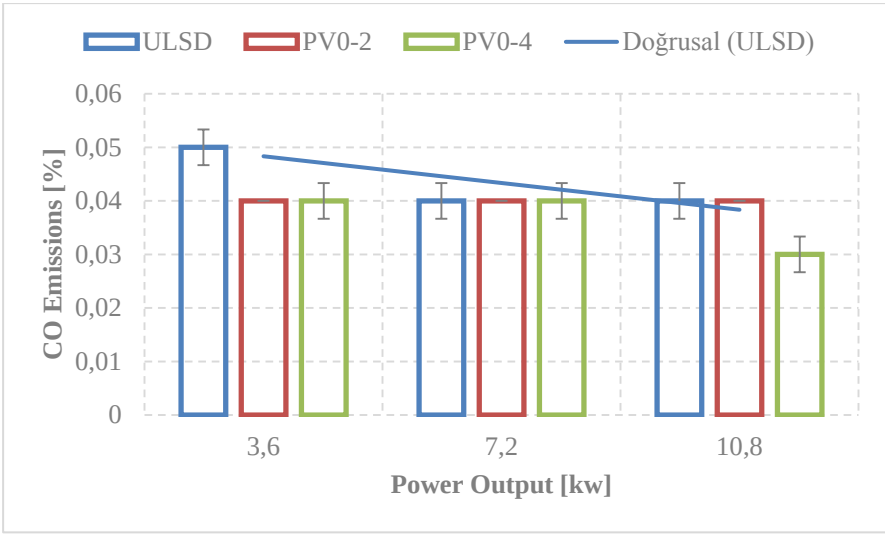

Figure 6. Carbon monoxide changes of test fuels depending on the load.

2.3.2. Carbon Dioxide (CO_2)

CO_2 emission in internal combustion engines is a colorless, odorless gas that emerges during combustion, directly harmless to human health. The carbon atom in the fuel combines with the oxygen in the air taken in the cylinders and forms CO_2 during its combustion. Although it is seen as the most harmless gas in vehicle emissions, when the limit values of CO_2 are exceeded, it causes ozone and greenhouse effect. With the increase of CO_2, the long-wavelength radiation from the sun is prevented from being reflected back into space, however, it causes the warming of the earth and therefore climate changes (Atmanli A, 2014). Figure 7,8 shows that the CO_2 emission produced by all test fuels increases in parallel with the increasing load. When the CO_2 values were examined, PVO-2 fuel produced 1.24% higher CO_2

than ULSD fuel and PVO-4 fuel produced 0.62% higher CO_2 than ULSD fuel.

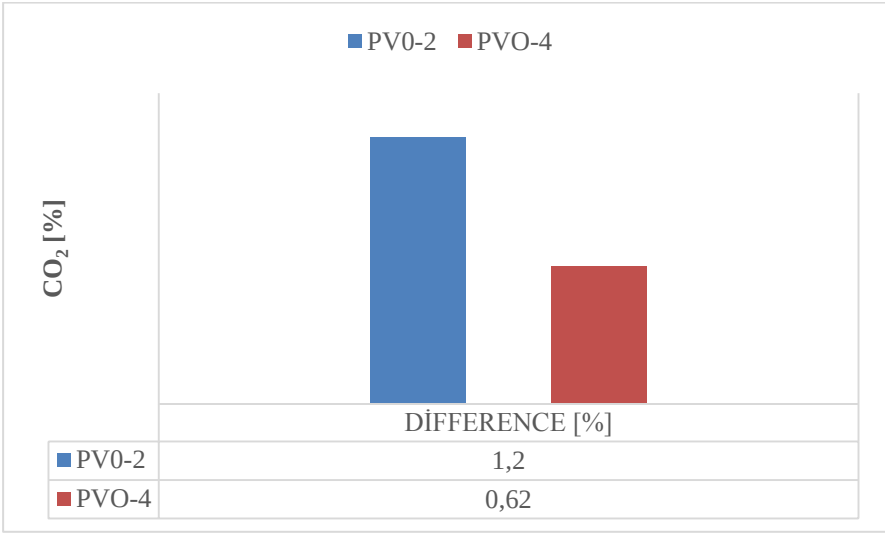

Figure 7. Percentage carbon dioxide differences of test fuels compared to ULSD fuel.

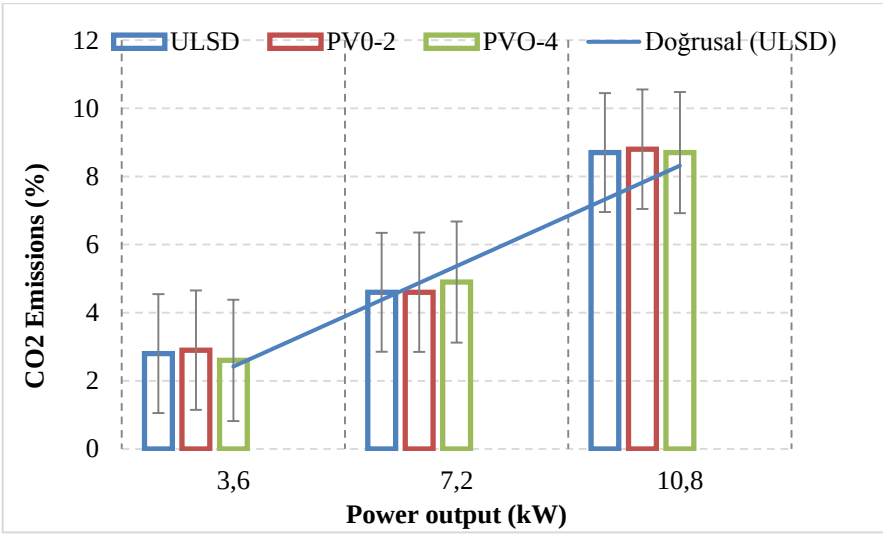

Figure 8. Test fuels load-dependent CO_2 emission change.

2.3.3. Hydrocarbon (HC)

Measuring the hydrocarbon (HC) in the exhaust gas at the end of the combustion in the cylinders means that the fuel does not burn partially or completely. The cause of HC emission formation is a function of temperature and oxygen (O_2) insufficiency, with incomplete combustion occurring as a result of too little fuel, too much air or too much fuel, too little air, in some areas in the cylinder, if the air / fuel mixture ratio is unstable. Oil cannot be completely combusted due to an increase in the fuel ratio, a reduction in the air ratio, and a lack of oxygen, resulting in the formation of HC. [26]. When the emission values of [HC] are examined in Figure 9,10, pure oil mixed fuels are PVO-2, PVO-4 respectively, from ULSD fuel. 1.87%, PVO-4 formed 3.12% lower HC. This decrease can be shown that the oxygen in the content of vegetable oils provides sufficient oxidation in the rich fuel-air mixture regions.

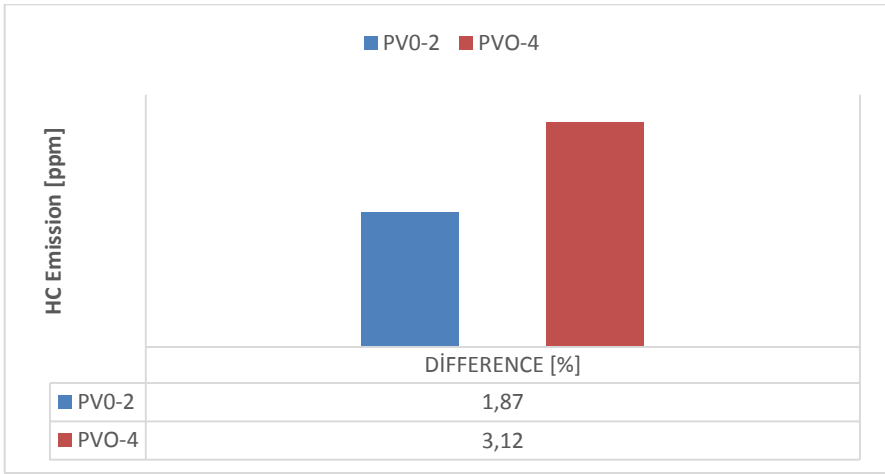

Figure 9. Percentage HC differences of test fuels compared to ULSD fuel.

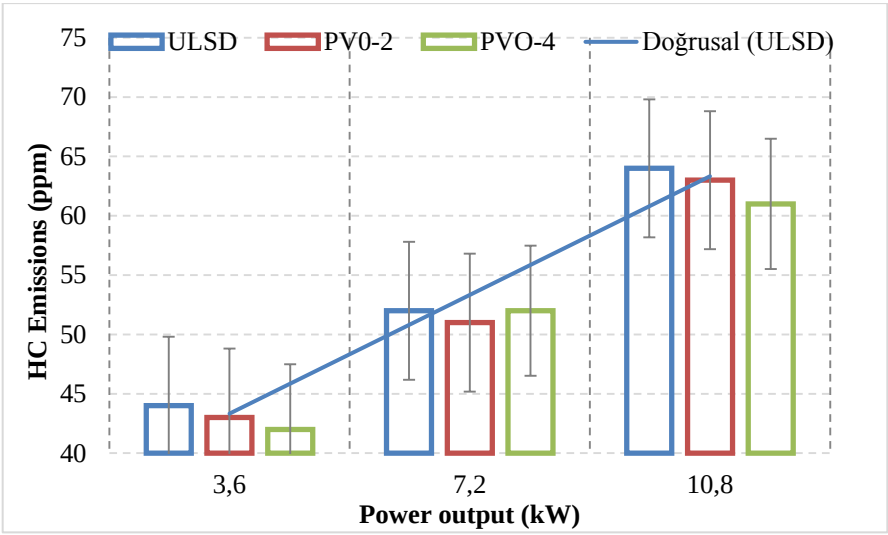

Figure 10. HC changes of test fuels depending on the load.

2.3.4. NOx Emission

This type of emission is expressed as NO_x, as nitrogen forms different oxides. Temperature, time and oxygen concentration are three important parameters that have an effect on NO_x formation (Borat, O. 1994). As the combustion improves, the NO_x emission will increase as the maximum combustion pressure and temperatures will increase. While NO_x emissions are maximized at theoretical Air / Fuel ratios, they decrease in case of moving away from the theoretical point. The explanation for the decrease in NO_x emissions in the case of depletion of the air/fuel ratio is slow combustion and a decrease in the overall combustion temperature and pressures, while the reason for the decrease in NO_x emissions in the case of enrichment of the air/fuel ratio is a lack of oxygen. [28]. In the Figure 11 and 12, when the NO_x values were examined, it was seen that the amount of pure oil in diesel

fuel increased volumetrically and the NO_X emission values increased (PVO-2: 0.39% increase, PVO-4: 2.81% increase). The explanation for the rise in NO_x emissions, which rises in lockstep with the amount of pure oil in diesel fuel material, is assumed to be that the amount of oxygen in the pure oil raises the temperature at the end of combustion, causing NO_x to form at these high temperatures. (Usta, N. 2005).

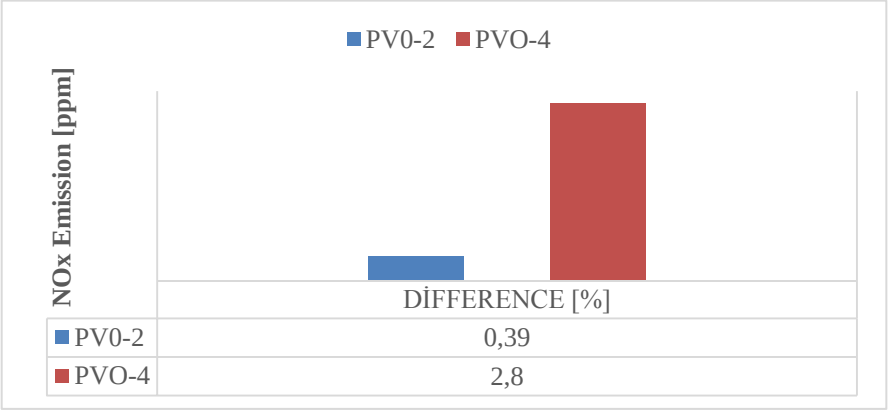

Figure 11. Percentage NO_x differences of test fuels compared to ULSD fuel.

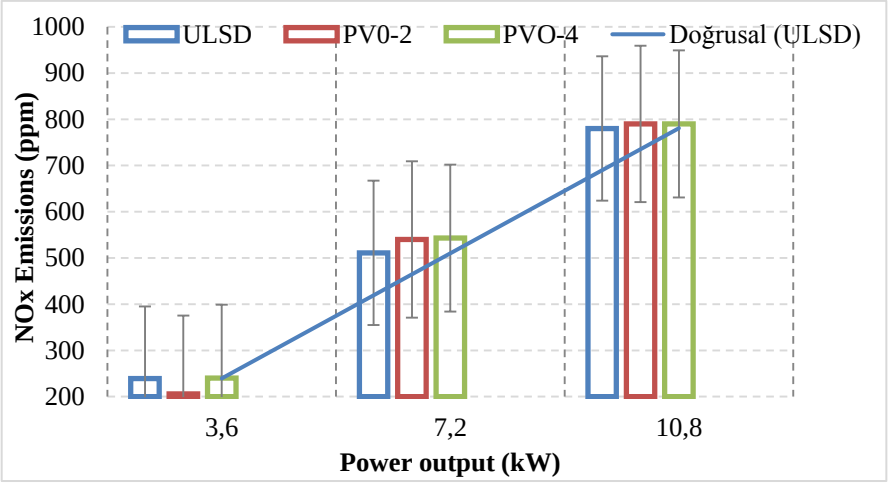

Figure 12. NO_x changes of test fuels depending on the load.

CONCLUSION

In this study, the pure microalgae oil obtained was tested by mixing it with diesel fuel in certain proportions in order to be used in diesel engines. The data obtained from the experiments are presented below:

- Both PVO-2 and PVO-4 fuels caused more fuel consumption than ULSD fuel, and as the amount of pure oil in the ULSD increased, the value of the oil increased in parallel.
- Both PVO-2 and PVO-4 fuels produced lower efficiency than ULSD fuel.
- Both PVO-2 and PVO-4 fuels produced lower CO emissions than ULSD fuel.
- CO_2 Conversions of PVO-2 and PVO-4 fuels are partially higher than ULSD fuel.
- PVO-2 and PVO-4 fuels produced more NOx emissions than ULSD fuel.

REFERENCES

Alibaş, A., Eyüboğlu, V. ve Kayık, S. (1993). Bitkisel yağların motor yakıtı olarak kullanılabilme olanakları. Mühendis ve Makine Dergisi, 34, 19-27.

Alkaya, B., Yıldırım, M. A., (2000). Taşıt Kaynaklı Kirleticilerin Azaltılma Yöntemleri. Ekoloji Çevre Dergisi, Ocak-Şubat-Mart 2000, 9(34):15-20, 2000.

Atabani, A.E. Silitonga,A.S. Badruddin,I.A. Mahlia, T.M.I. Masjuki, H.H. Mekhilef A, (2012). comprehensive review on biodiesel as an alternative energy resource and its characteristics Renew. Sustain. Energy Rev., 16 pp. 2070-2093.

Atmanli, A., Ileri, E., Yuksel, B, (2014). Experimental investigation of engine performance and exhaust emissions of a diesel engine fueled with diesel–n-butanol– vegetable oil blends. Energy Convers Manage, 81: 312-21.

Aydın, A. ve Keskin, A. (2000). Dizel motorlarda motorin, bitkisel yağlar ve alkol karışımlarının performans ve emisyona etkilerinin araştırılması. Yanma ve Hava Kirliliği Kontrolü V. Ulusal Sempozyumu, 19-21 Haziran, Elazığ, 149-158.

Barsic, N.J. ve Humke, A.L. (1982). Performance and emissions characteristics of a naturally aspirated diesel engine with vegetable oil fuels. Society of Automotiv Engineers, 810262, 1173-1187.

Birsen, B., (2008). Hidrojen yakıtının içten yanmalı motorlarda kullanılması, Yüksek Lisans Tezi, Erciyes Üniversitesi Fen Bilimleri Enstitüsü, Kayseri, 84s.

Borat, O., Balcı, M., Sürmen, A. (1994). Hava Kirlenmesi ve Kontrol Tekniği. Teknik Eğitim Vakfı Yayınları 3, Ankara, 1994.

Boyalı, A, (2008). İstanbul Teknik Üniversitesi Fen Bilimleri Enstitüsü'ne sunduğu "Hibrid Elektrikli Yol Taşıtlarının Modellenmesi ve Kontrolü".

Demirbas,A. (2017). Tomorrow's biofuels: goals and hopes Energy Sources Part A Recover. Util. Environ. Eff. 10.1080/15567036.2016.1252815

Demirsoy, M. ve Kındıroğlu, K. (1997). Diesel motorlarında alternatif yakıt olarak değişik yağların kullanılması. Otomotiv Teknolojisi Bilim Haftası'97, 26-30 Mayıs, Çukurova Üniversitesi Yayınları: Adana.

Ergeneman, M., Arslan, H., Mutlu, M, (1997). Motorlu Taşıtlardan kaynaklanan Kirleticiler kitabı, İstanbul.

García, J.F. Martín, M. López,C. Barrera, M. Torres García, Q.A. Zhang, P. Álvarez Mateos, (2019), Determination of the acidity of waste cooking oils by near infrared spectroscopy Processes, 7 pp. 1-7, 10.3390/pr7050304.

Gulum, M, Bilgin, A. Cakmak, A, (2015). Comparison of optimum reaction parameters of corn oil biodiesels produced by using sodium hydroxide (NaOH) and potassium hydroxide (KOH) J Faculty Eng Archit Gazi Univ, 30 (3), pp. 503-511.

He, Y. ve Bao, Y.D. (2002). Study on rapeseed oil as alternative fuel for a single-cylinder diesel engine. Renewable Energy, 28, 1447-1453.

Imdadul,H.K, et al(2016)..A comparative study of C4 and C5 alcohol treated diesel–biodiesel blends in terms of diesel engine performance and exhaust emission Fuel, 179, pp. 281-288.

İlkılıç, C., Çılğın, E., Aydın, H., (2015) Terebinth oil for biodiesel production and its diesel engine application Journal of the Energy Institute Volume 88, Issue 3, August 2015, Pages 292–303.

İlkılıç, C. ve Öner, C. (2003). Bir dizel motorunda ayçiçek yağı metil esteri ile motorin karışı kullanarak egzoz emisyonlarının incelenmesi. Fırat Üniversitesi Fen ve Mühendislik Bilimleri Dergisi, 15(4), 579- 588.

J.F. García-Martín, C.C. Barrios, F.J. Alés-Álvarez, A. Dominguez-Sáez, P. Alvarez-Mateos, (2018). Biodiesel production from waste cooking oil in an oscillatory flow reactor. Performance as a fuel on a TDI diesel engine Renew. Energy, 125, pp. 546-556, 10.1016/j.renene.2018.03.002.

J. Pereda Marín, F. Barriga Mateos, P. Álvarez Mateos (2003). Aprovechamiento de las oleinas residuales procedentes del proceso de refinado de los aceites

vegetales comestibles, para la fabricación de biodiesel Grasas y Aceites, 54, pp. 130-137.

Keleş.,G. (2012). Dizel Motorların Cng Ve Lpg Yakıtlarına Dönüşümünde Gerçek Çevrimin Teorik Ve Deneysel Çalışmalarla Optimizasyonu. İstanbul Teknik Üniversitesi Fen Bilimleri Enstitüsü. Yüksek Lisans Tezi.

Kumar,N,. Chauhan,S.R.(2013).Performance and emission characteristics of biodiesel from different origins: a review Renew Sustain Energy Rev, 21, pp. 633-658.

Martins A.A., Mata T.M., Oliveira O., Oliveira S., Mendes A.M., Caetano N.S. (2016). Sustainability evaluation of biodiesel from Arthrospira platensis and Chlorella vulgaris under mixotrophic conditions and salinity stress Chem. Eng. Trans. 49 10.3303/CET1649096.

Mata T.M., Martins A.A., Caetano N.S. Microalgae processing for biodiesel production Luque R., Melero J.A. (2012.). Advances in biodiesel production: Processes and technologies, Woodhead publishing series in energy, Woodhead Publishing, pp. 204-231, 10.1016/B978-0-85709-117-8.50009-5.

Mata T.M., Martins A.A., Caetano N.S(2010). Microalgae for biodiesel production and other applications: A review Renew Sustain Energy Rev, 14 (2010), pp. 217-232, 10.1016/j.rser.2009.07.020.

Mata T.M., Martins A.A., Sikdar S.K., Costa C.A.V., Caetano N.S (2013). Sustainability considerations about microalgae for biodiesel production Advanced biofuels and bioproducts, Springer New York, New York, NY, pp. 745-757.

Mrais Junior W.G., Gorgich M., Corrêa P.S., Martins A.A., Mata T.M., Caetano N.S . (2020). Microalgae for biotechnological applications: cultivation, harvesting and biomass processing Aquaculture, 528 (2020), 735562, 10.1016/j.aquaculture.2020.735562

Oliveira G.M., Caetano N., Mata T.M., Martins A.A. (2020). Biofixation of CO_2 emissions from natural gas combined cycle power plant Energy Rep, pp. 140-146, 10.1016/j.egyr.2019.08.032.

Oumer, A.N. Hasan, M.M. Baheta, A.T, Mamat, R A. Abdullah, A.A, (2018). Bio-based liquid fuels as a source of renewable energy: a review Renew Sustain Energy Rev, 88, pp. 82-98.

Pulkrabek, W.W. (2003). Engineering Fundamentals of the Internal Combustion Engine, Prentice Hall, New Jersey, 2003.

Sal, E., Hazar, H., Sap, S., Oner, M.C., Ilkılıc, C,. (2017). Exhaust Emission Analysis of Piston, Valve and Exhaust Pipe Chromium Carbide (Cr3C2) Coated LPG Engine. International Advanced Technologies Symposium (IATS'17), 19-22 October, Elazığ, Turkey.

Scholl, K.W., (1993). Sorenson S.C, Combustion of Soybean Oil Methyl Ester in a Direct Injection Diesel Engine, SAE Paper, No.930934

Stone, R., (1989). Motor Vehicle Fuel Economy, Macmillan Educational Ltd., Houndsmills, UK.

Usta,N., Öztürk,E ., Can,Ö., Conkur, ES., Nas,S., Con,AH., Can, AÇ ., Topcu.M., (2005) Energy Conversion. Biomass and bioenergy 28 (1), 77-86, 2005. 220.

Yücesu, H.S., Altın, R. ve Çetinkaya, S. (2001), Dizel motorlarında alternatif yakıt olarak bitkisel yağ kullanımının deneysel incelenmesi. Turkısh Journal of Engineering and Environmental Sciences, 25, 39-49.

CHAPTER 5

THE COMBINED EFFECTS OF HYDROGEN POST INJECTIONS AND FUMIGATION OF ETHANOL ON EMISSION AND PERFORMANCE IN A DIESEL ENGINE

Asst. Prof. Dr. Hüseyin GÜRBÜZ [1]

[1] Şırnak University, Faculty of Engineering, Mechanical Engineering Department, Automotive Department, Şırnak, Turkey. E-mail: huseyingurbuz@sirnak.edu.tr, ORCID ID: 0000-0002-3561-7786

INTRODUCTION

Pollutant emission standards were further tightened with Euro 5 and Euro 6 (Chong et al., 2018). Because pollutant emissions have started to permanently disrupt the environment, human health and global thermal balance (Smith et al., 2019). The fact that 30% of the global greenhouse gas is sourced from the transport sector, which only includes passenger cars, justifies the tightening of these emission standards. (EPA, 2019). Also, the cost of petroleum-based fuels has increased in recent years. However, the transportation sector meets most of its energy needs from gasoline and diesel (Tongroon et al., 2019). Conventional fuels produce NOx emission, which is greenhouse gas, especially owing to the high temperature in consequence of diesel combustion (Pedrozo et al., 2016). Ethanol and methanol, which have an important place among renewable alternative fuels, are commonly used fuels to control these emissions (He et al., 2018; Rakopoulos et al., 2019). In addition, ethanol is among the top renewable energy sources supported by the European Parliament (ICCT, 2018; Schöpe, 2008). Ethanol has the characteristics of high autoignition temperature, high evaporation temperature and low cetane number. Hence, ethanol cannot be utilized in diesel engine by conventional methods (Tutak et al., 2017). However, ethanol may be utilized in diesel engines with double injection, fumigation and emulsification methods (Bilgin et al., 2002; Satgé De Caro et al., 2001; Xiao et al., 2000). In addition, as the ethanol ratio increases due to phase separation and polar structure, ethanol and diesel do not show a homogeneous mix-

ture (Tutak et al., 2017). Anhydrous ethanol should be preferred because the amount of water in ethanol affects its solubility with diesel fuel (Datta et al., 2016; Lapuerta et al., 2007; Shahir et al., 2014). The diesel-ethanol mixture needs an emulsifier to prevent phase separation in the emulsion method (Kwanchareon et al., 2007; Tongroon et al., 2019). In addition, the emulsion must be heated against phase separation (Rakopoulos et al., 2019). Fumigation method is a process in which ethanol is atomized into the engine's intake air and evaporated (Damyanov et al., 2019; Heuser et al., 2015; Situ et al., 2013). It is suitable to use alcohols such as ethanol by fumigation method in diesel engines (Gürbüz et al., 2019).

Ignition delay and HRR increase with ethanol, which provides an almost homogeneous mixture with intake air in this method (Ghadikolaei et al., 2019). Also, in the fumigation method, ethanol can be directly injected into the cylinder (Tutak et al., 2018). However, an extra tank, a second injector, control card and some design changes are needed in this method (Gürbüz et al., 2019). The advantages of using ethanol-diesel dual fuel are limited thanks to the carbon element in the structure of ethanol and diesel. Therefore, hydrogen can be used as an additional fuel to produce cleaner and more efficient energy using ethanol diesel dual fuel. Since there is no carbon element in the hydrogen molecule (H_2) and consists only of hydrogen, just water is formed due to the combustion reaction with oxygen. The least NOx emission is released as the engine burns with high efficiency owing to the wide flammability interval of hydrogen (Mansor et al., 2017). Hy-

drogen can be directly injected into the cylinder and the sucked air. Nevertheless, low volumetric efficiency and low power are happened with fumigation of hydrogen intake manifold. Hydrogen direct injection into cylinder in a diesel engine is hard because of the high autoignition temperature of hydrogen (Bose et al., 2009). The hydrogen self-ignition heat 571^{o}C (Yapicioglu et al., 2018). Therefore, a spark plug-like igniter is needed in a diesel engine to inject hydrogen directly into the cylinder (Köse et al., 2013). When hydrogen is used directly as additional fuel, a combustion cycle occurs close to the ideal constant volume combustion cycle owing to the very high flame velocity and diffusion coefficient (Ji et al., 2009). Since the additional fuel must be mixed easily with air and main fuel in engines operating in dual mode, hydrogen is a substantial complimentary additional fuel because of its high combustibility and low pollutant emission (Dhole et al., 2014). Injection strategies have a serious contribution to homogeneous mixing and flammability. Also, direct injection of hydrogen provides greater volumetric efficiency and orderly combustion than port injection (Monemian et al., 2018). Hydrogen energizes aftertreatment apparatus such as lean NOx trap (LNT) to improve NOx reduction and desulfurization mechanisms (Dhole et al., 2014; Monemian et al., 2018). Poulston and Rajaram (Poulston et al., 2003) found that LNT ability increases with the use of hydrogen in thermally ancient catalysts. Heffel (Heffel, 2003) determined that with low mixtures in dual fuel mode, hydrogen can operate at no-load and partloads and reduce NOx emissions. Hydrogen also lowers NOx levels at

intermediate and low loads contrasted to diesel fuel (Mirica et al., 2015).

Combustion quality in internal combustion engines can be increased with various injection strategies (Moiz et al., 2016). NOx emission levels can be reduced by pilot injection, while soot emissions can be decreased post injection(G. Wu et al., 2019). Quadais et al. (Abu-Qudais et al., 2000) worked on emulsion and fumigation methods of ethanol in CI engine. They noticed a 51% reduction in soot emissions and a 55% increase in CO emissions with 20% ethanol fumigation. Ghadikolaeia et al. (Ghadikolaei et al., 2019) worked on effects of ethanol with emulsion and fumigation method in diesel engine. Ignition delay and heat release rate increased with the fumigation of ethanol compared to diesel. Mariasiu et al. (Mariasiu et al., 2015) worked on the effects of 15% ethanol by volume with fumigation and emulsion method in diesel engine. With the fumigation method, NOx, HC and specific fuel consumption decreased compared to the emulsion method. Monemian et al. (Monemian et al., 2020) researched the experimental and numerical effect of fumigation of hydrogen in a diesel engine on driving cycles. Combustion simulation tests of hydrogen and diesel were performed in the GT Power software. With more hydrogen at low load, CO and soot emissions were depleted. Talibi et al. (Talibi et al., 2014) examined the impacts of hydrogen injection into the inlet air of normal aspirated diesel engine. The experiments were implemented at different loads and constant injection. Tests showed reductions in THC, particulate matter, CO emissions however led to a

large increment in NOx emissions. Saravanan and Nagarajan (Saravanan et al., 2010) researched the impacts of hydrogen on diesel engine in double form experiments. The injection angle and injection time of hydrogen were controlled by the electronic control unit. NOx emission and thermal efficiency increased while the smoke emission reduced in all operational loads. Boretti (Boretti, 2011) examined the effects of adding hydrogen in a dual mode diesel engine. The consequences seen that the heat release rate increases with the supplementation of hydrogen, the combustion time was shortened and the engine power increased. Jafarmadar et al. (Jafarmadar, 2014) made exergy analysis on hydrogen and diesel in dual mode engine. They discovered that the energy ratio of hydrogen increased the temperature and pressure entering the cylinder, reducing exergy efficiency. M. Masood, et al.(Masood et al., 2007), in a CFD study examining the effects of hydrogen, found that the NOx emission raised with the rise in the amount of hydrogen involved in the burning.

Different applications of hydrogen in conventional engines have recently increased in research because hydrogen provides a high combustion ratio and a substantial reduction in harmful emissions (Boretti, 2011; Hafiz et al., 2018; Jafarmadar, 2014; Masood et al., 2007; Saravanan et al., 2010). In addition, although the effects of hydrogen as the main fuel and the injection fuel in intake airport have been investigated, few works have been done to research the influence of hydrogen as a post-injection fuel on emissions and performance in diesel engines operating with ethanol fumigation. In this study, the emission

and performance results of the diesel engine were determined primarily by using diesel fuel. In the second step, the changes of 10% ethanol fumigation on emissions and performance were experimentally examined. In the third step, the engine modelled with AVL Boost software separately for ethanol fumigation and diesel. After verifying the numerical models, effects of different post injection strategies of hydrogen in engine run with the ethanol fumigation on NOx emissions, Particulate Matter (PM) and engine performance were inquired.

The main goal of this paper is to analyze the effects of combined use of hydrogen and ethanol on diesel-induced harmful emissions, which is a deadly threat to health and the environment. Hence, the presented research will make a significant contribution to this very weak issue, as post-injection strategies are focused on injection of hydrogen at different crank angles in the CI engine working with ethanol fumigation and diesel main fuel.

1. METHODOLOGY

In the paper, the diesel engine was connected to a DC dynamometer loaded with resistance. The CI engine tests were done from 1100 r/min to 2200 r/min The CI engine tests were done from 1100 r/min to 2200 r/min. In the second stage, the effects of ethanol fumigation an injector controlled by an ECU card designed with Arduino on emission and performance were investigated experimentally in a diesel engine, whose emission and performance levels were determined by diesel in the first stage. Ethanol of 99.9% purity was used in the experiments. This is the reason why high purity ethanol is

used, it provides better blends of diesel with others pure ethanol (Zhu et al., 2011). In ethanol experiments, 10% ethanol (FE10) was used by fumigation method. The experiment system stand is seen in Figure 1. The engine speed was measured by a sensitive proximity sensor. Fuel consumption was determined with precision scales and fuel meters. Emission measurements were measured with AVL 415S filter paper smoke meter and AVL Dicom 4000.

In the third stage, the engine was modeled separately for diesel and FE10 fuels with AVL Boost 2016v software. Experimental data obtained using diesel and FE10 fuels have been verified by tests with this model engine. The FE10 simulation model engine rearranged to hydrogen injection strategies. The same amount of hydrogen was ejected in every post injection strategy. Post hydrogen injections were applied in the engine operating with ethanol fumigation and diesel main fuel. Thus, the effects of ethanol and hydrogen on polluting emissions from diesel were investigated.

2. SIMULATION MODEL AND VALIDATION

In the research, the turbocharged experiment test engine was modeled in one dimension with AVL Boost software. The block diagram of this model engine is shown in Figure 2. The model was first validated with diesel experimental study data. This model was then developed for ethanol fumigation and validated with ethanol experiment data.

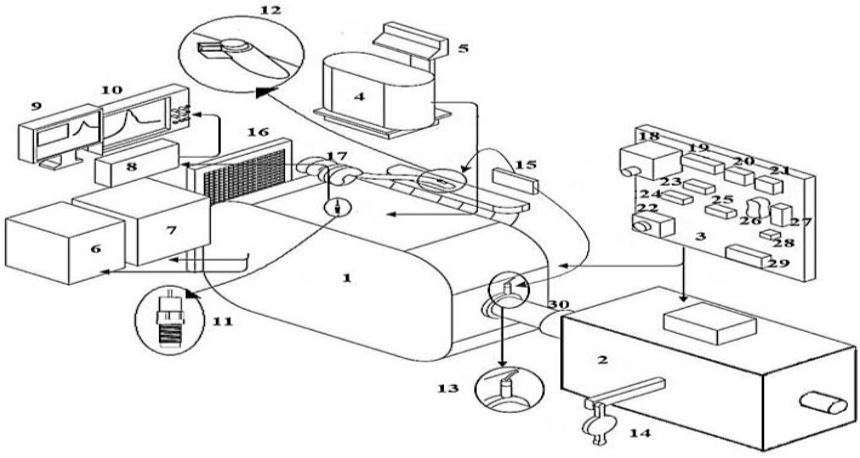

1-Engine, 2-DC dynamometer, 3-Control panel, Fuel tank, 5-Precision balance, 6-AVL emission analyzer, 7-AVL Soot analyzer, 8-Amplifier, 9-Computer, 10-Oscilloscope, 11-Pressure sensor, 12-Ethanol injector, 13-Proximity speed sensor, 14-Load cell, 15-Arduino ECU, 16-Radiator, 17-Turbochargers, 18-DC motor controller, 19-Load indicator, 20-Voltmeter, 21-Ammeter, 22-Emergency stop button, 23-Engine speed indicator, 24-Coolant inlet temperature, 25-Coolant outlet temperature, 26-Exhaust temperature, 27-Fuel temperature, 28-Air moisture meter, 29-Date and clock, 30-Pressure sensor

Figure 1. Experimental system setup.

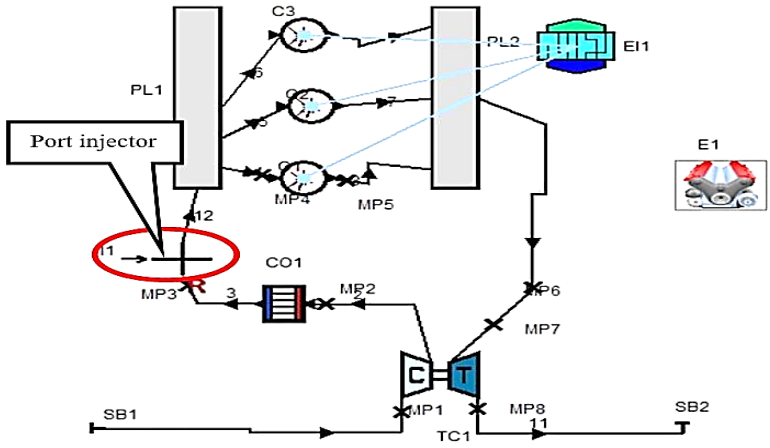

Figure 2. Block schema model of test engine.

The cylinder pressures of the FE10 experiment and simulation tests were compared to verify the engine model. The ignition delay was altered in regard to the average effective pressure curve for hydrogen utilization of the model. In addition, according to the combustion velocity of hydrogen, the combustion time was determined again. To get more accurate results of the model verification, the in-cylinder pressure data at low (1400 r/min), medium (1600 r/min) and high (2000 r/min) engine speeds were compared separately in Figure 3. The verification results showed that the experiment and simulated cylinder pressure results almost exactly overlapped at three different engine speeds. Therefore, the overlap of the experimental and simulation two pressure data indicates that the verification of the model is acceptable.

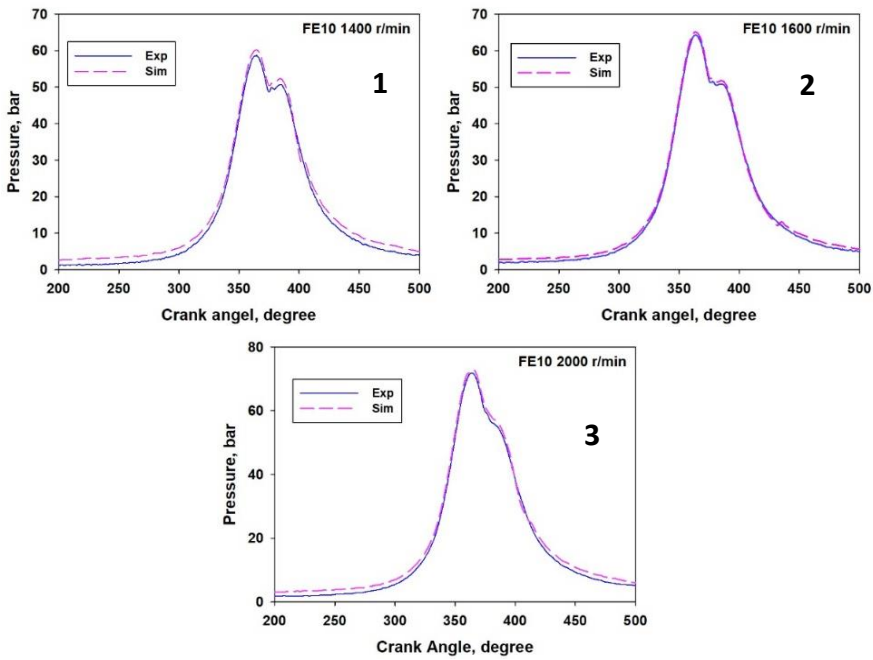

Figure 3. Validation of model software with cylinder pressure results.

Moreover, the model engine torque was compared with experimental data to validation the model. Comparison of the outcomes of engine torque of the model and experiment are seen in Table 1. The table shown that experiment and model data are quite in tune with each other. The error rate of data between experiment and model is less than 1% at almost all speeds, and less than 3% only at highest speed. Models with an error rate of less than 4% between the motor torque test and simulation test can be considered as verified. Therefore, due to such low error rate, the model was validated and used with confidence.

Table 1. Comparison of engine torque of AVL model by experimental tests at some engine speeds.

Engine speed [r/min]	**Engine torque [Nm]**		
	AVL model	**Experiment**	**Error [%]**
1100	165.823	164.08	1.0622
1200	165.641	164.21	0.8714
1300	165.788	164.85	0.5691
1400	165.862	165.22	0.3885
1500	167.777	167.07	0.4231
1600	169.668	169.38	0.1711
1700	164.838	164.76	0.0473
1800	167.232	164.64	1.5743
1900	160.272	158.87	0.8824
2000	160.465	160.23	0.1466
2100	150.972	149.23	1.1673
2200	107.066	104.04	2.9085

3. INJECTION STRATEGY

Three various injection strategies seen in Figure 4 were done. In injection strategies, only hydrogen was injected as a post-fuel in the model engine powered with diesel and ethanol fumigation.

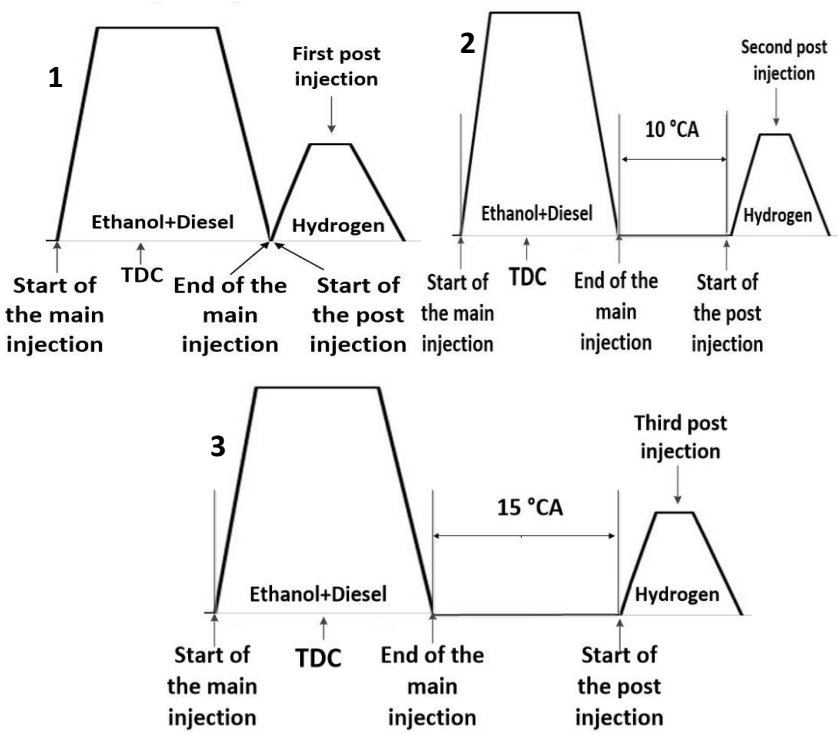

Figure 4. Injection Test Strategies.

In the first injection strategy, as soon as the main injection was completed, hydrogen post injection (HP0) was carried out at 0 °CA (crank angle). In the second injection strategy, after the main injection was completed, hydrogen post injection (HP10) was applied at 10 °CA. Finally, after the main injection was completed, hydrogen post injec-

tion (HP15) was applied at 15 °CA. The amount of hydrogen injected was applied evenly in all injection strategies.

4. RESULTS AND DISCUSSION

All experimental and simulation tests were performed at various engine velocities from 1100 r/min to 2200 r/min. In the graphs, only diesel experiments D-Exp, 10% ethanol fumigation experiment and simulation results, respectively, FE10-Exp and FE10-Sim, and hydrogen post injection tests HP0, HP10 and HP15, respectively.

Figure 5 shows engine power. Compared with the diesel results, the engine power was determined to be 35.49 kW, with an increase of 7.8% at 2000 rpm with ethanol fumigation. The average engine power of the HP0, HP10 and HP15 hydrogen post injections was 30.89kW, 29.86kW and 29.30 kW, respectively, with an increase of 8.49%, 4.87% and 2.94% compared to the FE10-Sim. Engine power increased as the post fuel injection of hydrogen approached the main fuel injection. Therefore, the highest engine powers were obtained in the HP0 test.

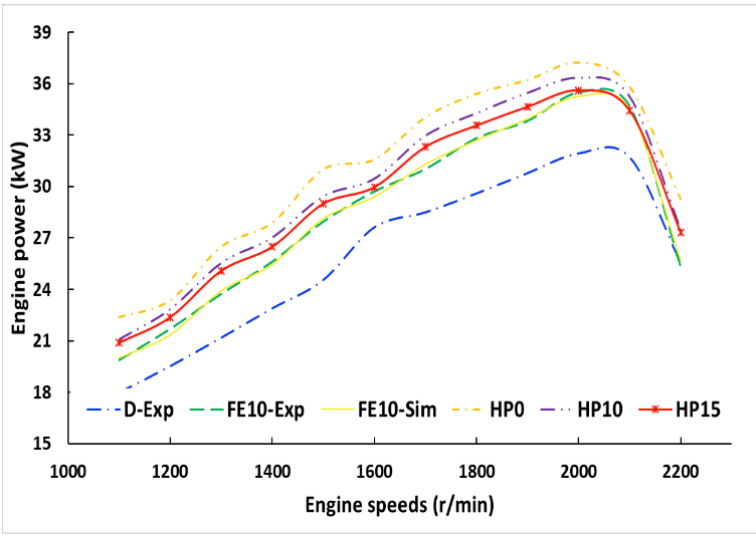

Figure 5. The impact of ethanol fumigation and post injections of hydrogen on engine power.

BSFC (Brake specific fuel consumption) is presented in Figure 6. BSFC was remarkably dropped at low engine speeds with FE10 fuel compared to diesel, however, slightly increased at high engine speeds. In simulation tests, the specific fuel consumption of hydrogen in all three-post injection strategies reduced at all engine speeds compared to the FE10-Sim. BSFC decreased at low and middle speeds with the effect of ethanol and hydrogen. Comparing the HP0and HP10 tests with the FE10-Sim test in terms of total consumption, the injection tests decreased significantly such as 9.01% and 11.07%. If the hydrogen injected into the cylinder comes together with sufficient oxygen, BSFC decreases due to complete combustion (Deb et al., 2015).

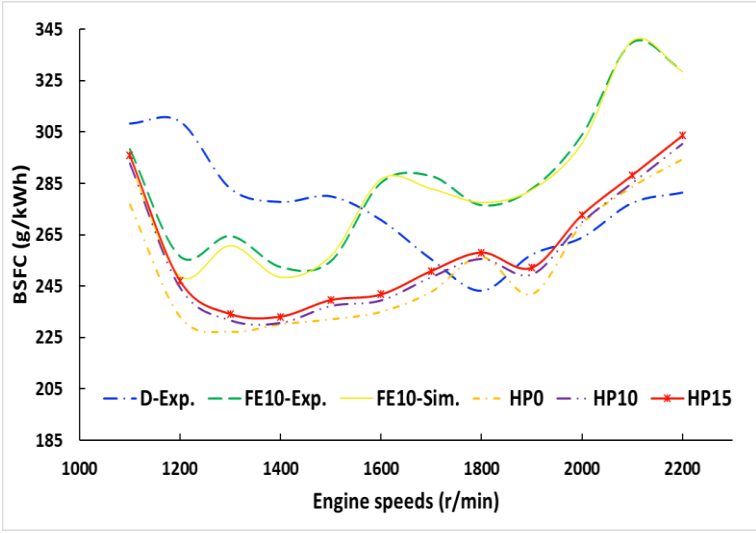

Figure 6. The impact of ethanol fumigation and post injections of hydrogen on BSFC.

NOx emission changes are seen in Figure 7. NOx emissions raised with FE10. Because this increase is owing to the high evaporation temperature of ethanol, the self-ignition heat, the increased heat of the cylinder and the ethanol ratio in the mixture (An et al., 2013; Jamrozik et al., 2020). NOx emission increased considerably with hydrogen injection on ethanol fumigation and diesel. As the hydrogen post injection approached the TDC, NOx emission increased. Hence, the HP0 strategy has maximized NOx emissions, while with HP15, it has significantly decreased compared to other strategies. If the post injection is delayed excessively after the main injection without changing the injection amount, NOx emission decrease (Y. Wu et al., 2019). The reason why NOx emission increases with the supplement of hydrogen; hydrogen holds the in-cylinder temperature at higher levels for longer (Saravanan et al., 2008).

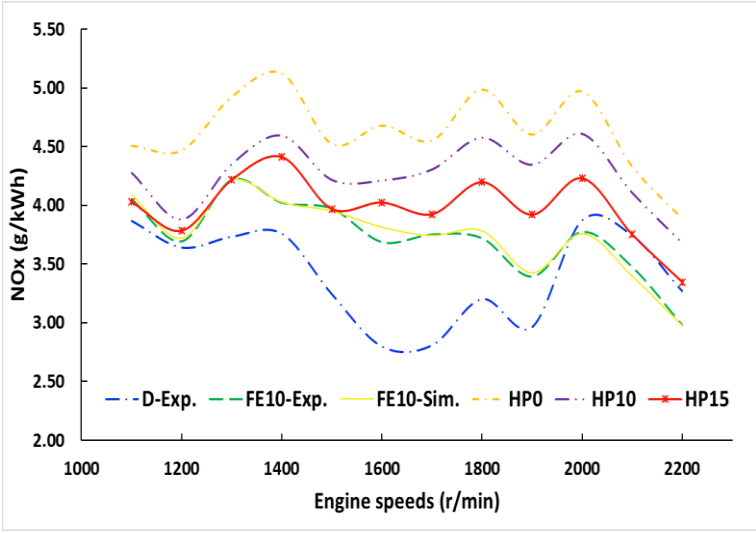

Figure 7. The impact of ethanol fumigation and post injections of hydrogen on NOx emission.

Figure 8 shows the changes of soot emission. At low engine speeds, there was a considerable reduce in soot emission with FE10. However, an increase in soot emission occurred at medium and high engine speeds. Soot emission was further reduced with hydrogen post injection. The least soot emission occurred in HP0 tests. As the post injection time approached the main injection, the soot emission decreased. In addition, in the HP0 strategy test, soot emission was less than diesel fuel with the addition of hydrogen. When there is enough oxygen, the combustion efficiency improves with additional hydrogen (Christodoulou et al., 2014). In the Hydrogen post injection tests, soot emission decreased by 35%, 11.36% and 9.21% for HP0, HP10 and HP15, respectively. However, soot emission increased slightly at medium and high engine speeds with the HP10 post injection according to the diesel D-Exp test. The increase in soot emission with

HP10 (10 °CA) may have been due to the lowering of cylinder temperature by late post injection.

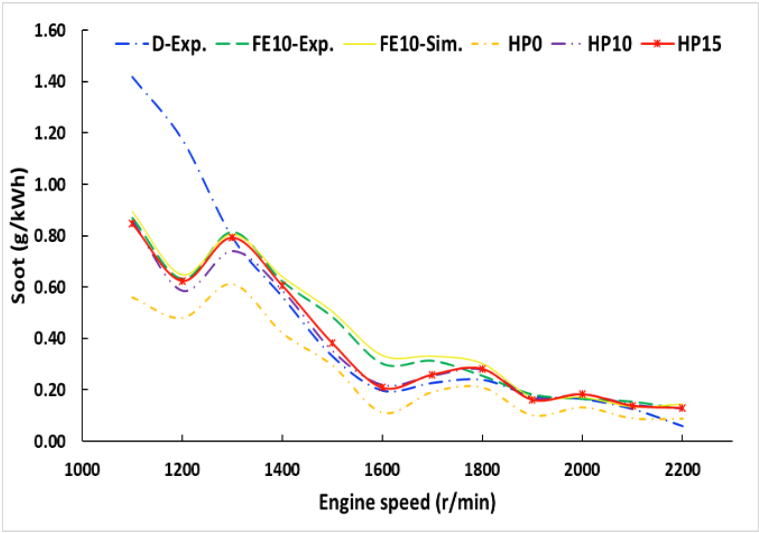

Figure 8. The effect of ethanol fumigation and post injections of hydrogen on soot emission.

CONCLUSIONS

In this research, the influences of ethanol on emissions and performance by fumigation method in diesel engine were investigated experimentally. In addition, in the diesel engine modeled with AVL Boost software and operated with ethanol fumigation, the impacts of hydrogen post-injection strategies on emissions and performance were numerically analyzed. The following results were obtained in the study:

- In ethanol fumigation tests, engine power increased compared to diesel fuel. This increase was approximately 9.59% on average of all engine speeds. The analysis shown that, the engine power

was highly dependent on hydrogen injection timing. Engine power that raised with ethanol fumigation increased even more with hydrogen injection optimization. However, the engine power obtained with the closest post injection to the main fuel injection was greater than the other post injections. For the two post-injection strategies of hydrogen with 0 °CA and 10 °CA, this power increase was 8.49% and 4.87%, respectively.

- Specific fuel consumption increased with ethanol fumigation. In addition, hydrogen post injection reduced specific fuel consumption by 11.28% and 9.47% in post 1 and post 2 strategies, respectively, in the engine powered by diesel and ethanol fumigation.
- NOx emission increased with FE10-Exp and hydrogen post injection strategies compared to D-Exp. As Hydrogen injection strategies move away from main diesel injection, NOx emission decreased.
- Soot emissions have dropped significantly at low engine speeds with ethanol fumigation. However, soot emission raised at middle and high engine speeds. Soot emission was importantly reduced with hydrogen post injections at low and medium engine speeds compared to the FE10. With the HP0 strategy, the least soot emission was achieved in this strategy, since hydrogen injected closer to the TDC increases the combustion efficiency.
- Post hydrogen injection crank angle can be widened to compensate for increased NOx emissions.

NOMENCLATURE

BSFC	Brake specific fuel consumption
CA	Crank angle
DC	Direct current
ECU	Electronic control unit
g	Gram
H_2	Hydrogen
HRR	Heat release rate
J	Joule
kW	Kilowatt
LNT	Lean NOx trap
NOx	Oxides of nitrogen
r/min	Revolution per minute
TDC	Top dead center
THC	Total hydrocarbon
PM	Particulate matter

REFERENCES

Abu-Qudais, M., Haddad, O., & Qudaisat, M. (2000). The effect of alcohol fumigation on diesel engine performance and emissions. *Energy Conversion and Management*, *41*(4), 389–399. doi: 10.1016/S0196-8904(99)00099-0

An, H., Yang, W. M., Maghbouli, A., Li, J., Chou, S. K., & Chua, K. J. (2013). A numerical study on a hydrogen assisted diesel engine. *International Journal of Hydrogen Energy*, *38*(6), 2919–2928. doi: 10.1016/j.ijhydene.2012.12.062

Bilgin, A., Durgun, O., & Şahin, Z. (2002). The effects of diesel-ethanol blends on diesel engine performance. *Energy Sources*, *24*(5), 431–440. doi: 10.1080/00908310252889933

Boretti, A. (2011). Advances in hydrogen compression ignition internal combustion engines. *International Journal of Hydrogen Energy*, *36*(19), 12601–12606. doi: 10.1016/j.ijhydene.2011.06.148

Bose, P. K., & Maji, D. (2009). An experimental investigation on engine performance and emissions of a single cylinder diesel engine using hydrogen as inducted fuel and diesel as injected fuel with exhaust gas recirculation. *International Journal of Hydrogen Energy*, *34*(11), 4847–4854. doi: 10.1016/j.ijhydene.2008.10.077

Chong, H. S., Park, Y., Kwon, S., & Hong, Y. (2018). Analysis of real driving gaseous emissions from light-duty diesel vehicles. *Transportation Research Part D: Transport and Environment*, *65*, 485–499. doi: 10.1016/j.trd.2018.09.015

Christodoulou, F., & Megaritis, A. (2014). Experimental investigation of the effects of simultaneous hydrogen and nitrogen addition on the emissions and combustion of a diesel engine. *International Journal of Hydrogen Energy*, *39*(6), 2692–2702. doi: 10.1016/j.ijhydene.2013.11.124

Damyanov, A., & Hofmann, P. (2019). Operation of a diesel engine with intake manifold alcohol injection. *Automotive and Engine Technology*, *4*(1–2), 17–28. doi: 10.1007/s41104-019-00040-2

Datta, A., & Mandal, B. K. (2016). Impact of alcohol addition to diesel on the performance combustion and emissions of a compression ignition engine. *Applied Thermal Engineering*, *98*, 670–682. doi: 10.1016/j.applthermaleng.2015.12.047

Deb, M., Sastry, G. R. K., Bose, P. K., & Banerjee, R. (2015). An experimental study on combustion, performance and emission analysis of a single cylinder, 4-stroke DI-diesel engine using hydrogen in dual fuel mode of operation. *International Journal of Hydrogen Energy*, *40*(27), 8586–8598. doi: 10.1016/j.ijhydene.2015.04.125

Dhole, A. E., Yarasu, R. B., Lata, D. B., & Baraskar, S. S. (2014). Mathematical modeling for the performance and emission parameters of dual fuel diesel engine using hydrogen as secondary fuel. *International Journal of Hydrogen Energy*, *39*(24), 12991–13001. doi: 10.1016/j.ijhydene.2014.06.084

EPA. (2019). *Sources of Greenhouse Gas Emissions*. Retrieved from https://www.epa.gov/ghgemissions/sources-greenhouse-gas-emissions

Ghadikolaei, M. A., Cheung, C. S., & Yung, K. F. (2019). Study of combustion, performance and emissions of a diesel engine fueled with ternary fuel in blended and fumigation modes. *Fuel*, *235*, 288–300. doi: 10.1016/j.fuel.2018.07.089

Gürbüz, H., & Sandalcı, T. (2019). Investigation of Effects of Fumigation on Performance and Emission in Dual Fuel Engines Injection-Controlled With Electronic Card. *International Journal of Engineering Research and Advanced Technology*, *5*(3), 24–31. doi: 10.31695/ijerat.2019.3400

Hafiz, N. M., Mansor, M. R. A., & Wan Mahmood, W. M. F. (2018). Simulation of the combustion process for a CI hydrogen engine in an argon-oxygen atmosphere. *International Journal of Hydrogen Energy*, *43*(24), 11286–11297. doi: 10.1016/j.ijhydene.2018.05.022

He, T., Chen, Z., Zhu, L., & Zhang, Q. (2018). The influence of alcohol additives and EGR on the combustion and emission characteristics of diesel engine under high-load condition. *Applied Thermal Engineering*, *140*(May), 363–372. doi: 10.1016/j.applthermaleng.2018.05.064

Heffel, J. W. (2003). NOx emission reduction in a hydrogen fueled internal combustion engine at 3000 rpm using exhaust gas recirculation. *International Journal of Hydrogen Energy*, *28*(11), 1285–1292. doi: 10.1016/S0360-3199(02)00289-6

Heuser, B., Kremer, F., Pischinger, S., Rohs, H., Holderbaum, B., & Körfer, T. (2015). An Experimental Investigation of Dual-Fuel Combustion in a Light Duty Diesel Engine by In-Cylinder Blending of Ethanol and Diesel. *SAE International Journal of Engines*, *9*(1), 11–25. doi: 10.4271/2015-01-1801

ICCT. (2018). *Final recast RED II: Renewable Energy Directive for 2021-2030 in the European Union* (Issue July). Retrieved from https://www.theicct.org/sites/default/files/publications/EU_Fuels_Policy_Update_20180719.pdf

Jafarmadar, S. (2014). Exergy analysis of hydrogen/diesel combustion in a dual fuel engine using three-dimensional model. *International Journal of Hydrogen Energy*, *39*(17), 9505–9514. doi: 10.1016/j.ijhydene.2014.03.152

Jamrozik, A., Grab-Rogaliński, K., & Tutak, W. (2020). Hydrogen effects on combustion stability, performance and emission of diesel engine. *International Journal of Hydrogen Energy*. doi: 10.1016/j.ijhydene.2020.05.049

Ji, C., & Wang, S. (2009). Effect of hydrogen addition on the idle performance of a spark ignited gasoline engine at stoichiometric condition. *International Journal of Hydrogen Energy*, *34*(8), 3546–3556. doi: 10.1016/j.ijhydene.2009.02.052

Köse, H., & Ciniviz, M. (2013). An experimental investigation of effect on diesel engine performance and exhaust emissions of addition at dual fuel mode of hydrogen. *Fuel Processing Technology*, *114*, 26–34. doi: 10.1016/j.fuproc.2013.03.023

Kwanchareon, P., Luengnaruemitchai, A., & Jai-In, S. (2007). Solubility of a diesel–biodiesel–ethanol blend, its fuel properties, and its emission characteristics from diesel engine. *Fuel*, *86*(7–8), 1053–1061. doi: 10.1016/J.FUEL.2006.09.034

Lapuerta, M., Armas, O., & García-Contreras, R. (2007). Stability of diesel-

bioethanol blends for use in diesel engines. *Fuel*, *86*(10–11), 1351–1357. doi: 10.1016/j.fuel.2006.11.042

Mansor, M. R. A., Abbood, M. M., & Mohamad, T. I. (2017). The influence of varying hydrogen-methane-diesel mixture ratio on the combustion characteristics and emissions of a direct injection diesel engine. *Fuel*, *190*, 281–291. doi: 10.1016/j.fuel.2016.11.010

Mariasiu, F., Burnete, N. V., Moldovanu, D., Varga, B. O., Iclodean, C., & Kocsis, L. (2015). Effects of bioethanol ultrasonic generated aerosols application on diesel engine performances. *Thermal Science*, *19*(6), 1931–1941. doi: 10.2298/TSCI140703108M

Masood, M., Ishrat, M. M., & Reddy, A. S. (2007). Computational combustion and emission analysis of hydrogen-diesel blends with experimental verification. *International Journal of Hydrogen Energy*, *32*(13), 2539–2547. doi: 10.1016/j.ijhydene.2006.11.008

Mirica, I., Cernat, A., Pana, C., Negurescu, N., & Nutu, C. (2015). PERFORMANCE COMPARISON BETWEEN HYDROGEN AND DIESEL FUEL FUELLED COMPRESSION IGNITION ENGINE. *U.P.B. Sci. Bull., Series D*, *77*(4), 217–228.

Moiz, A. A., Ameen, M. M., Lee, S. Y., & Som, S. (2016). Study of soot production for double injections of n-dodecane in CI engine-like conditions. *Combustion and Flame*, *173*, 123–131. doi: 10.1016/j.combustflame.2016.08.005

Monemian, E., & Cairns, A. (2020). Hydrogen Fumigation on HD Diesel Engine: An Experimental and Numerical Study. In Diesel and Gasoline Engines (pp. 1–24). IntechOpen. doi: 10.5772/intechopen.89425

Monemian, E., Cairns, A., Gilmore, M., Newman, D., & Scott, K. (2018). Evaluation of intake charge hydrogen enrichment in a heavy-duty diesel engine. *Proceedings of the Institution of Mechanical Engineers, Part D: Journal of Automobile Engineering*, *232*(1), 139–147. doi: 10.1177/0954407017738375

Pedrozo, V. B., May, I., Dalla Nora, M., Cairns, A., & Zhao, H. (2016). Experimental analysis of ethanol dual-fuel combustion in a heavy-duty diesel en-

gine: An optimisation at low load. *Applied Energy*, *165*, 166–182. doi: 10.1016/j.apenergy.2015.12.052

Poulston, S., & Rajaram, R. R. (2003). Regeneration of NOx trap catalysts. *Catalysis Today*, *81*(4), 603–610. doi: 10.1016/S0920-5861(03)00158-5

Rakopoulos, C. D., Rakopoulos, D. C., Kosmadakis, G. M., & Papagiannakis, R. G. (2019). Experimental comparative assessment of butanol or ethanol diesel-fuel extenders impact on combustion features, cyclic irregularity, and regulated emissions balance in heavy-duty diesel engine. *Energy*, *174*, 1145–1157. doi: 10.1016/j.energy.2019.03.063

Saravanan, N., & Nagarajan, G. (2010). Performance and emission studies on port injection of hydrogen with varied flow rates with Diesel as an ignition source. *Applied Energy*. doi: 10.1016/j.apenergy.2010.01.014

Saravanan, N., Nagarajan, G., Sanjay, G., Dhanasekaran, C., & Kalaiselvan, K. M. (2008). Combustion analysis on a DI diesel engine with hydrogen in dual fuel mode. *Fuel*, *87*(17–18), 3591–3599. doi: 10.1016/j.fuel.2008.07.011

Satgé De Caro, P., Mouloungui, Z., Vaitilingom, G., & Berge, J. C. (2001). Interest of combining an additive with diesel-ethanol blends for use in diesel engines. *Fuel*, *80*(4), 565–574. doi: 10.1016/S0016-2361(00)00117-4

Schöpe, M. (2008). Renewable energy directive. *European Wind Energy Conference and Exhibition 2008*, *1*, 32–38.

Shahir, S. A., Masjuki, H. H., Kalam, M. A., Imran, A., Fattah, I. M. R., & Sanjid, A. (2014). Feasibility of diesel-biodiesel-ethanol/bioethanol blend as existing CI engine fuel: An assessment of properties, material compatibility, safety and combustion. In Renewable and Sustainable Energy Reviews (Vol. 32, pp. 379–395). doi: 10.1016/j.rser.2014.01.029

Situ, R., Ireland, G., Bodisco, T., & Brown, R. (2013). *Thermodynamic Modeling of Ethanol Fumigation in a Diesel Engine*. 1568–1574. Retrieved from www.mssanz.org.au/modsim20131568

Smith, C. J., Forster, P. M., Allen, M., Fuglestvedt, J., Millar, R. J., Rogelj, J., & Zickfeld, K. (2019). Current fossil fuel infrastructure does not yet commit us to 1.5 °C warming. *Nature Communications*, *10*(1), 101. doi:

10.1038/s41467-018-07999-w

Talibi, M., Hellier, P., Balachandran, R., & Ladommatos, N. (2014). Effect of hydrogen-diesel fuel co-combustion on exhaust emissions with verification using an in-cylinder gas sampling technique. *International Journal of Hydrogen Energy*. doi: 10.1016/j.ijhydene.2014.07.039

Tongroon, M., Saisirirat, P., Suebwong, A., Aunchaisri, J., Kananont, M., & Chollacoop, N. (2019). Combustion and emission characteristics investigation of diesel-ethanol-biodiesel blended fuels in a compression-ignition engine and benefit analysis. *Fuel*, *255*. doi: 10.1016/j.fuel.2019.115728

Tutak, W., Jamrozik, A., Bereczky, Á., & Lukacs, K. (2018). Effects of injection timing of diesel fuel on performance and emission of dual fuel diesel engine powered by diesel/E85 fuels. *Transport*, *33*(3), 633–646. doi: 10.3846/transport.2018.1572

Tutak, W., Jamrozik, A., Pyrc, M., & Sobiepański, M. (2017). A comparative study of co-combustion process of diesel-ethanol and biodiesel-ethanol blends in the direct injection diesel engine. *Applied Thermal Engineering*, *117*, 155–163. doi: 10.1016/j.applthermaleng.2017.02.029

Wu, G., Zhou, X., & Li, T. (2019). Temporal evolution of split-injected fuel spray at elevated chamber pressures. *Energies*, *12*(22). doi: 10.3390/en12224284

Wu, Y., Wang, P., Muhammad Farhan, S., Yi, J., & Lei, L. (2019). Effect of post-injection on combustion and exhaust emissions in DI diesel engine. *Fuel*, *258*, 116131. doi: 10.1016/J.FUEL.2019.116131

Xiao, Z., Ladommatos, N., & Zhao, H. (2000). The effect of aromatic hydrocarbons and oxygenates on diesel engine emissions. *Proceedings of the Institution of Mechanical Engineers, Part D: Journal of Automobile Engineering*, *214*(3), 307–332. doi: 10.1243/0954407001527448

Yapicioglu, A., & Dincer, I. (2018). Performance assesment of hydrogen and ammonia combustion with various fuels for power generators. *International Journal of Hydrogen Energy*, *43*(45), 21037–21048. doi: 10.1016/j.ijhydene.2018.08.198

Zhu, L., Cheung, C. S., Zhang, W. G., & Huang, Z. (2011). Combustion, perfor-

mance and emission characteristics of a DI diesel engine fueled with ethanol–biodiesel blends. *Fuel*, *90*(5), 1743–1750. doi: 10.1016/J.FUEL.2011.01.024

CHAPTER 6

THE INVERSE PROBLEM OF STURM-LIOUVILLE OPERATOR WITH DISCONTINUITY CONDITIONS

Assist. Prof. Dr. Özge AKÇAY [1]

[1] Munzur University, Engineering Faculty, Department of Computer Engineering, Tunceli, Turkey. E-mail: ozgeakcay@munzur.edu.tr ORCID ID: 0000-0001-9691-666X

INTRODUCTION

Inverse spectral problems arises when the linear operator is reconstructed from its spectral characteristics, for example spectral data (the sequences of eigenvalues and norming constants), spectral function, two spectra, scattering data, Weyl function, etc. In this work, the inverse problem of Sturm-Liouville boundary value problem is considered and state that the eigenfunctions of this problem have a discontinuity in an interior point of the finite interval. In that case, let us take the boundary value problem generated by the Sturm-Liouville equation

$$-y''+q(x)y=\lambda^2 y, \quad x\in(0,\pi), \tag{1}$$

with the discontinuity conditions at $x=a\in\left(\frac{\pi}{2},\pi\right)$

$$y(a+0)=\alpha y(a-0), \quad y'(a+0)=\alpha^{-1}y'(a-0), \tag{2}$$

and boundary conditions

$$y'(0)=y'(\pi)+hy(\pi)=0, \tag{3}$$

where $q(x)\in L_2(0,\pi)$ is real valued-function, $\alpha>0$ and h are real constant numbers, λ is a spectral parameter.

Boundary value problems for Sturm-Liouville equation with discontinuities within the interval arise in mathematics, physics, geophysics and other fields of natural sciences (see Anderssen, 1997; Gomilko and Pivovarchik, 2002; Hald, 1984; Tikhonov and Samarskii, 1990; Willis, 1984 and etc.), that's why there are so many

studies on such problems and the studies continue to improve. For instance, the direct and/or inverse problems (according to the different spectral characteristics) of the Sturm-Liouville problem with discontinuity conditions at interior points of the finite interval are examined in the works (Akcay, 2018; Akcay, 2019; Akcay, 2020; Huseynov and Dostuyev, 2016; Freiling and Yurko, 2001; Amirov, Ozkan and Keskin 2009; Guseinov and Mammadova, 2014; Kadakal and Muhktarov, 2006; Muhktarov and Aydemir, 2017; Muhktarov, Olğar, Aydemir and Jabbarov 2018; Şen, 2017; Wang, 2015; C. F. Yang and X. P. Yang, 2009; Zheng, Cai, Li and Zhang, 2018) and the references therein.

The results obtained in this paper can be given as follows: firstly, it is proved that the eigenfunctions of the problem (1)-(3) form a complete system in $L_2(0,\pi)$ and then the eigenfunction expansion formula is obtained. Secondly, we examine the inverse spectral problem of the problem (1)-(3) that is indicated in the way: to determine the potential $q(x)$ and the boundary constant h according to spectral data of the problem (1)-(3). Therefore, the fundamental equation of the inverse problem is constructed and the uniqueness theorem for the solution of inverse problem by spectral data is proved. Finally, an algorithm for the construction of the potential $q(x)$ from the spectral data is given.

1. MATERIALS AND METHODS

To solve the inverse problem stated above, we use Gelfand-Levitan-Marchenko (GLM) method. In this method, we use the transformation

operator and a linear integral equation (named by GLM equation or fundamental equation) is satisfied by the kernel of the transformation operator plays the central role. Whereas, considered problem has a discontinuity condition (2) at the point $x = a$, so the solution of the Sturm-Liouville equation (1) with discontinuity condition (2) is different from the transformation operator, it has the form of integral representation in which the kernel function $H(x,s)$ has a discontinuity along the line $s = 2a - x$ for $a < x < \pi$. This integral representation is known from the work (Akcay, 2018) (in case of $\beta = 0$ in the second discontinuity condition of this work) as follows:

The solution of equation (1) under the discontinuity conditions (2) and initial conditions

$$e(0,\lambda) = 1, \qquad e'(0,\lambda) = i\lambda \tag{4}$$

is defined by $e(x,\lambda)$ and the integral representation of the solution $e(x,\lambda)$ is as follows:

$$e(x,\lambda) = e_0(x,\lambda) + \int_{-x}^{x} H(x,s)e^{i\lambda s}ds, \tag{5}$$

where

$$e_0(x,\lambda) = \begin{cases} e^{i\lambda x}, & 0 < x < a, \\ \alpha_1 e^{i\lambda x} + \alpha_2 e^{i\lambda(2a-x)}, & a < x < \pi, \end{cases}$$

here $\alpha_1 = \frac{1}{2}\left(\alpha + \frac{1}{\alpha}\right)$, $\alpha_2 = \frac{1}{2}\left(\alpha - \frac{1}{\alpha}\right)$, the kernel $H(x,.) \in L_1(-x,x)$ for each $x \in (0,\pi)$ and satisfies the inequality.

$$\int_{-x}^{x} |H(x,s)|\,ds \le e^{c\sigma(x)} - 1, \qquad \sigma(x) = \int_0^x (x-\xi)\,|q(\xi)|\,d\xi.$$

Moreover, the kernel $H(x,s)$ has a discontinuity along the line $s = 2a - x$ for $a < x < \pi$ and provide the following properties:

$$H(x,x) = \begin{cases} \frac{1}{2}\int_0^x q(\xi)\,d\xi, & 0 < x < a, \\ \frac{\alpha_1}{2}\int_0^x q(\xi)\,d\xi, & a < x < \pi, \end{cases}$$

$$H(x,2a-x+0) - H(x,2a-x-0) =$$

$$= \frac{\alpha_2}{2}\left(\int_a^x q(\xi)\,d\xi - \int_0^a q(\xi)\,d\xi\right), \quad a < x < \pi,$$

$$H(x,-x) = 0.$$

Therefore, in this work, we use the integral representation (5) when solving the inverse spectral problem of Sturm-Liouville problem (1)-(3) by applying the GLM method. In the finite interval, the inverse Sturm-Liouville problems are studied by using the GLM method in the works (Akcay, 2020; Akhmedova and Huseynov, 2010; Guliyev, 2005; Huseynov and Dostuyev, 2016; Karahan and Mamedov, 2017; Nabiev, Gürdal and Saltan 2016). Moreover, note that the comprehensive information on the development of the theory of

inverse problems and the GLM method are given in (Agranovich and Marchenko, 1963; Freiling and Yurko, 2001; Levitan, 1987; Levitan and Sargsjan, 1991; Marchenko, 2011).

Now, to discuss in detail the obtained results we need some preliminary facts about the spectral properties of the problem (1)-(3):

Let $\zeta(x,\lambda)$ and $\upsilon(x,\lambda)$ be the solutions of the equation (1) with the conditions (2) satisfying the initial conditions, respectively.

$$\begin{aligned} &\zeta(0,\lambda)=1, \qquad &&\zeta'(0,\lambda)=0,\\ &\upsilon(\pi,\lambda)=-1, \qquad &&\upsilon'(\pi,\lambda)=h. \end{aligned} \tag{6}$$

The function $\zeta(x,\lambda)$ has the form which is obtained from the solution $e(x,\lambda)$ formulated by (5):

$$\zeta(x,\lambda)=\zeta_0(x,\lambda)+\int_0^x L(x,s)\cos\lambda s ds, \tag{7}$$

where

$$\zeta_0(x,\lambda)=\begin{cases}\cos\lambda x, & 0<x<a,\\ \alpha_1\cos\lambda x+\alpha_2\cos\lambda(2a-x), & a<x<\pi\end{cases}$$

and $L(x,s)=H(x,s)+H(x,-s)$. Moreover, from this equality, we have

$$L(x,x)=\begin{cases}\dfrac{1}{2}\displaystyle\int_0^x q(\xi)d\xi, & 0<x<a,\\ \dfrac{\alpha_1}{2}\displaystyle\int_0^x q(\xi)d\xi, & a<x<\pi.\end{cases} \tag{8}$$

The characteristic function of the boundary value problem (1)-(3) is in the form

$$\phi(\lambda) = \upsilon'(0,\lambda) = \zeta'(\pi,\lambda) + h\zeta(\pi,\lambda). \tag{9}$$

The function $\phi(\lambda)$ is an entire function in λ, so it has a countable number of zeros $\{\lambda_p\}$ and the numbers $\{\lambda_p^2\}$ are the eigenvalues of the boundary value problem (1)-(3). The solutions $\zeta(x,\lambda_p)$ and $\upsilon(x,\lambda_p)$ are eigenfunctions of the problem (1)-(3) and there exists $\{\tau_p\}$ such that

$$\upsilon(x,\lambda_p) = \tau_p \zeta(x,\lambda_p), \quad \tau_p \neq 0. \tag{10}$$

The following asymptotic formula of the eigenvalues $\{\lambda_p^2\}_{p\geq 0}$ of the problem (1)-(3) is valid:

$$\lambda_p = \tilde{\lambda}_p + \frac{s_p}{\tilde{\lambda}_p} + \frac{k_p}{p},$$

where $\tilde{\lambda}_p = p + h_p$, $\{h_p\} \in l_\infty$, $\{s_p\} \in l_\infty$ and $\{k_p\} \in l_2$ (see Amirov, Ozkan and Keskin, 2009). Moreover, the norming constants of the boundary value problem (1)-(3) is defined by

$$\gamma_p := \int_0^\pi \zeta^2(x,\lambda_p)\,dx$$

and the relation holds:

$$\dot{\phi}\left(\lambda_p\right)=2\lambda_p\gamma_p\tau_p,\qquad \dot{\phi}\left(\lambda\right)=\frac{d}{d\lambda}\phi\left(\lambda\right). \tag{11}$$

Note that consider $G_\delta := \left\{\lambda : \left|\lambda-\tilde{\lambda}_p\right|\geq\delta\right\}$, then the inequality holds:

$$\left|\phi\left(\lambda\right)\right|\geq C_\delta\left|\lambda\right|e^{\left|\mathrm{Im}\,\lambda\right|\pi},\qquad \lambda\in G_\delta \tag{12}$$

here δ is a sufficiently small positive number (see Amirov, Ozkan and Keskin, 2009). Furthermore, putting the asymptotic behavior in (9) as $\left|\lambda\right|\to\infty$

$$\zeta\left(x,\lambda\right)=\alpha_1\cos\lambda x+\alpha_2\cos\lambda\left(2a-x\right)+O\left(\frac{1}{\left|\lambda\right|}e^{\left|\mathrm{Im}\,\lambda\right|x}\right),\quad a<x<\pi,$$

we have as $\left|\lambda\right|\to\infty$

$$\phi\left(\lambda\right)=-\lambda\left(\alpha_1\sin\lambda\pi-\alpha_2\sin\lambda(2a-\pi)\right)+O\left(e^{\left|\mathrm{Im}\,\lambda\right|\pi}\right). \tag{13}$$

2. RESULTS

2.1. Eigenfunction Expansion

Theorem 1.

i. The eigenfunctions $\left\{\zeta\left(x,\lambda_p\right)\right\}_{p\geq0}$ of the problem (1)-(3) form a complete system in $L_2\left(0,\pi\right)$.

ii. If $h(x)\in AC[0,a]\cap AC[a,\pi]$ and satisfy the conditions (2) and (3), then the function $h(x)$ has the uniformly convergent eigenfunction expansion

$$h(x)=\sum_{p=0}^{\infty}c_p\zeta\left(x,\lambda_p\right),\quad c_p=\frac{1}{\gamma_p}\int_0^{\pi}h(s)\zeta\left(s,\lambda_p\right)ds. \tag{14}$$

Proof.

i. Denote

$$\rho(x,s,\lambda)=\frac{1}{\phi(\lambda)}\begin{cases}\upsilon(x,\lambda)\zeta(s,\lambda), & s\le x,\\ \zeta(x,\lambda)\upsilon(s,\lambda), & s\ge x\end{cases} \tag{15}$$

and take into account the function

$$y^*(x,\lambda)=\int_0^{\pi}\rho(x,s,\lambda)h(s)ds. \tag{16}$$

The function $y^*(x,\lambda)$ is the solution of the following problem:

$$\begin{gathered}-y^*{}''+q(x)y^*=\lambda^2y^*+h(x),\\ y^*(a+0,\lambda)=\alpha y^*(a-0,\lambda),\quad y^*{}'(a+0,\lambda)=\alpha^{-1}y^*{}'(a-0,\lambda),\\ y^*{}'(0,\lambda)=y^*{}'(\pi,\lambda)+hy^*(\pi,\lambda)=0.\end{gathered} \tag{17}$$

It follows from (10) and (11) that

$$\upsilon\left(x,\lambda_p\right)=\frac{\dot\phi(\lambda)\left(\lambda_p\right)}{2\lambda_p\gamma_p}\zeta\left(x,\lambda_p\right).$$

Taking into account this relation, the expressions (15) and (16), we have

$$\operatorname*{Res}_{\lambda=\lambda_p}y^*(x,\lambda)=\frac{1}{2\lambda_p\gamma_p}\zeta\left(x,\lambda_p\right)\int_0^{\pi}h(s)\zeta\left(s,\lambda_p\right)ds. \tag{18}$$

Let $h(x)\in L_2(0,\pi)$ be such that

$$\int_0^{\pi} h(s)\zeta\left(s,\lambda_p\right)ds=0,\qquad p\geq 0.$$

It is obtained from (18) that $\operatorname*{Res}_{\lambda=\lambda_p} s\, y^*\left(x,\lambda\right)\equiv 0$. Then, $y^*\left(x,\lambda\right)$ is entire function of λ for each $x\in\left(0,\pi\right)$. Moreover, it follows from (12) and the estimates

$$\zeta\left(x,\lambda\right)=O\left(e^{|\mathrm{Im}\,\lambda|x}\right),\qquad \upsilon\left(x,\lambda\right)=O\left(e^{|\mathrm{Im}\,\lambda|(\pi-x)}\right),\quad |\lambda|\to\infty$$

that for a fixed $\delta>0$ and sufficiently large $\lambda^*>0$:

$$\left|y^*\left(x,\lambda\right)\right|\leq\frac{C_\delta}{\lambda},\quad \lambda\in G_\delta,\quad |\lambda|\geq\lambda^*.$$

As a result, we find $y^*\left(x,\lambda\right)\equiv 0$ by applying the maximum principle and Liouville theorem. Thus, from this fact and (17), we have $h(x)\equiv 0$ almost everywhere on $\left(0,\pi\right)$.

ii. Since $\zeta\left(x,\lambda\right)$ and $\upsilon\left(x,\lambda\right)$ are solutions of the homogeneous problem (1)-(3), we transform $y^*\left(x,\lambda\right)$ as follows:

$$y^*\left(x,\lambda\right)=\frac{h(x)}{\lambda^2}+\frac{1}{\lambda^2}\left[z_1\left(x,\lambda\right)+z_2\left(x,\lambda\right)\right],\qquad (19)$$

where

$$z_1\left(x,\lambda\right)=\frac{1}{\phi\left(\lambda\right)}\left\{\upsilon\left(x,\lambda\right)\int_0^x\zeta\,'\left(s,\lambda\right)v\left(s\right)ds+\right.$$

$$+\zeta(x,\lambda)\int_x^\pi \upsilon'(s,\lambda)v(s)ds\Big\}, \quad v(s):=h'(s),$$

$$z_2(x,\lambda)=\frac{1}{\phi(\lambda)}\Big\{-hh(\pi)\zeta(x,\lambda)+\upsilon(x,\lambda)\int_0^x q(s)\zeta(s,\lambda)h(s)ds$$

$$+\zeta(x,\lambda)\int_x^\pi q(\zeta)\upsilon(s,\lambda)h(s)ds\Big\}.$$

Applying the standard method in the work (Freiling and Yurko, 2001), we calculate

$$\lim_{\substack{|\lambda|\to\infty \\ \lambda\in G_\delta}} \max_{0\le x\le\pi} \left|z_k(x,\lambda)\right|=0, \quad k=1,2. \tag{20}$$

Take into account the following contour integral:

$$J_m(x)=\frac{1}{2\pi i}\int_{C_m}\lambda y^*(x,\lambda)d\lambda,$$

where $C_m=\left\{\lambda:\left|\tilde{\lambda}_m\right|+\frac{b}{2}\right\}$ and here $b=\inf_{n\neq k}\left|\tilde{\lambda}_n-\tilde{\lambda}_k\right|>0$. Using (19), we get

$$J_m(x)=h(x)-\varepsilon_m(x), \tag{21}$$

where

$$\varepsilon_m(x)=-\frac{1}{2\pi i}\int_{C_m}\frac{1}{\lambda}\left[z_1(x,\lambda)+z_2(x,\lambda)\right]d\lambda$$

and it follows from (20) that

$$\lim_{m\to\infty}\max_{0\le x\le\pi}\left|\varepsilon_m(x)\right|=0. \tag{22}$$

Moreover, applying the residue theorem, it is found that

$$J_m(x)=2\sum_{p=0}^{m}\operatorname*{Re}_{\lambda=\lambda_p} s\,\lambda y^*(x,\lambda)=\sum_{p=0}^{m}c_p\zeta(x,\lambda_p), \tag{23}$$

where

$$c_p=\frac{1}{\gamma_p}\int_0^{\pi}h(s)\zeta(s,\lambda_p)ds.$$

Consequently, as $m\to\infty$ it follows from (21)-(23) that the eigenfunction expansion formula (14) is obtained.

Corollary 2. The eigenfunctions $\left\{\zeta(x,\lambda_p)\right\}_{p\ge0}$ form a complete and orthogonal system in $L_2(0,\pi)$, so it creates an orthogonal basis in $L_2(0,\pi)$. Moreover, for $h(x)\in L_2(0,\pi)$ the Parsevale quality holds:

$$\int_0^{\pi}\left|h(s)\right|^2ds=\sum_{p=0}^{\infty}\gamma_p\left|c_p\right|^2.$$

2.2. The Uniqueness of Inverse Problem

Consider the function

$$F(x,s)=\sum_{p=0}^{\infty}\left(\frac{\zeta_0(x,\lambda_p)\zeta_0(s,\lambda_p)}{\gamma_p}-\frac{\zeta_0(x,\tilde{\lambda}_p)\zeta_0(s,\tilde{\lambda}_p)}{\gamma_p^0}\right), \tag{24}$$

where γ_p^0 are norming constants of the problem (1)-(3) where $q(x) \equiv 0.$

Theorem 3. The kernel appearing in representation (7) satisfies the following equation which is defined as fundamental equation of inverse problem for each $x \in (0, \pi]$:

$$\tilde{L}(x,s) + F(x,s) + \int_0^x \tilde{L}(x,z) F(z,s) dz = 0, \quad 0 < s < x, \tag{25}$$

where

$$\tilde{L}(x,s) = \begin{cases} L(x,s), & 0 < s < x < a \ \text{ and } \ 0 < s < 2a - x, \ x > a, \\ L(x,s) - \dfrac{\alpha_2}{\alpha_1} L(x, 2a - s), & 2a - x < s < a < x, \\ \dfrac{1}{\alpha_1} L(x,s), & a < s < x. \end{cases} \tag{26}$$

Proof. It is obtained from the expression $\zeta_0(x,\lambda)$ that

$$\cos \lambda x = \begin{cases} \zeta_0(x,\lambda), & 0 < x < a, \\ \dfrac{1}{\alpha_1} \zeta_0(x,\lambda) - \dfrac{\alpha_2}{\alpha_1} \zeta_0(2a - x, \lambda), & a < x < \pi. \end{cases}$$

Taking into account this formula, the solution (7) is converted to the following form:

$$\zeta(x,\lambda) = \zeta_0(x,\lambda) + \int_0^x L(x,s) \zeta_0(s,\lambda) ds, \qquad x < a$$

and

$$\zeta(x,\lambda)=\zeta_0(x,\lambda)+\int_0^a L(x,s)\zeta_0(s,\lambda)ds+\int_a^x \frac{1}{\alpha_1}L(x,s)\zeta_0(s,\lambda)ds$$
$$-\int_{2a-x}^{a}\frac{\alpha_2}{\alpha_1}L(x,2a-s)\zeta_0(s,\lambda)ds,\qquad a<x.$$

Consequently, we get

$$\zeta(x,\lambda)=\zeta_0(x,\lambda)+\int_0^x \tilde{L}(x,s)\zeta_0(s,\lambda)ds, \tag{27}$$

where $\tilde{L}(x,s)$ is in the form of (26). Moreover, according to (27),

$$\zeta_0(x,\lambda)=\zeta(x,\lambda)+\int_0^x \tilde{N}(x,s)\zeta(s,\lambda)ds. \tag{28}$$

It is obtained from (27) and (28) that

$$\sum_{p=0}^{m}\frac{\zeta(x,\lambda_p)\zeta_0(s,\lambda_p)}{\gamma_p}=\sum_{p=0}^{m}\frac{\zeta_0(x,\lambda_p)\zeta_0(s,\lambda_p)}{\gamma_p}$$
$$+\int_0^x \tilde{L}(x,z)\sum_{p=0}^{m}\frac{\zeta_0(z,\lambda_p)\zeta_0(s,\lambda_p)}{\gamma_p}dz$$

and

$$\sum_{p=0}^{m}\frac{\zeta(x,\lambda_p)\zeta_0(s,\lambda_p)}{\gamma_p}=\sum_{p=0}^{m}\frac{\zeta(x,\lambda_p)\zeta(s,\lambda_p)}{\gamma_p}$$
$$+\int_0^s \tilde{N}(s,z)\sum_{p=0}^{m}\frac{\zeta(x,\lambda_p)\zeta(z,\lambda_p)}{\gamma_p}dz.$$

Then, using these equalities, we can write

$$\Psi_m(x,s)=\psi_{m_1}(x,s)+\psi_{m_2}(x,s)+\psi_{m_3}(x,s)+\psi_{m_4}(x,s) \qquad (29)$$

where

$$\Psi_m(x,s)=\sum_{p=0}^{m}\left(\frac{\zeta(x,\lambda_p)\zeta(s,\lambda_p)}{\gamma_p}-\frac{\zeta_0(x,\tilde{\lambda}_p)\zeta_0(s,\tilde{\lambda}_p)}{\gamma_p^0}\right),$$

$$\psi_{m_1}(x,s)=\sum_{p=0}^{m}\left(\frac{\zeta_0(x,\lambda_p)\zeta_0(s,\lambda_p)}{\gamma_p}-\frac{\zeta_0(x,\tilde{\lambda}_p)\zeta_0(s,\tilde{\lambda}_p)}{\gamma_p^0}\right),$$

$$\psi_{m_2}(x,s)=\int_0^x\tilde{L}(x,z)\sum_{p=0}^{m}\left(\frac{\zeta_0(z,\lambda_p)\zeta_0(s,\lambda_p)}{\gamma_p}-\frac{\zeta_0(z,\tilde{\lambda}_p)\zeta_0(s,\tilde{\lambda}_p)}{\gamma_p^0}\right)dz,$$

$$\psi_{m_3}(x,s)=\int_0^x\tilde{L}(x,z)\sum_{p=0}^{m}\frac{\zeta_0(z,\tilde{\lambda}_p)\zeta_0(s,\tilde{\lambda}_p)}{\gamma_p^0}dz,$$

$$\psi_{m_4}(x,s)=-\int_0^s\tilde{N}(s,z)\sum_{p=0}^{m}\frac{\zeta(x,\lambda_p)\zeta(z,\lambda_p)}{\gamma_p}dz.$$

Let $h(x)\in AC[0,a]\cap AC[a,\pi]$. Then, from Theorem 1 and the expression (24) we calculate

$$\lim_{m\to\infty}\max_{0\le x\le\pi}\left|\int_0^{\pi}h(s)\Psi_m(x,s)ds\right|=\lim_{m\to\infty}\max_{0\le x\le\pi}\left|\sum_{p=0}^{m}c_p\zeta(x,\lambda_p)-\sum_{p=0}^{m}c_m^0\zeta_0(x,\tilde{\lambda}_p)\right|$$

$$\le\lim_{m\to\infty}\max_{0\le x\le\pi}\left|h(x)-\sum_{p=0}^{m}c_p\zeta(x,\lambda_p)\right|$$

$$+\lim_{m\to\infty}\max_{0\le x\le\pi}\left|h(x)-\sum_{p=0}^{m}c_p^0\zeta_0(x,\tilde{\lambda}_p)\right|=0, \qquad (30)$$

$$\lim_{m\to\infty}\int_0^{\pi} h(s)\psi_{m_1}(x,s)\,ds=\int_0^{\pi} h(s)F(x,s)\,ds, \tag{31}$$

$$\lim_{m\to\infty}\int_0^{\pi} h(s)\psi_{m_2}(x,s)\,ds=\int_0^{\pi} h(s)\left(\int_0^{x}\tilde{L}(x,z)F(z,s)\,dz\right)ds, \tag{32}$$

$$\lim_{m\to\infty}\int_0^{\pi} h(s)\psi_{m_3}(x,s)\,ds=\int_0^{x} h(z)\tilde{L}(x,z)\,dz, \tag{33}$$

$$\lim_{m\to\infty}\int_0^{\pi} h(s)\psi_{m_4}(x,s)\,ds=-\int_x^{\pi} h(s)\tilde{N}(s,x)\,ds. \tag{34}$$

Thus, it is obtained from (29)-(34) that

$$\int_0^{\pi} h(s)F(x,s)\,ds+\int_0^{\pi} h(s)\left(\int_0^{x}\tilde{L}(x,z)F(z,s)dz\right)ds$$

$$+\int_0^{x}\tilde{L}(x,s)h(s)ds-\int_x^{\pi} h(s)\tilde{N}(s,x)ds=0.$$

Since $\tilde{L}(x,s)=\tilde{N}(x,s)=0$ for $x<s$ and $h(x)$ can be chosen arbitrary, we have

$$F(x,s)+\tilde{L}(x,s)+\int_0^{x}\tilde{L}(x,z)F(z,s)\,dz-\tilde{N}(s,x)=0.$$

The above equation yields the fundamental equation (25) for $s<x$.

Lemma 4. The fundamental equation (25) has a unique solution $\tilde{L}(x,.)\in L_2(0,x)$ for each $x\in(0,\pi]$.

Proof. We will demonstrate that the homogenous equation

$$w(s)+\int_0^x F(\xi,s)w(\xi)d\xi=0 \tag{35}$$

has only trivial solution $w(s)=0$. Let $w(s)$ be a solution of the equation (35) and $w(s)=0$ for $s\in(x,\pi)$. In that case,

$$\int_0^x w^2(s)ds+\int_0^x\int_0^x F(\xi,s)w(\xi)w(s)d\xi ds=0$$

or by means of (24), we get

$$\int_0^x w^2(s)ds+\sum_{p=0}^{\infty}\frac{1}{\gamma_p}\left(\int_0^x \zeta_0(s,\lambda_p)w(s)ds\right)^2$$

$$-\sum_{p=0}^{\infty}\frac{1}{\gamma_p^0}\left(\int_0^x \zeta_0(s,\tilde{\lambda}_p)w(s)ds\right)^2=0.$$

Applying the Parseval equality,

$$\int_0^x w^2(s)ds=\sum_{p=0}^{\infty}\frac{1}{\gamma_p^0}\left(\int_0^x w(s)\zeta_0(s,\tilde{\lambda}_p)ds\right)^2,$$

we obtain

$$\sum_{p=0}^{\infty}\frac{1}{\gamma_p}\left(\int_0^x w(s)\zeta_0(s,\lambda_p)ds\right)^2=0.$$

Since $\gamma_n>0$ and the system $\{\zeta_0(s,\lambda_p)\}_{p\geq 0}$ is complete in $L_2(0,\pi)$ from the statement i in the Theorem 1, we find $w(s)=0.$

Now, let us point out the problem (1)-(3) as $T\left(q(x),h\right)$ and take the problem $\hat{T}\left(\hat{q}(x),\hat{h}\right)$ which is the same form as T but with different coefficients.

Theorem 5. Assume that $\lambda_p=\hat{\lambda}_p$ and $\gamma_p=\hat{\gamma}_p,\quad p\geq 0.$ In that case $q(x)=\hat{q}(x)$ almost everywhere on $\left(0,\pi\right)$ and $h=\hat{h}.$ That is, the operator T is uniquely determined by the specification of the spectral data $\left\{\lambda_p^2,\gamma_p\right\}_{p\geq 0}$.

Proof. It follows from (24) that $F\left(x,s\right)=\hat{F}\left(x,s\right).$ Thus, it is obtained from the equation (25) that $\tilde{L}\left(x,s\right)=\hat{\tilde{L}}\left(x,s\right).$ Using the formula (8) and (26), we find

$$\tilde{L}\left(x,x\right)=\frac{1}{2}\int_0^x q\left(\xi\right)d\xi. \tag{36}$$

This relation yields $q(x)=\hat{q}(x)$ almost everywhere on $\left(0,\pi\right).$ Taking into account (13), we have $\dot{\phi}\left(\lambda_p\right)\equiv\dot{\hat{\phi}}\left(\lambda_p\right)$ and $\tau_p=\hat{\tau}_p$ from the equality (11). It is obtained from (6) and (10) that $h=\hat{h}.$

Algorithm 6. The construction of potential $q(x)$ according to the spectral data $\left\{\lambda_p^2,\gamma_p\right\}_{p\geq 0}$ is as follows:

- From the given spectral data $\left\{\lambda_p^2,\gamma_p\right\}_{p\geq 0}$ build $F\left(x,s\right)$ by the formula (24),

- Calculate $\tilde{L}(x,s)$ by solving the fundamental equation (25),
- Find $q(x)$ from the relation (36).

REFERENCES

Agranovich, Z.S. and Marchenko, V.A. (1963). The inverse problem of scattering theory. New York and London: Gordon and Breach Science Publishers.

Akcay, O. (2018). The representation of the solution of Sturm-Liouville equation with discontinuity conditions. *Acta Mathematica Scientia, 38B(4),* 1195-1213.

Akcay, O. (2019). On the boundary value problem for discontinuous Sturm-Liouville operator. *Mediterranean Journal of Mathematics, 16(1)*,7. https://doi.org/10.1007/s00009-018-1279-5

Akcay, O. (2020). Uniqueness theorems for inverse problems of discontinuous Sturm-Liouville operator. *Bulletin of the Malaysian Mathematical Sciences Society*. https://doi.org/10.1007/s40840-020-01041-3

Akhmedova, E.N. and Huseynov, H.M. (2010). On inverse problem for Sturm-Liouville operator with discontinuous coefficients. *Izv. Saratov Univ. (N.S.), Ser. Math. Mech. Inform. 10(1)*, 3-9 (in Russian).

Amirov, R.K., Ozkan, A.S. and Keskin, B. (2009). Inverse problems for impulsive Sturm-Liouville operator with spectral parameter linearly contained in boundary conditions. *Integral Transforms and Special Functions, 20(8),* 607-618.

Anderssen, R.S. (1997). The effect of discontinuous in density and shear velocity on the asymptotic overtone structure of torsional eigenfrequencies of the earth. *Geophys J. R. Astr. Soc. 50,* 303-309.

Freiling, G. and Yurko, V.A. (2001). Inverse Sturm-Liouville problems and their applications. Huntington, NY: Nova Science Publishers Inc.

Gomilko, A. and Pivovarchik, V. (2002). On basis properties of a part of eigenfunctions of the problem of vibrations of a smooth inhomogeneous string damped at the midpoint. *Math. Nachr. 245*, 72-93.

Guliyev, N.J. (2005). Inverse eigenvalue problems for Sturm-Liouville equations with spectral parameter linearly contained in one of the boundary conditions. *Inverse Problems, 21*, 1315-1330.

Guseinov, I.M. and Mammadova, L.I. (2014). Reconstruction of the diffusion equation with singular coefficients for two spectra. *Doklady Mathematics, 90*, 401-404.

Hald, O.H. (1984). Discontinuous inverse eigenvalue problems. *Comm. Pure Appl. Math. 37*, 539-577.

Huseynov, H.M. and Dostuyev, F.Z. (2016). On determination of Sturm-Liouville operator with discontinuity conditions with respect to spectral data. *Proc. Inst. Math. Mech. Natl. Acad. Sci. Azerb. 42(2)*, 143-153.

Kadakal, M, and Mukhtarov, O.S. (2006). Discontinuous Sturm-Liouville problems containing eigenparameter in the boundary conditions. *Acta Mathematica Sinica, English Series, 22(5),* 1519-1528.

Karahan, D. and Mamedov, K.R. (2017). On an inverse problem for Sturm-Liouville equation. *Eur. J. Pure Appl. Math. 10(3),* 535-543.

Levitan, B.M. (1987). Inverse Sturm-Liouville problems. Utrecht: VNU Sci Press.

Levitan, B.M. and Sargsjan, I.S. (1991). Sturm-Liouville and Dirac operators. Dordrecht, Boston, London: Kluwer Academic Publishers.

Marchenko, V.A. (2011). Sturm-Liouville operators and applications. Providence, Rhode Island: AMS Chelsea Publishing.

Mukhtarov, O.S. and Aydemir, K. (2017). The eigenvalue problem with interaction conditions at one interior singular point. *Filomat, 31(17),* 5411-5420.

Mukhtarov, O.S., Olğar, H., Aydemir, K. and Jabbarov, I.S. (2018). Operator-pencil realization of one Sturm-Liouville problem with transmission conditions. *Applied and Computational Mathematics, 17(2),* 284-294.

Nabiev, A.A., Gürdal, M. and Saltan, S. (2016). Inverse problems for the Sturm-Liouville equation with the discontinuous coefficient. *J. Appl. Anal. Comput. 7(2)*, 559-580.

Şen, E. (2017). Sturm-Liouville problems with retarded argument and a finite number of transmission conditions. *Electronic Journal of Differential Equations, 2017(310),* 1-8.

Tikhonov, A.N. and Samarskii, A.A. (1990). Equations of mathematical physics. Dover, NewYork: Dover Books on Physics and Chemistry.

Wang, Y.P. (2015). Inverse problems for discontinuous Sturm-Liouville operators with mixed spectral data. *Inverse Problems in Science and Engineering, 23(7),* 1180-1198.

Willis, C. (1984). Inverse problems for torsional modes. *Geophys. J. R. Astr. Soc. 78,* 847-853.

Yang, C.F. and Yang, X.P. (2009). An interior inverse problem for the Sturm-Liouville operator with discontinuous conditions. *Applied Mathematics Letters, 22,* 1315-1319.

Zheng, Z., Cai, J., Li, K. and Zhang, M. (2018). A discontinuous Sturm-Liouville problem with boundary conditions rationally dependent on the eigenparameter. *Boundary Value Problems, 2018:103.* https://doi.org/10.1186/s13661-018-1023-x

CHAPTER 7

A MODERN APPROACH TO THE LOADING CONFIGURATION OF PATTERNS IN FRAMES

Asst. Prof. Dr. Muhammed Ernur AKINER [1]

[1] Akdeniz University, Vocational School of Technical Sciences, Environmental Protection and Control, Antalya, Turkey.
E-mail: ernurakiner@akdeniz.edu.tr. ORCID ID: 0000-0002-5192-2473

INTRODUCTION

Building codes permit pattern loads to be arranged to provide the most unfavorable internal forces in building frames' structural analysis. Hundreds of patterns loading configurations must be performed, mainly if the structural analysis of multistory systems is performed according to this law. Such pattern loading arrangements are not feasible and economical, even with the most modern desktop technologies. Therefore, various pattern loading arrangements have been proposed in previous studies. Prof. Richard W. Furlong and Prof. Ugur Ersoy have published two well documented critical studies regarding pattern loading arrangements. This paper's key motivation is to review these two previous articles on pattern loading arrangements, suggest a new methodology, and simplify all three different approaches by planning computer programs. Design tables, consisting of the most unfavorable internal forces required for design, will be ordered automatically using the prepared software applications. These tables would also be in a suitable format that the designer can quickly read and use. Consequently, the time required for the concrete frame structural examination would be reduced, making it easier for a designer to work. The author's suggested solution, regardless of the number of spans and floors of a building structure, needs only five loading arrangements for patterns.

In the structural analysis phase of multistory buildings' design, the engineer must analyze live load patterns placed on the building frame floors. Building codes such as ACI 318-99, sec. 8.9.2 (ACI, 1977), TS

500-2000, sec. 6.3.3 (TSE, 2000) and others require analyses based on live load arrangements producing the most unfavorable effects on members. This requirement leads to hundreds of loading cases in the analysis of multistory structures. However, this may not be practical even with the use of the most recent desktop technology, and except supercomputers, all personal computers have limited capacity. It is known that if the number of live load arrangement increases, the probability of a specific live load arrangement occurring decreases (Ersoy, 1992). Also, internal forces in any element are not affected by the loadings on far away spans. Therefore, a reasonable number of pattern loading cases should be analyzed to obtain sufficiently accurate results. Proper arrangements are suggested by Prof. Richard W. Furlong, Prof. Ugur Ersoy, and the author of this paper, which are called Furlong Approach (FA), Ersoy Approach (EA), and Approach Number 3 (AN3). Even with computer programs, inputting loads for each pattern loading case of each approach by hand is time-consuming. Also, during inputting, loads can be inputted onto the wrong element, yielding a false result. Another problem is identifying maximum internal forces from the resulting internal forces of each loading case of each approach. The selected maximum results of each loading case must be compared with each other, and maximum values must be taken as internal design forces. Also, this procedure should be repeated for all the approaches to get the most unfavorable effects. Another motivation of this paper is to shorten the time taken in the structural analysis phase of the structural design process. Accordingly, an easy method is needed to generate pattern loading arrangements

and do analysis according to these arrangements. Hence, computer codes for realizing this motivation were written in the "FORTRAN Visual Workbench v 1.00" programming language (Fortran, 1993). This paper aims to generate computer programs to automate pattern loading arrangements and apply pattern loads onto beams of frame structures according to approaches proposed by Richard W. Furlong, Ugur Ersoy, and the author of this paper, respectively. Hence, the methods of Richard W. Furlong, Ugur Ersoy, and the author of this paper were coded separately. Another objective is to quickly solve internal forces and identify maximum internal forces from each loading case resulting in internal forces. Ultimate results of each loading case were selected, and these results were compared with each other, and design tables were prepared using these maximum values, computer codes automatically generate all these phases. A designer can use design tables to start design directly. The methodology's main stages for this paper's objective are developing live load arrangements, analysis by stiffness method, finding member forces, and drawings generated live load arrangements. Illustrations were done for a visual explanation of the ideas of each approached live load arrangement.

1. METHODOLOGY

This research considers the problem of pattern loading arrangements in frames. Pattern loading is a phenomenon that occurs when live loads are present on some of the beams of the frame, but no live loads are present on the other beams of the frame. For example, imagine a

floor that sits beneath two different rooms in a home. If one day there is a person in one room but no one in the other room, this is a possible pattern load condition. Pattern loading only concerns live loads. Dead loads are always present and do not affect by pattern loading. According to Cavadas et al. (2020), load combinations can bedone in the order shown in Figure 1. This general approach is time-consuming and involves complex computations. Genetic algorithms are search algorithms based on the mechanics of natural selection and natural genetics. Their basic idea behind nature itself is the "Survival of the Fittest" (Zalzala & Fleming, 1997). In a genetic algorithm, in every generation, a new set of artificial creatures (strings) are created using bits (0 or 1), and the fittest of every string or chromosome is calculated (Jenkins, 1997). If they are strong enough to survive to the next generation, their genetic information is exploited to the new generation, thus exchanging its information to seek new and fitter strings in the preceding generations (Demirel, 1999). Leading operators of a Simple Genetic Algorithm: 1. Selection and Reproduction; 2. Crossover; 3. Mutation (Artar and Daloğlu, 2015; Toğan and Daloğlu, 2006). According to Turğut and Arslan (2001), pattern loads can be generated by using Genetic Algorithms. Turğut and Arslan (2001) worked on continuous beams, and they tried to develop pattern loading arrangements that cause the most unfavorable effects.

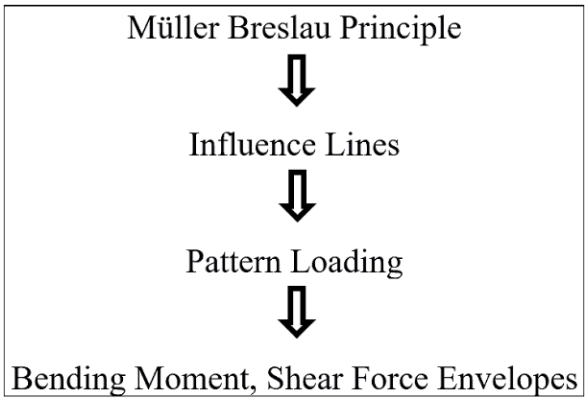

Figure 1. General approach for live load arrangements in a manner that the most unfavorable effects are created.

As seen in Table. 1, in addition to their advantages, genetic algorithms have many drawbacks. Especially for pattern loading arrangements, Genetic Algorithms are mostly applicable for small structures such as indeterminate continuous beams or small frames. During the load combination process, too many files must be opened and read. More complex calculations are needed to obtain the internal forces' unfavorable values found during this optimization process. These mentioned drawbacks show that getting the optimum design values is time-consuming and needs to be developed or supercomputer technology rather than standard desktop technology. However, more simple methods can be used for the optimization process, and the most unfavorable internal forces for the design process can be found by using these methods.

Table 1. Advantages and disadvantages of Genetic Algorithms.

Technology	Advantage	Disadvantage
Genetic Algorithms	• Particularly well suited for challenging problems where little is known about the underlying search space. • Widely applicable. • Easy to incorporate other methods. • It can be run interactively, accommodate user proposed solutions. • Provide many alternative solutions.	• There is no guarantee for the optimal solution within finite time. • Weak theoretical basis. • May need parameter tuning. • Often computationally expensive and slow.

1.1. Furlong Approach

Furlong Approach aims to get maximum internal forces in beams and columns with the least number of reasonable live load arrangements (Furlong 1981). In Furlong Approach, many loading cases are defined due to the number of frame structure spans. Using Eq. (1), the total number of loading cases for the frame structure can be calculated.

$$\text{nlc of FA} = 2 + (m-1) \quad (1)$$

Where “nlc,”“FA,”“m,”“2”, (m-1) are indicating the number of loading cases, Furlong Approach, the total number of spans, number of loading cases for positive span moments, number of loading cases for negative support moments, respectively. Loading cases along with the programming idea of FA is shown in Figure 2. Each circle indicates one floor; each space between dots on circles indicates a

single beam; thick curves on the circles indicate pattern loads; arrows indicate equivalent joint forces of pattern loads.

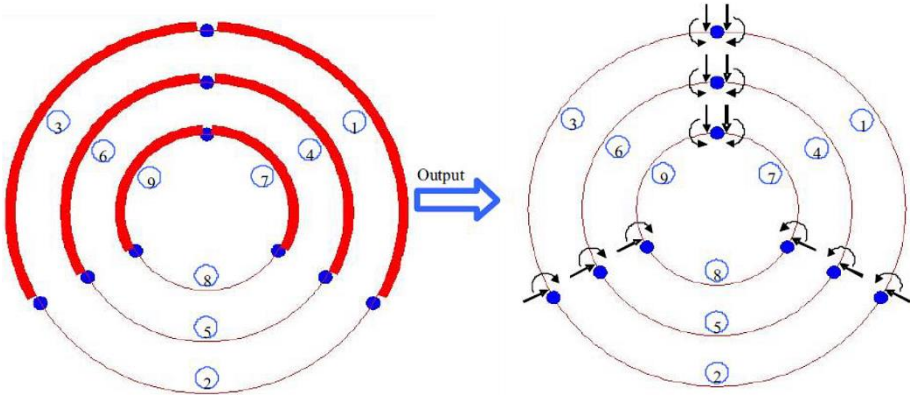

Figure 2. Loading cases of Furlong Approach and the programming idea.

1.2. Ersoy Approach

Ersoy's approach requires analyzing five cases irrespective of the number of stories and beams (Ersoy, 1992). A reasonable number of cases should be interpreted to obtain sufficiently accurate results (Ersoy, 1992). Loading cases along with the programming idea of EA is shown in Figure 3. In EA, two beams are loaded at the top story starting from the first beam, and the third one is unloaded. This loading continues until all beams at the top story are dealt with. This loading continues by skipping one beam in each story until all beams and stories are dealt with (Ersoy and Ozcebe, 1998).

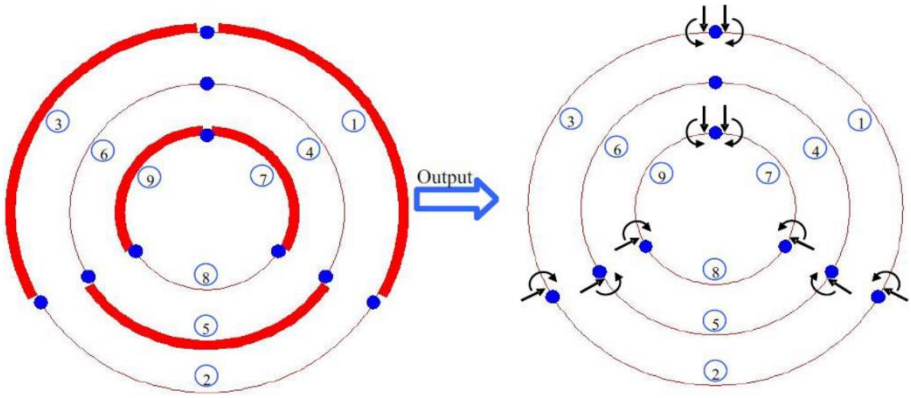

Figure 3. Loading cases of Ersoy Approach and the programming idea.

1.3. Approach Number 3

Approach Number 3 requires the analysis of five cases irrespective of the number of stories and beams. The aim of Approach Number 3 is, as the aim of the Furlong Approach and Ersoy Approach, to obtain sufficiently accurate results with a reasonable number of loading cases. The first two loading cases are Classical Checkerboard Loading and the first two loading case of the Ersoy Approach. Loading cases for finding maximum negative moments are different from Furlong and Ersoy's Approaches. Loading cases of AN3 along with the programming idea of AN3 is shown in Figure 4. Helix indicates all beams. In AN3, starting from the first beam, two adjacent beams are loaded, and the third one is unloaded at the upper left. This loading continues until all beams are dealt with.

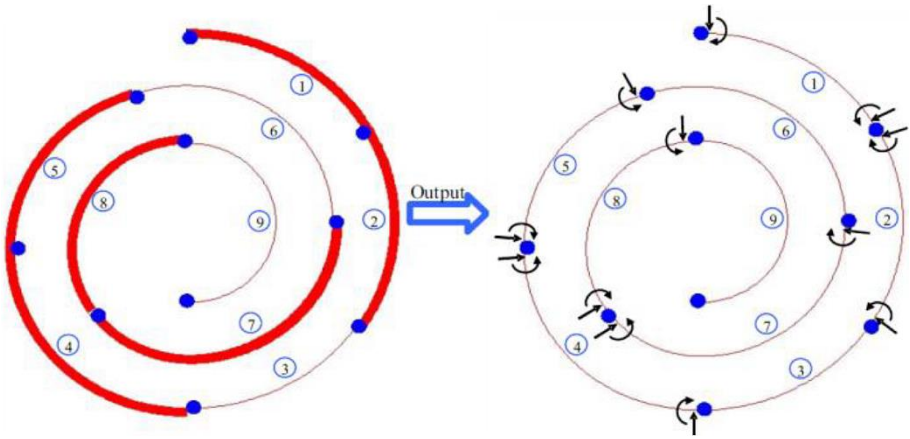

Figure 4. Loading cases of Approach Number 3 and the programming idea.

According to Balfour (1992), distributed loads on beam elements can be converted into equivalent joint forces. Therefore, loaded structure can be analyzed by computer programs quickly. According to Hibbeler (1990), this method is used for the structure analyzed by the hand calculation's stiffness method. Beam elements of the frame structure are considered components of a matrix, "m" is the total number of spans and "lvl" is the total number of floors. Therefore, "m" is the column number and "lvl" is the row number of this matrix,as seen in Eq. (2).

$$m\begin{bmatrix} Beam\_1 & Beam\_2 & Beam\_3 \\ Beam\_4 & Beam\_5 & Beam\_6 \\ Beam\_7 & Beam\_8 & Beam\_9 \end{bmatrix}^{lvl} \quad (2)$$

Using the Do loop, which changes from 1 to m, each span number can be defined, and by using the second Do loop, which varies from 1 to lvl, each beam number can be determined. Computer codes were written in Fortran programming language for all three approaches

(CCFA, CCEA, and CCAN3). Parts of each computer code are shown in Figure 5.

2. RESULTS AND DISCUSSIONS

According to "TS 500-2000" (TSE, 2000), unfavorable loads must be considered for the building design. An example frame 3x4 is shown in Figure 6. In this frame, factored loads are in kN per meter (kN/m). Load Combination is; Fd=1.0G+1.0Q, where G is dead load, Q is live load. Section properties for each element of the frame are given as: for beams; E=28,000,000 kN/m^2, A=0.1125 m^2, I=0.001898 m^4, for columns; E=28,000,000 kN/m^2, A=0.1225 m^2, I=0.001250 m^4.

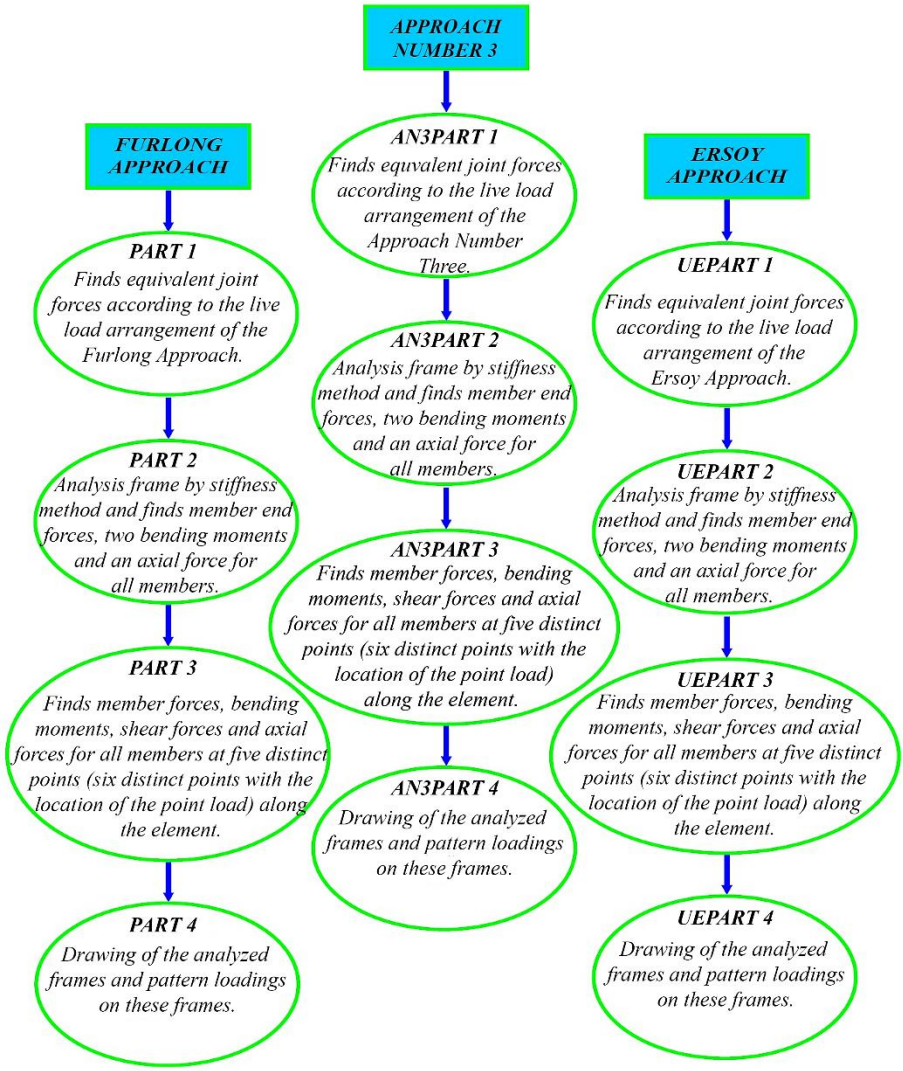

Figure 5. Programming logic and parts of three approaches.

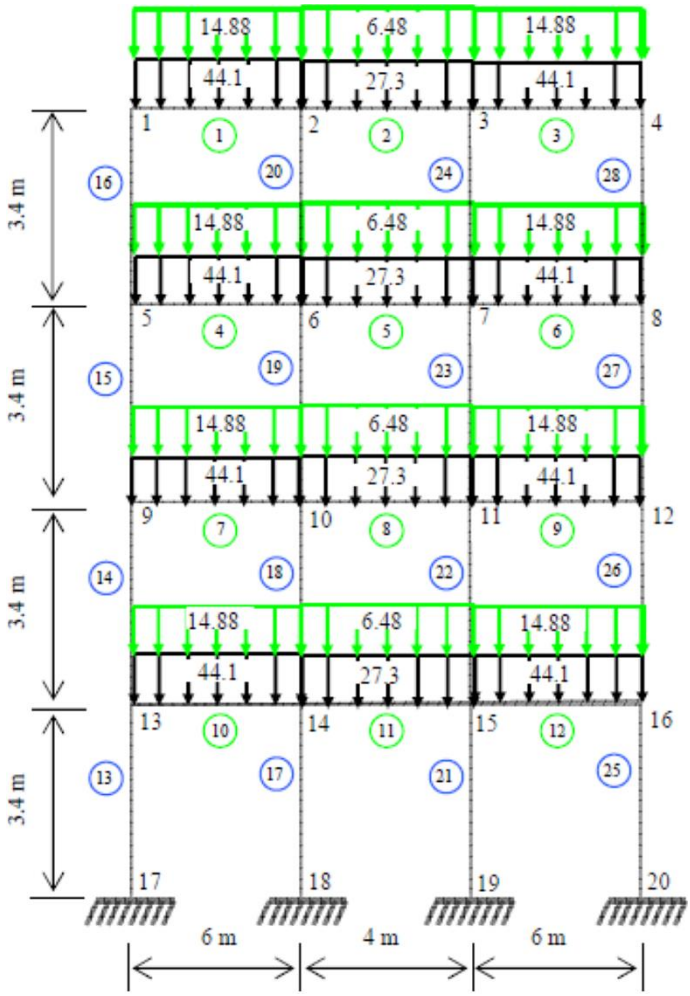

Figure 6. Example frame for the analysis (green for live load, black for dead load).

Results from computer codes (CCFA, CCEA, and CCAN3) are shown in Table 2. Note that the most critical frame elements where the most unfavorable loads have occurred were presented.

Table 2. Comparison of CCFA, CCEA, and CCAN3 results for the frame in Fig. 6.

Beam no	Design internal forces	CCFA				CCEA				CCAN3			
		i-end	span (+)	span (-)	j-end	i-end	span (+)	span (-)	j-end	i-end	span (+)	span (-)	j-end
		Along the element				Along the element				Along the element			
1	M (kN.m)	-121	124	34	-163	-122	127	32	-164	-121	127	32	-163
	V (kN)	171			-184	171			-185	171			-184
	N (kN)		-62				-63				-62		
5	M (kN.m)	-60	11	-14	-60	-70	16	-20	-72	-61	16	-20	-61
	V (kN)	68			-68	73			-74	68			-68
	N (kN)		7				7				7		
7	M (kN.m)	-152	107	27	-167	-151	-110	24	-169	-152	110	24	-167
	V (kN)	175			-179	175			-180	175			-179
	N (kN)		-7				-13				-7		
9	M (kN.m)	-167	107	27	-152	-168	110	24	-151	-167	110	24	-152
	V (kN)	179			-175	180			-175	179			-175
	N (kN)		-7				-14				-7		
11	M (kN.m)	-72	5	-22	-72	-74	8	-25	-77	-72	8	-25	-72
	V (kN)	70			-70	72			-73	70			-70
	N (kN)		6				6				6		
Column no	Design internal forces	CCFA				CCEA				CCAN3			
		i-end	span (+)	span (-)	j-end	i-end	span (+)	span (-)	j-end	i-end	span (+)	span (-)	j-end
		Along the element				Along the element				Along the element			
14	M(kN.m)	84	43	-39	-80	84	44	-41	-81	84	44	-41	-80
	V (kN)	-48			-48	-49			-49	-48			-48
	N (kN)		-521				-477				-521		
17	M (kN.m)	-21	26	-5	42	-22	28	-6	45	-22	28	-6	45
	V (kN)	18			18	20			11	20			20
	N (kN)		-1001				-939				-1001		
23	M (kN.m)	50	26	-23	-47	53	28	-25	-48	50	27	-25	-47
	V (kN)	-28			-28	-30			-30	-28			-28
	N (kN)		-501				-489				-501		

If we want to apply all possible load combinations, there will be many pattern loads cases. On the other hand, using FA, EA, and AN3 decreases (Table 3).

Table 3. Comparison of the total number of loading cases (LC) for the example frame according to FA, EA, AN3, and all possible load combinations.

Number of LC of FA	Number of LC of EA	Number of LC of AN3	Number of LC of All Possible Load Combinations
4	5	5	$2^n = 2^{12} = 4096$

CONCLUSIONS

This study's programming ideology is a useful example for those interested in programming in structural engineering. The author's alternative approach (AN3) and computer codes (CCFA, CCEA, and CCAN3) were presented. The proposed method is straightforward, applicable, and efficient for programming.

This research investigated the previous studies done by Furlong and Ersoy and developed the third approach called approach number three (AN3). The new proposal influenced the genetic algorithms based on the mechanics of natural selection or, in other words, the survival of the fittest. A new approach requires analyzing five cases only irrespective of the number of stories and beams. The AN3 has the aim to obtain sufficiently accurate results with a reasonable number of loading cases. Loading cases of the Furlong and Ersoy approaches are classical checkerboard loading. AN3 has different loading cases for finding maximum negative moments, starting from the first beam, at the upper left, two adjacent beams are loaded, and the third one is unloaded. This loading continues until all beams are dealt with.

Using computer programs (computer codes) short time is taken in the structural design purpose analysis phase. A designer and students can easily handle these programs and get design tables. By using these design tables, the engineer can start design directly. Results show that all three approaches give unfavorable internal forces that were very close to each other. However, the proposed alternative Approach (AN3) easier to apply for any building frame regardless of the number of spans and story.

REFERENCES

ACI (1997). Building code requirements for structural concrete (ACI 318-99). *Section 8.9.2, American Concrete Institute, Detroit, USA.*

Artar, M., & Daloğlu, A. (2015). Çok katlı kompozit çelik çerçevelerin genetik algoritma ile dinamik sınırlayıcılı optimizasyonu. *Teknik Dergi, 26*(2), 7077-7098.

Balfour, J. A. D. (1992). *Computer Analysis of Structural Frameworks,* Blackwell Scientific Publications, Great Britain, London.

Cavadas, F., Costa, B. J. A., Figueiras, J. A., Pimentel, M., & Félix, C. (2020). *Data-Driven Damage Detection Based on Moving-Loads Responses-The Luiz I Bridge,* In European Workshop on Structural Health Monitoring (pp. 837-846), Springer, Cham.

Demirel, L. (1999). *Genetic algorithms in engineering optimization,* MSc thesis, Department of Aerospace Engineering, Istanbul Technical University, Istanbul.

Ersoy, U. (1992). Çok katlı yapıların çözümünde hareketli yük düzenlemesi. *IMO Teknik Dergi, YAZI 40*, 555-561.

Ersoy, U., & Ozcebe, G. (2001). *Betonarme-Temel İlkeler TS 500-2000 ve Türk Deprem Yönetmeliğine (1998) Göre Hesap,* Evrim Yayınevi ve Bilgisayar San. Tic. Ltd. Sti., İstanbul.

Fortran (1993). *Fortran Visual Workbench v 1.00,* Microsoft Corporation, USA.

Furlong, R. W. (1981). Rational analysis of multistory concrete structures. *Concrete International. American Concrete Inst., 3*(6), 29-35.

Hibbeler, R. C. (1990). *Structural Analysis,* Macmillan Publishing Company, (pp. 645-658), USA.

Jenkins, W. M. (1997). Plane frame optimum design environment based on genetic algorithm. *Journal of Structural Engineering, ASCE, 118*(11), 3103-3112.

Toğan, V., & Daloğlu, A. (2006). Genetik Algoritma ile Üç Boyutlu Kafes Sistemlerin Şekil ve Boyut Optimizasyonu. *Teknik Dergi, 17*(82), 3809-3825.

TSE (2000). *Türk Standardı, TS 500-Betonarme Yapıların Tasarım ve Yapım Kuralları,* Section 6.3.3, Türk Standartları Enstitüsü, Ankara, Turkey, 18 pp.

Turğut, P., & Arslan, A. (2001). Sürekli bir kirişte maksimum momentlerin genetik algoritmalar ile belirlenmesi. *Dokuz Eylül Üniversitesi Mühendislik Fakültesi Fen ve Mühendislik Dergisi*, *3*(3), 1-9.

Zalzala, A. M. S., Fleming, P. J. (1997). *Genetic Algorithms in Engineering Systems*, The Institution of Electrical Engineers, (pp. 3-17), London, United Kingdom.

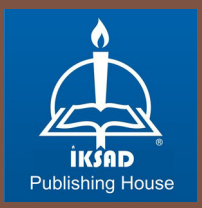

ISBN: 978-625-7636-73-5